UNIVERSIDADE FEDERAL DO PARANÁ

VINICIUS ANTUNES FERREIRA DA SILVA

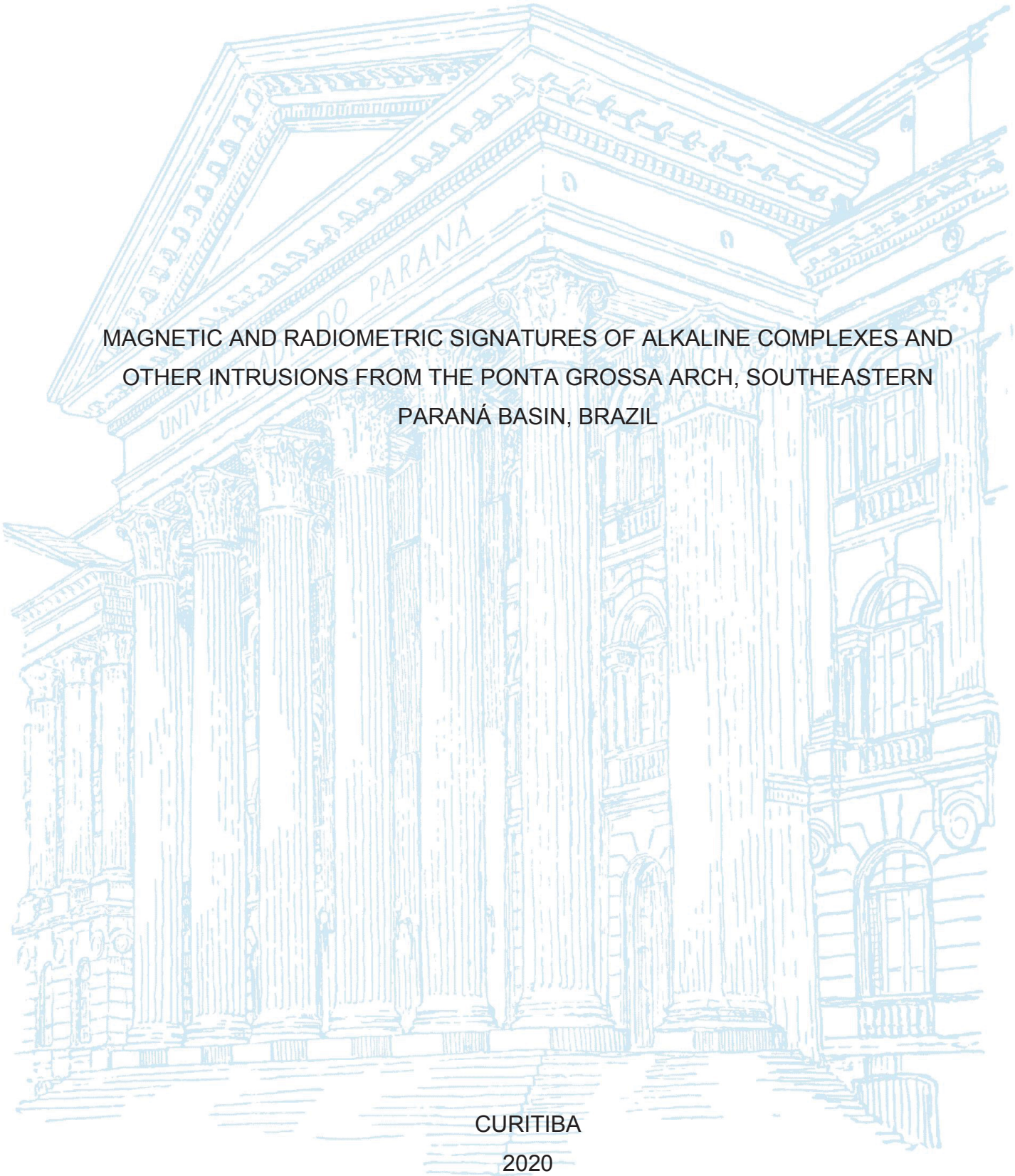

MAGNETIC AND RADIOMETRIC SIGNATURES OF ALKALINE COMPLEXES AND OTHER INTRUSIONS FROM THE PONTA GROSSA ARCH, SOUTHEASTERN PARANÁ BASIN, BRAZIL

CURITIBA

2020

VINICIUS ANTUNES FERREIRA DA SILVA

MAGNETIC AND RADIOMETRIC SIGNATURES OF ALKALINE COMPLEXES AND OTHER INTRUSIONS FROM THE PONTA GROSSA ARCH, SOUTHEASTERN PARANÁ BASIN, BRAZIL

Dissertação apresentada ao curso de Pós-Graduação em Geologia, Setor de Ciências da Terra, Universidade Federal do Paraná, como requisito parcial à obtenção do título de Mestre em Geologia Exploratória.

Orientador: Prof. Dr. Francisco J. F. Ferreira

CURITIBA

2020

Catalogação na Fonte: Sistema de Bibliotecas, UFPR
Biblioteca de Ciência e Tecnologia

S586m Silva, Vinicius Antunes Ferreira da
Magnetic and radiometric signatures of alkaline complexes and other intrusions from the Ponta Grossa arch, southeastern Paraná Basin, Brazil [recurso eletrônico] / Vinicius Antunes Ferreira da Silva. – Curitiba, 2020.

Dissertação - Universidade Federal do Paraná, Setor de Ciências da Terra, Programa de Pós-Graduação em Geologia, 2020.

Orientador: Francisco José Fonseca Ferreira.

1. Rochas ígneas alcalinas. 2. Carbonatitos. 3. Geofísica. I. Universidade Federal do Paraná. II. Ferreira, Francisco José Fonseca. III. Título.

CDD: 552.1

Bibliotecária: Vanusa Maciel CRB- 9/1928

TERMO DE APROVAÇÃO

Os membros da Banca Examinadora designada pelo Colegiado do Programa de Pós-Graduação em GEOLOGIA da Universidade Federal do Paraná foram convocados para realizar a arguição da Dissertação de Mestrado de **VINICIUS ANTUNES FERREIRA DA SILVA** intitulada: **MAGNETIC AND RADIOMETRIC SIGNATURES OF ALKALINE COMPLEXES AND OTHER INTRUSIONS FROM THE PONTA GROSSA ARCH, SOUTHEASTERN PARANÁ BASIN, BRAZIL**, sob orientação do Prof. Dr. FRANCISCO JOSÉ FONSECA FERREIRA, que após terem inquirido o aluno e realizada a avaliação do trabalho, são de parecer pela sua APROVAÇÃO no rito de defesa.

A outorga do título de mestre está sujeita à homologação pelo colegiado, ao atendimento de todas as indicações e correções solicitadas pela banca e ao pleno atendimento das demandas regimentais do Programa de Pós-Graduação.

CURITIBA, 29 de Abril de 2020.

Assinatura Eletrônica
02/05/2020 16:44:53.0
FRANCISCO JOSÉ FONSECA FERREIRA
Presidente da Banca Examinadora (UNIVERSIDADE FEDERAL DO PARANÁ)

Assinatura Eletrônica
29/04/2020 17:59:30.0
WELITOM RODRIGUES BORGES
Avaliador Externo (UNIVERSIDADE DE BRASÍLIA)

Assinatura Eletrônica
02/05/2020 17:59:17.0
ODERSON ANTÔNIO DE SOUZA FILHO
Avaliador Externo (COMPANHIA DE PESQUISA DE RECURSOS MINERAIS)

Dedico à Iara

ACKNOWLEDGMENTS

I would like to thank my mother, Iara, for the continuous support and motivation during this work. You are the greatest. Mental fortitude is a must to finish a research and I would like to acknowledge your time and effort giving me strength to accomplish the task.

To my father and sister, Pedro e Renata, for all your help.

I would also like to thank Ravena for our discussions about life and issues in academia. Thanks my sweetheart.

To my advisor, Professor Francisco, for the support.

To the thesis committee, Prof. Welitom Rodrigues Borges and Dr. Oderson Antônio de Souza Filho, who kindly accepted the invitation to revise this work and contribute with suggestions to the final version.

To my mentor in Mentoring365, John Robert Kusiak, who gave me a lot of insightful advices about life and career in just three months of mentoring.

To the people in the ResearchGate website who replied me and helped to improve discussions about topics related to this thesis. Big kudos also for Mario Sigismondi who teach me about the power spectrum method.

To all my friends in the Laboratory for Research in Applied Geophysics (LPGA), specially to Rafael Canata for the moments of fun and friendship during the hardships of writing. Also, for helping me to find a committee member just in a few days before my defense. You are the true hero. To Luizemara who helped me showing me techniques which were used in this work.

To my friends at the Instituto de Terras, Cartografia e Geologia do Paraná (ITCG) for the suggestions, advices and interesting chats about geology and other topics.

Two tenured professors, an assistant professor, and a grad student walk into a bar and order [See below for full text options]

by "Shit Scademics Say"

RESUMO

Localizada próxima do limite sudeste da Bacia do Paraná, Brasil, a Província Alcalina do Arco de Ponta Grossa (PAAPG) é composta por rochas alcalinas, carbonatíticas-alcalinas e gabroicas. Rochas alcalinas têm recebido muita atenção nos últimos anos devido a sua associação com carbonatitos que podem hospedar mineralizações de elementos de terras raras e fosfatos. Essas rochas podem ser identificadas e definidas em escalas regionais a de detalhe por levantamentos aéreos multiparamétricos que contribuem para o mapeamento geológico e a exploração mineral. Nesta dissertação, dados aeromagnéticos e aerogamaespectrométricos foram avaliados para as seguintes rochas da PAAPG: complexos Bairro da Cruz, Banhadão, Barra do Itapirapuã, Mato Preto e Tunas, Fonolito Barra do Teixeira, Nefelina sienito Itapirapuã e Gabro José Fernandes. Estimativas de profundidade das fontes magnéticas foram analisadas através do espectro de potência, soluções da deconvolução de Euler 3D e inclinação do sinal analítico. Realizou-se o delineamento do arcabouço magnético-estrutural da área de estudo através da primeira derivada vertical. Além disso, foram feitas inversões 3D de susceptibilidade magnética para os corpos Bairro da Cruz, José Fernandes e Tunas. Mapas básicos (K, eU e eTh) e ternário (R-K, G-eTh, B-eU) foram criados para explicar a concentração dos radioelementos assim como foram gerados 14 mapas de razões e 3 parâmetros normalizados pelo tório. Níveis mínimos, máximos e médios dos radioelementos foram apresentados para cada intrusão, bem como suas concentrações relativas de K, eU e eTh para os pontos amostrados do levantamento. Cada complexo alcalino foi também avaliado com base em perfis empilhados de dados radiométricos e magnéticos oriundos das linhas de voo. Os resultados magnéticos revelaram fontes rasas para a área de estudo, em torno de 500 m de profundidade. Anomalias dipolares significativas com polaridade normal foram associadas aos corpos ígneos Bairro da Cruz, José Fernandes e Tunas. Os modelos 3D apresentaram valores de susceptibilidade magnética coerentes com os de gabros e rochas alcalinas publicados na literatura. Dados gamaespectrométricos mostraram que o elemento mais radioativo nos corpos ígneos foi o tório equivalente. Das unidades estudadas, as formadas majoritariamente por carbonatitos apresentaram os maiores teores de eU e eTh. O trabalho desta dissertação contribuiu para as características geológicas e geofísicas das rochas alcalinas do Arco de Ponta Grossa.

Palavras-chave: Geofísica aérea. Província Alcalina do Arco de Ponta Grossa. Rochas alcalinas.

ABSTRACT

Located near the southeastern limit of Paraná Basin, Brazil, the Ponta Grossa Arch Alkaline Province (PGAAP) is comprised of alkaline, carbonatitic-alkaline, and gabbroic rocks. Alkaline rocks have received much attention in recent years due to being associated with carbonatites that may host rare earth elements and phosphates mineralizations. These rocks can be identified and defined in regional to fine-detail scales by multi-parameter airborne surveys contributing to geological mapping and mineral exploration. In this thesis, airborne magnetic and gamma-ray spectrometric data were evaluated for the following rocks of PGAAP: Bairro da Cruz, Banhadão, Barra do Itapirapuã, Mato Preto, and Tunas complexes, Barra do Teixeira Phonolite, Itapirapuã Nepheline syenite, and José Fernandes Gabbro. Depth estimates of magnetic sources were analyzed through the power spectrum, Euler 3D deconvolution solutions, and tilt angle techniques. Delineation of the magnetic-structural framework for the study area was generated using the first vertical derivative. Additionally, 3D inversions of magnetic susceptibilities were performed for Bairro da Cruz, José Fernandes, and Tunas. Basic maps (K, eU, and eTh) and a ternary one (R-K, G-eTh, B-eU) were generated to explain radioelements concentration as well as 14 ratios and 3 thorium-normalized maps. Minimum, maximum, and average radioelements levels were presented for each intrusion as well as their relative concentrations of K, eU, and eTh of sampled data points. Each alkaline complex was also evaluated based on stacked profiles from flight lines comprising radiometric and magnetic data. Magnetic results revealed shallow sources for the study area, around 500 m depth. Noteworthy dipolar anomalies with normal polarity are associated with the Bairro da Cruz, José Fernandes, and Tunas igneous bodies. The 3D models showed magnetic susceptibilities values in agreement with the ones published for gabbros and alkaline rocks. Gamma-ray spectrometric data displayed that the most radioactive element in the igneous bodies was equivalent thorium. From the units studied, the ones composed mainly by carbonatites showed the highest contents of eU and eTh. The current work of this thesis has contributed to the geology and geophysical characteristics of the alkaline rocks in the Ponta Grossa Arch.

Keywords: Airborne geophysics. Ponta Grossa Arch Alkaline Province. Alkaline rocks.

LIST OF FIGURES

LIST OF TABLES

CONTENTS

1 INTRODUCTION

1.1 MOTIVATION

The Ponta Grossa Arch (PGA) is an uplifted domain located in southeastern Paraná Basin and its Precambrian basement (**Figure 1**). The arch hosts alkaline and carbonatitic-alkalic intrusions. These complexes were studied by Almeida (1983) who labeled them as the Ponta Grossa Arch Alkaline Province (PGAAP). Most of this province is situated between the southern parts of the Guapiara (Ferreira et al. 1981) and the São Jerônimo-Curiúva (Vieira 1973; Ferreira 1982) lineaments.

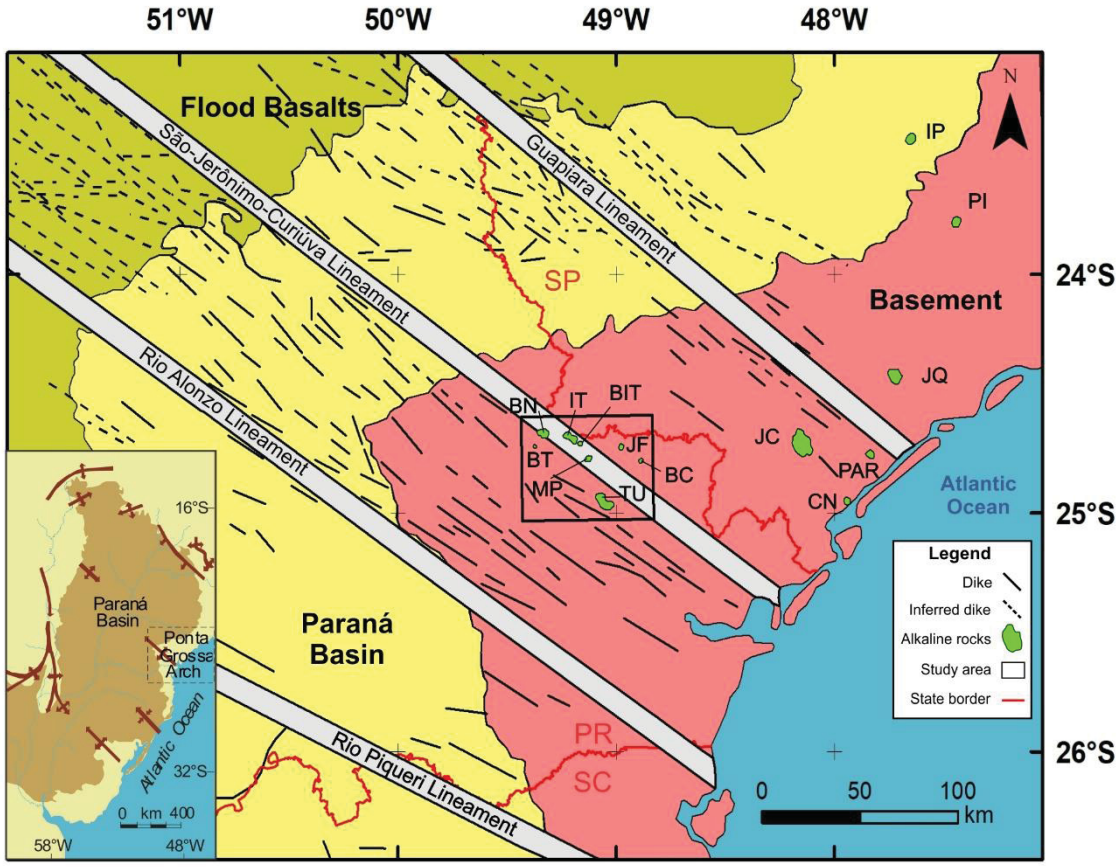

Figure 1. Sketch map of the Ponta Grossa Arch Alkaline Province (modified from Ruberti et al. 2005; Gomes et al. 2018). Alkaline complexes: Bairro da Cruz (BC), Barra do Itapirapuã (BIT), Banhadão (BN), Barra do Teixeira (BT), Cananéia (CN), Ipanema (IP), Itapirapuã (IT), Jacupiranga (JC), José Fernandes (JF), Juquiá (JQ), Mato Preto (MP), Pariquera-Açu (PAR), Piedade (PI), and Tunas (TU). States: São Paulo (SP), Paraná (PR), and Santa Catarina (SC).

Alkaline intrusions have been recognized and detailed in different scales by airborne magnetics and gamma-ray spectrometric surveys. These surveys contribute to a variety of geological and geophysical interpretation and modeling applications, such as geological mapping and mineral exploration (Airo et al. 2014), as well as the discovery of uranium

deposits in alkaline igneous complexes (e.g. Cercado Mine in Poços de Caldas, Forman and Angeiras 1981). For example, aeromagnetic maps aid the interpreter in verifying anomalies that coincide with outcropping alkaline intrusions, or even those with no surface manifestation, as well as to verify possible structural control on such intrusions (Marangoni and Mantovani 2013; Louro et al. 2019). Aeromagnetic maps may also reveal typical magnetic features such as circular anomalies for carbonatitic-alkaline bodies which coincide with their radiometric responses (Airo 2015). Modeling of these bodies in subsurface could aid in reducing costs prior to mining (Marangoni and Mantovani 2013). As for radiometrics, alkaline rocks tend to enrich in equivalent thorium (eTh), which forms complex ions with sulfides, carbonates, and phosphates (Airo 2015). Furthermore, carbonatitic-alkalic complexes may show potential for rare earth elements (REE), niobium, and vermiculite mineralizations which are resources with economic importance for Brazil (Gomes and Comin-Chiaramonti 2005).

The PGAAP was studied by Ulbrich and Gomes (1981), Almeida (1983) and several authors, including Comin-Chiaramonti and Gomes (2005), Gomes et al. (2011), and Gomes and Comin-Chiaramonti (2017), who did an extensive review about the Mesozoic-Cenozoic alkaline magmatism in the Brazilian platform. The area has also been studied by Marangoni and Mantovani (2013), who characterized and reviewed state-of-the-art potential field (magnetic and gravimetric) signatures in the PGAAP and other alkaline provinces in Brazil. However, these authors have not reported geophysical signatures of all the bodies from the PGAAP, but for Ipanema (IP), Jacupiranga (JC), Juquiá (JQ), Pariquera-Açu (PAR), and Tunas (TU). In addition, all the works compiled by Marangoni and Mantovani (2013) used previous and lower-resolution aerogeophysical data (i.e. flight lines spaced with 1 km or more) than the 2011 airborne survey contracted by the Geological Survey of Brazil - CPRM (CPRM 2011).

Although a variety of geophysical studies were applied in Brazilian alkaline rocks, not all the provinces have been studied in detail by different geophysical methods (Marangoni and Mantovani 2013). Little attention has been paid to the use of gamma-ray spectrometric data along with the magnetic one. The aim of this study was to define what are the airborne magnetic and radiometric signatures of eight bodies in the PGAAP, namely: Bairro da Cruz, Banhadão, Itapirapuã, Barra do Itapirapuã, Barra do Teixeira, José Fernandes, Mato Preto, and Tunas. High-resolution aeromagnetics (HRAM), according to Sheriff (2002) definition, and radiometric datasets were analyzed in order to assess the pattern of anomalies over the area comparing them with other previous studies.

1.2 ORGANIZATION OF THE THESIS

This thesis comprises seven chapters. While Chapter **1** gives an overview and aim of the study, Chapter **2** is a compilation of studies regarding the magmatism in the South America platform and the Ponta Grossa Arch. A more detailed view of preceding geological and geophysics analyses of alkaline bodies in the area of study is also given in this chapter. Chapter **3** will outline the theory behind the magnetic and radiometric methods used for the airborne survey data. In Chapter **4**, “Material and Methods”, provides a summary of the techniques and its parameters utilized for the processing of airborne survey data. In Chapter **5**, results and discussion about the eight bodies of the PGAAP is given in a scientific article format alongside other items required for further publication. Chapter **6** outlines the results of basic statistics for the survey height lines. Chapter **7**, “Final remarks”, summarizes the findings in the study area and suggests future works to be carried.

Appendices present a detailed routine to calculate the average flight height by line (Appendix 1), the values of parameters used in inversions (Appendix 2), and radiometric images of the study area (Appendix 3).

2 GEOLOGICAL SETTING

2.1 MAGMATISM IN THE SOUTH AMERICAN PLATFORM

Four main geotectonic units constitute the South American plate. One of them is the South American platform, defined as the continent part that was not affected by the Andean orogenies (Almeida 1967; Almeida et al. 1981, 2000) and where Brazil is most located. This platform is surrounded by the younger terrains of the continent, defined by the Patagonian platform (south-central), the Andean chain, placed to the west, and the domain of oceanic crust which constitutes the eastern unit of the plate (Riccomini et al. 2005; Alkmim 2015).

The area where Brazil resides in the South American platform, called the Brazilian platform, is comprised of Archaean to Proterozoic cratons surrounded by Neoproterozoic orogenic belts and covered by Phanerozoic sediments (e.g. Paraná Basin) (**Figure 2**) (Riccomini et al. 2005).

The Brazilian and South American platforms have been through magmatic activity comprising alkaline and alkaline-carbonatitic complexes starting in the Permian-Triassic and lasting until the Oligocene period. The majority of these complexes in Brazil are of Late Cretaceous age (Gomes and Comin-Chiaramonti 2005).

Alkaline province, according to Almeida (1983), is a term used to define areas of occurrence of clusters of alkaline bodies, with specific rock associations and ages, and are grouped mainly on the basis of their geological setting and recognizable tectonic features (Riccomini et al. 2005; Gomes and Comin-Chiaramonti 2005).

Even though there is no clear consensus about the definition of alkaline rocks, they may be classified as situated above the X - Y and X - Z lines in the Total Alkalis-Silica - TAS (Na_2O + K_2O vs SiO_2) graph (Gill 2010). They can vary from ultramafic to felsic and are deficient in silica and/or alumina with respect to alkalis (Na_2O, K_2O, and CaO) (Fitton and Upton 1987).

The South American platform alkaline rocks are found primarily intruding into the Precambrian crystalline basement or the Paraná Basin Paleozoic sediments. As first suggested by Almeida (1971, 1972), the distribution of the alkaline rocks in the South America platform is controlled by regional tectonics. It is assumed for the whole magmatism that an old structure frame of the basement and positive, parallel elongated deep fractures (arches) have been important for the emplacement of such rocks (Gomes and Comin-Chiaramonti 2005). The frame is comprised of lineaments whose trend are for NE-SW, N-S, and WNW-ESE and faulting zones, active since the Precambrian times and subject to intense reactivation in the Mesozoic named the Wealdian reactivation (Almeida 1966) while the deep fractures are

mainly NW-trending, transversal to the major axis of the Paraná Basin and generally surround it (Gomes and Comin-Chiaramonti 2005).

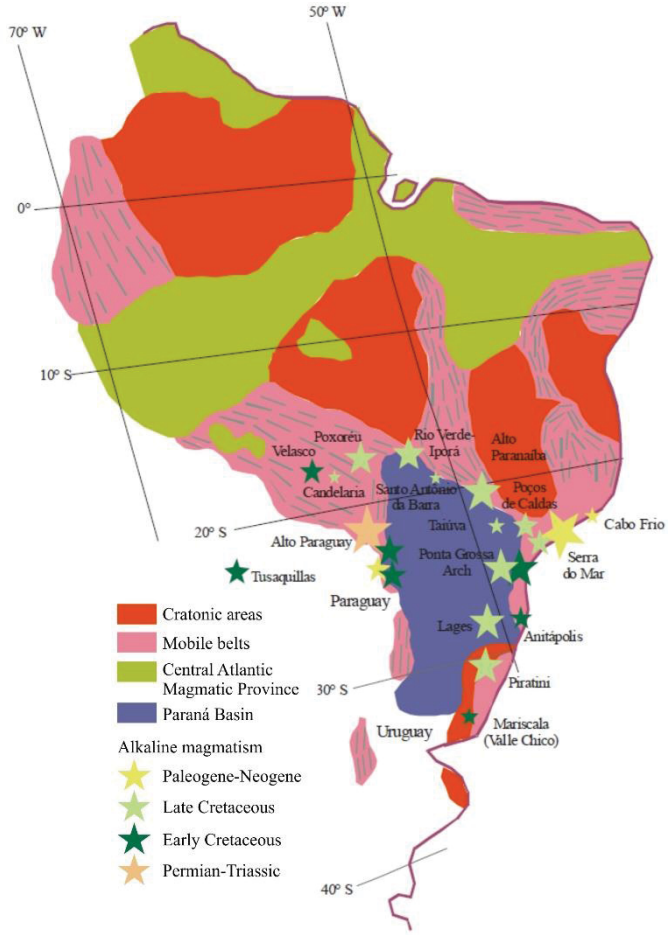

Figure 2: Distribution of the post-Paleozoic alkaline magmatism dispersal in and around the Paraná Basin in the South American Platform. The size of the stars is roughly proportional to the erupted volumes (Gomes and Comin-Chiaramonti 2005, modified).

According to Riccomini et al. (2005), in the context of the Paraná Basin, seven alkalines provinces could be recognized in its borders (**Figure 3**) due to tectonic and geological-geophysical evidence. These provinces are Alto Paraguay, Ponta Grossa Arch, Valle Chico, Misiones, Central Paraguay, Amambay, and Rio Apa. Many of the alkaline magmatism occurrences in Brazil studies consist only of preliminary geological and petrographic data. This is associated with the lack of stable rocks due to weathering processes (Gomes and Comin-Chiaramonti 2005). Usually studies attention is more focused on occurrences that have an economical interest and good facilities for geological expeditions (e.g. Jacupiranga carbonatite) (Gomes and Comin-Chiaramonti 2005).

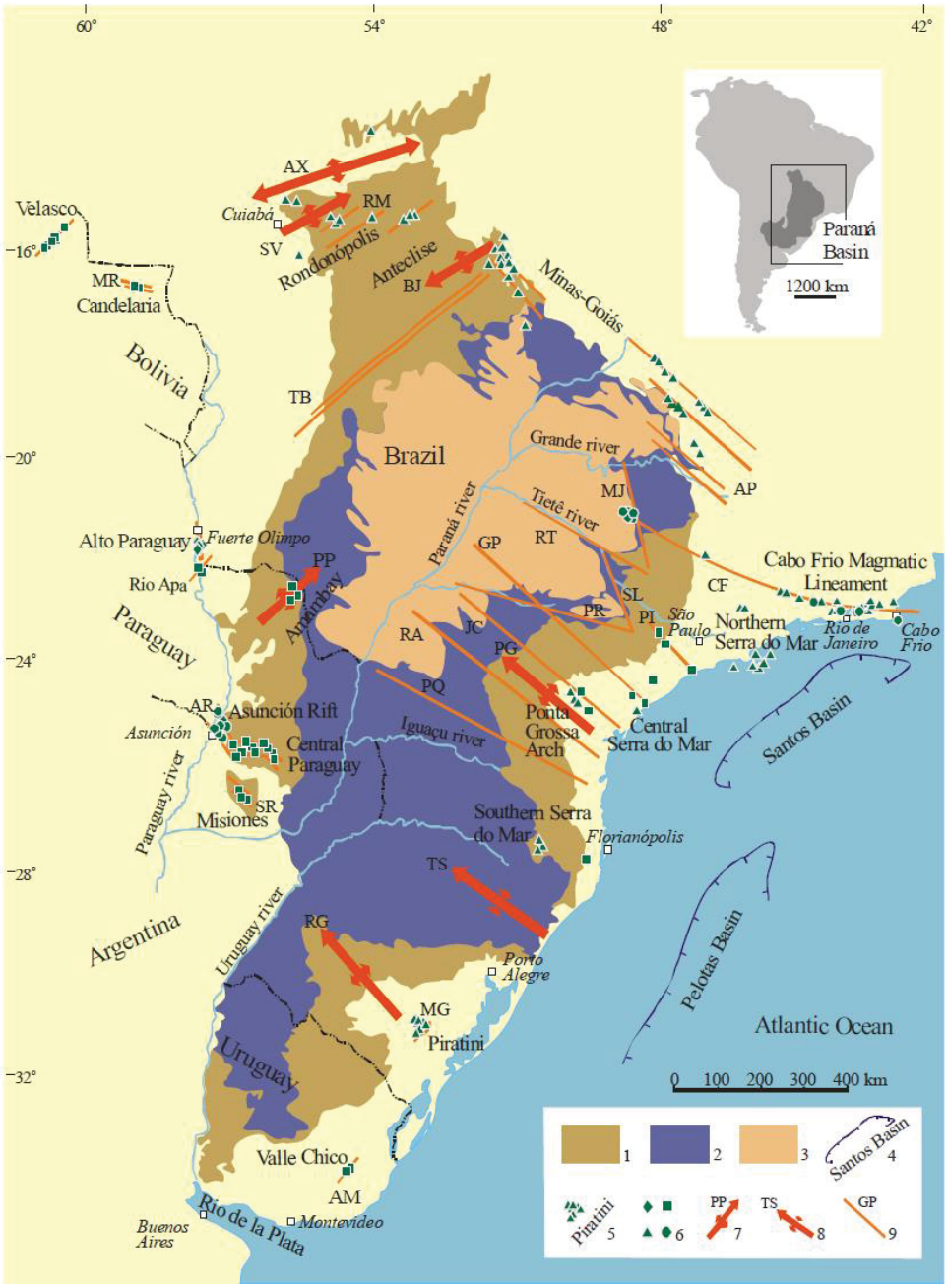

Figure 3. Schematic map of the Brazilian Platform central-southeastern alkaline provinces associated with major structural features: 1) Late Ordovician to Early Cretaceous Paraná Basin; 2) Early Cretaceous tholeiitic lava flows; 3) Late Cretaceous Bauru Basin; 4) offshore marginal basins; 5) Alkaline provinces; 6) Age of alkaline rocks (diamonds, Permian-Triassic; squares, Early Cretaceous; triangles, Late Cretaceous; circles, Paleogene); 7) Axes of main archs (AX, Alto Xingu; SV, São Vicente; BJ, Bom Jardim de Goiás; PG, Ponta Grossa; RG, Rio Grande; PP, Ponta Porã); 8) Torres Syncline; 9) Major fracture zones, in part deep lithospheric faults (Rifts: MR, Mercedes; RM, Rio das Mortes; MG, Moirão; SR, Santa Rosa; AR, Asunción; Lineaments: TB, Transbrasiliano; AP, Alto Paranaíba; MJ, Moji-Guaçu; CF, Cabo Frio; RT, Rio Tietê; SL, São Carlos-Leme; PR, Paranapanema; PI, Piedade; GP, Guapiara; JC, São Jerônimo-Curiúva; RA, Rio Alonzo; PQ, Rio Piquiri; AM, Santa Lucía-Aiguá-Merin) (Riccomini et al. 2005).

Extensional environments are the tectonic setting for the emplacement of alkaline rocks in the Brazilian platform (Gomes and Comin-Chiaramonti 2005). Riccomini et al. (2005)

based on geological, structural, and geophysical data obtained during the ‘90s and 2000s period have identified strike-slip (wrenching) fault zones along the current borders of sedimentary basins and associated structures as a control for alkaline bodies. These structures allowed alkaline magmas to be emplaced in the region.

Riccomini et al. (2005) and references therein demonstrated that the alkaline magmatism in the central-southeastern Brazilian platform took place in four main stages according to geochronological data, as follows:

1) Permian-Triassic age: possibly linked to the propagation of stress related to the Cape and Sierra de la Ventana (Australes) fold belts (Tankard et al. 1995) to the inner parts of the continent.

2) Early Cretaceous age: with three minor pulses - older, coeval and younger than the tholeiitic magmatism of the Paraná basin – could be considered equivalent to the rift stage in marginal Atlantic basins.

3) Late Cretaceous age: corresponded to the Atlantic margin oceanic stage.

4) Paleogene age: related to the evolution of continental rift systems in southeastern Brazil and eastern Paraguay.

Changes in the stress-fields led to a reactivation of discontinuities in the Permian-Triassic, Cretaceous, and Paleogene. Thus, alkaline magmatism in the central-southeastern Brazilian Platform emplaced in those fault zones (Riccomini et al. 2005).

Gomes and Comin-Chiaramonti (2005) reported that the alkaline magmatism in the South American platform started in Permo-Triassic periods during the third of the four geological evolution main stages of the Paraná Basin, which is represented by general uplifts that promoted significant erosional processes and the final development of NW-trending arch structures. K/Ar, Ar/Ar, and Rb/Sr datings reveal that the alkaline magmatism in Brazil has an age between 250 and 50 Ma (Gomes and Comin-Chiaramonti 2005). Ar-Ar isotopic data in the African counterpart of the PGAAP showed that both provinces have similar age, with the former situated between 137 and 127 Ma (Milner et al. 1995; Renne et al. 1996).

A complete explanation of the long-term (Permian-Triassic to Cenozoic, c. 210 Ma) alkaline magmatism source of heating in the central-southeastern Brazilian Platform is not yet defined. One hypothesis is that the source is usually associated with mantle plumes (Riccomini et al. 2005). However, many aspects related to the genesis and tectonic controls of the continental alkaline magmatism are not fully understood and its properties, such as provenance, extent and age distribution, do not support this idea (Riccomini et al. 2005). For example, available Ar-Ar geochronological data and the distribution of alkaline rocks along

tectonic features do not make evident any age distribution pattern. Another hypothesis for the mantle source is based on $^{87}Rb/^{87}Sr$ and $^{147}Sm/^{143}Nd$ isotopic ratios (Gibson et al. 1995, 1997; Comin-Chiaramonti et al. 1995, 1997, 1999; Thompson et al. 1998; Ulbrich et al. 2003) disregards the mantle plume source idea (Riccomini et al. 2005). The totality of the data is concentrated next or below to the Bulk Earth line in Hart's Sr-Nd diagram (Hart 1988), thus showing an evident full lithospheric mantle source for the magmatism (Riccomini et al. 2005).

2.2 LOCAL GEOLOGY (PONTA GROSSA ARCH AND ITS ALKALINE PROVINCE)

The Ponta Grossa Arch (PGA) is an uplifted megastructure that extends for about 600 km in a northwest-southeast trending and its hinge line dips toward NW, i.e. in the inner part of the Paraná Basin (Piccirillo and Melfi 1988; Piccirillo et al. 1990). It comprises several northwest trending tholeiitic dike swarms (Ferreira 1982; Ussami et al. 1994) and also four significant magnetic lineaments in the same direction, namely the Guapiara (Ferreira et al. 1981), São Jerônimo-Curiúva (Vieira 1973), Rio Alonzo (Vieira 1973), and Piqueri lineaments (Ferreira 1982).

The structural lineaments of the Ponta Grossa Arch acted as a pipe for the tholeiitic lava. For example, the Guapiara Lineament was a 600 km long and 20-60 km wide fissure-zone throughout a large volume of basaltic magma was intruded as dikes (Riccomini et al. 2005).

According to Ferreira (1982) and Raposo and Ernesto (1995), the arch is delimited by the Guapiara lineament in the northeast, by the Piqueri or Rio Piqueri in the southeast while the arch central region has the São Jerônimo-Curiúva and Rio Alonzo lineaments (**Figure 1**). These structures have lengths around 600 km and have a width between 20 and 100 km. They may also be related to the arch uplift and conditioned the alkaline and tholeiitic magmatism distribution (Ferreira et al. 1984). However, Almeida (1982) defined the Rio Ivaí lineament as the southern limit of the Ponta Grossa Arch based on remote sensor data.

The Guapiara lineament, according to Ferreira et al. (1981), integrates two important geological features: the Guapiara Fissure (Algarte 1972) and the Serra da Fartura Fault (Vieira 1973).

The São Jerônimo-Curiúva and Rio Alonzo lineaments represent continuities for NW and SE of faults that have the same designation defined by Vieira (1973), while the Rio Piqueri lineament was first described by Ferreira (1982).

In the Mesozoic, tectono-magmatic activities gave rise to extensive basaltic magmatism reactivating the Ponta Grossa Arch, represented by a dense swarm of diabase,

diorite, porphyry diorite, and quartz-diorite dikes. The relationship between arching and the appearance of parallel crustal fractures, filled by basic dikes, demonstrates that the same conditions could lead to eventual accommodation of alkaline intrusive bodies. In the Cerro Azul Geological Sheet (Brumatti et al. 2015), the northwest alignment of the alkaline intrusives, parallel to the Ponta Grossa Arch, is visible (Arioli and Salazar Jr. 2015).

The PGAAP is one of the twelve provinces located below the 15º S parallel by Almeida (1983). This author pointed out thirteen intrusions in this arch, named: Banhadão, Barra do Itapirapuã, Barra do Rio Ponta Grossa, Barra do Teixeira, Cananéia, Itanhaém, Itapirapuã, Jacupiranga, Juquiá, Mar Pequeno (Sabaúma, SP), Mato Preto, Sete Quedas, and Tunas. In addition, two more bodies were suggested by airborne magnetic data: Pariquera-Açu and Registro (Ferreira and Algarte 1979). The former was corrobored by ground magnetic data and petrography by Ferreira et al. (1987) and the latter was interpreted as a subsurface body, covered by alluvium deposits of the Ribeira de Iguape river (Mantovani et al. 2005).

Riccomini et al. (2005) has grouped the alkaline rocks in fifteen provinces considering the PGAAP with rocks belonging to the Early Cretaceous while its Late Cretaceous counterpart (e.g Barra do Teixeira, Cananéia, and Tunas) belongs to the Serra do Mar Alkaline Province. In addition, these authors suggested that the Ponta Grossa Arch Province should be expanded to the northeast and south from its original area to include Ipanema, Salto de Pirapora, Piedade, Itanhaém, and Anitápolis alkaline bodies. These new limits would correspond to the extent of Early Cretaceous uplift along the arch. All the Lower Cretaceous alkaline bodies in the Ponta Grossa Arch, except Anitapólis, show a striking control along the northwest direction (Riccomini et al. 2005).

While the majority of alkaline intrusions from the Lower Cretaceous (e.g. Jacupiranga, Juquiá, Pariquera-Açu, ~130 Ma) are considered contemporaneous to the Serra Geral Group tholeiitic magmatism, the suites related to to the Upper Cretaceous (~85 Ma), such as Tunas, Mato Preto, and Cananeia, present their formation after this event (Gomes et al. 2011). Gomes et al. (2018) reported that 10 Ma after the Serra Geral basaltic volcanism, the alkaline activity was renewed about 110 Ma with the Tunas intrusion close to the Ponta Grossa Arch axis and then 20 Ma after the alkaline magmatism reached its peak being characterized by the Upper Cretaceous intrusions.

Ferreira and Algarte (1979) were the first authors to delineate the aeromagnetic and scintillometric responses of the major alkaline rocks in the Paraná and São Paulo states. These data allowed to infer that the alkaline intrusions could be genetically and temporally linked to the diabase dikes of the Ponta Grossa Arch and the opening processes of the South Atlantic Ocean.

The anomalies in the area around the Guapiara magnetic lineament have normal polarity typical of southern hemisphere dipolar anomalies (positive pole to the north and negative pole to the south). The bodies of Jacupiranga, Cananéia, and Pariquera-Açu have normal polarity while one of the dipoles studied by Marangoni and Mantovani (2013) revealed a reversed magnetic orientation (i.e. Juquiá Complex). The normal and reverse magnetization directions for these igneous bodies may indicate the presence of carbonatite (Marangoni and Mantovani 2013). Intrusions that do not host carbonatites demonstrated reduced to the pole anomalies with highly concentrated magnetization and well-defined 3D geometry whereas alkaline rocks containing carbonatites usually exhibit double polarization (Marangoni and Mantovani 2013).

With regard to Ponta Grossa Arch dikes, it is reported that they are remanently magnetized with a predominance of normal polarity according to paleomagnetic studies done by Raposo and Ernesto (1995).

2.3 DESCRIPTION OF THE BODIES

A summary of petrological and geophysical studies is presented for the eight bodies of the study area (**Figure 1**) containing their ages and occurrence of carbonatites and rare earth elements mineralizations (**Table 1**).

2.3.1 Bairro da Cruz (BC) Complex

The Bairro da Cruz Complex (**Figure 4**) is located on the Bocaiúva do Sul municipality (24º52’ S, 49º23’ W), Paraná state, and it was discovered during the mapping of the Apiaí Quadrangle done by the Geological Survey of Brazil and the Brazilian National Department of Mineral Resources (CPRM and DNPM 1977).

This complex is a small volcanic center of approximately 1 km^2 showing an oval shape and irregular contours. At the time it was discovered it was largely eroded at the surface (Hama et al. 1977). Most of the volcanic building is topped by thick colluvium deposits, which are distributed blocks and boulders of fresh rocks. Field trip results revealed the existence of coarse (olivine-gabbros) and fine (phonolites) varieties, as well as possible basic alkaline affinity rocks at more saturated terms in the central part and the western border of Bairro da Cruz complex. The country rocks are mainly comprised of amphibole-schists and calc-silicate rocks (Hama et al. 1977). Additionally, numerous small dikes (maximizing 1 m of width) cut these gabbroic rocks in the area (Hama et al. 1977; Almeida 2016).

K/Ar dating in pyroxene-amphibole resulted in an age of 230±17 Ma for the Bairro da Cruz Complex (Hama et al. 1977). These authors suggest that this intrusion, alongside the

José Fernandes gabbro, represents a previous basic-alkaline magmatism that occurred before the wide basaltic extrusion in the Paraná Basin.

Another isotopic dating in the area was made by Almeida et al. (2017) who used a sample of a phlogopite lamprophyre from a basanite dike located near the São Jerônimo-Curiúva Lineament, next to the edge of the aeromagnetic anomaly associated with the Bairro da Cruz alkaline intrusion. The Ar-Ar ratio showed an age of 133.7±0.1 Ma.

Table 1. Summary of the main characteristics of the igneous rocks in the study area.

Rock name	Main lithotypes	Main classification	Coordinates	Age (Ma)	Carbonatites and REE reported
Bairro da Cruz (BC) Complex	Olivine-gabbros and phonolites	Alkaline, basic, intrusive/volcanic	24º52' S, 49º23' W	230±17[a], Upper Triassic	No
Banhadão (BN) Complex	Nepheline syenites and phonolites	Alkaline, basic, intrusive	24º39' S, 49º23' W	110-106[b], Lower Cretaceous	No
Itapirapuã (IT) Nepheline syenite	Undersaturated syenites	Alkaline, basic, intrusive	24°41'27" S, 49°08'30" W	106-102[c], Lower Cretaceous	No
Barra do Itapirapuã (BIT) Carbonatite	Carbonatites (plug)	Alkaline - carbonatite, intrusive	24°41'30'' S, 49°13'00'' W	129±19[d], Lower Cretaceous	Yes
Barra do Teixeira (BT) Phonolite	Peralkaline phonolites (plug)	Alkaline, basic, volcanic	49º26' S, 49º41' W	78-73[d,e], Upper Cretaceous	No
José Fernandes (JF) Gabbro	Variety of gabbros	Basic, intrusive	24°43'30" S, 48°58'59" W	134.93±0.16[f], Lower Cretaceous	No
Mato Preto (MP) Complex	Nepheline syenites, phonolites, and carbonatites	Alkaline (carbonatites), basic, intrusive	24°45' S, 49°12' W	76-62[d,e], Upper Cretaceous to Paleocene	Yes
Tunas (TU) Complex	Syenites and alkali syenites	Alkaline, felsic, intrusive	24°57' S, 49°06' W	85-70[d,g,h,i] Upper Cretaceous	No

References: [a] Hama et al. (1977), [b] Gomes et al. (2018), [c] Ruberti et al. (1997), [d] Cordani and Hasui (1968), [e] Sonoki and Garda (1988), [f] Almeida (2016), [g] Gomes et al. (1987), [h] Rugenski (2006), [i] Siga Jr. et al. (2007).

Due to the difficulty of access, this intrusion has few references about it (Hama et al. 1977; Faleiros et al. 2012). The large majority of works reviewing the alkaline magmatism in the Ponta Grossa Arch did not cite this complex.

Ferreira and Algarte (1979) reported values of 500 and -250 nT for the intrusion. Almeida (2016) using the geophysical airborne survey from CPRM (2011) showed that the Bairro da Cruz complex has a dipolar magnetic anomaly.

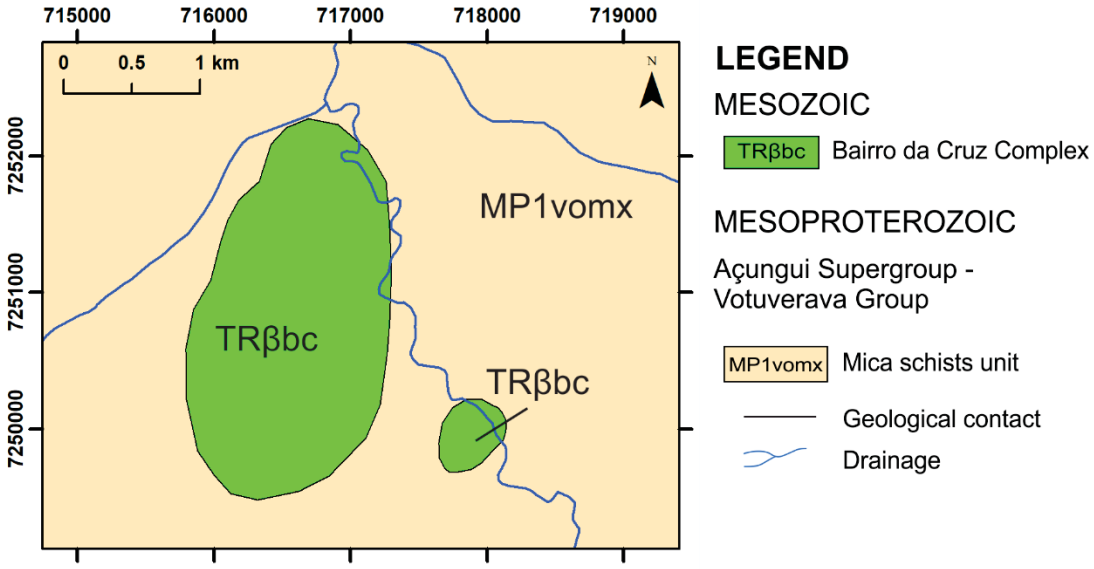

Figure 4. Geological map of the Bairro da Cruz Complex (modified from Morais et al. 2012).

2.3.2 Banhadão (BN) Complex

The Banhadão alkaline intrusion (24º39' S, 49º23' W, **Figure 5**) is located at 20 km NE of Cerro Azul town, Paraná state, between the Sete Quedas river and Fecho creek in the Ribeira Valley (Hama et al. 1977). It has an area of 8 km^2 approximately (Gomes et al. 2018) and it was emplaced into the Neoproterozoic Três Córregos granitic suite (Hama et al. 1977; Brumatti et al. 2015).

The first known studies about this intrusion were made by Algarte (1972) and Kaefer and Algarte (1972) and, more extensively, by Ruberti (1984) and Ruberti and Gomes (1984).

Algarte (1972) and Kaefer and Algarte (1972) demonstrated that the intrusion is composed of nepheline syenites and phonolites. Among the syenites, there are the following varieties: foyaite, nepheline-sodalite-syenlte, muniongite, ijolite, alkali-syenlte, and others (Hama et al. 1977).

Most of the complex is composed of different foid syenite-foidite rock types, sometimes not differentiated in the geological map (Ruberti et al. 2012). Ruberti and Gomes (1984) described the presence of a phlogopite melteigite body at the central-eastern portion of the complex and of a pipe-like, well-defined late body of nepheline syenites at the western section.

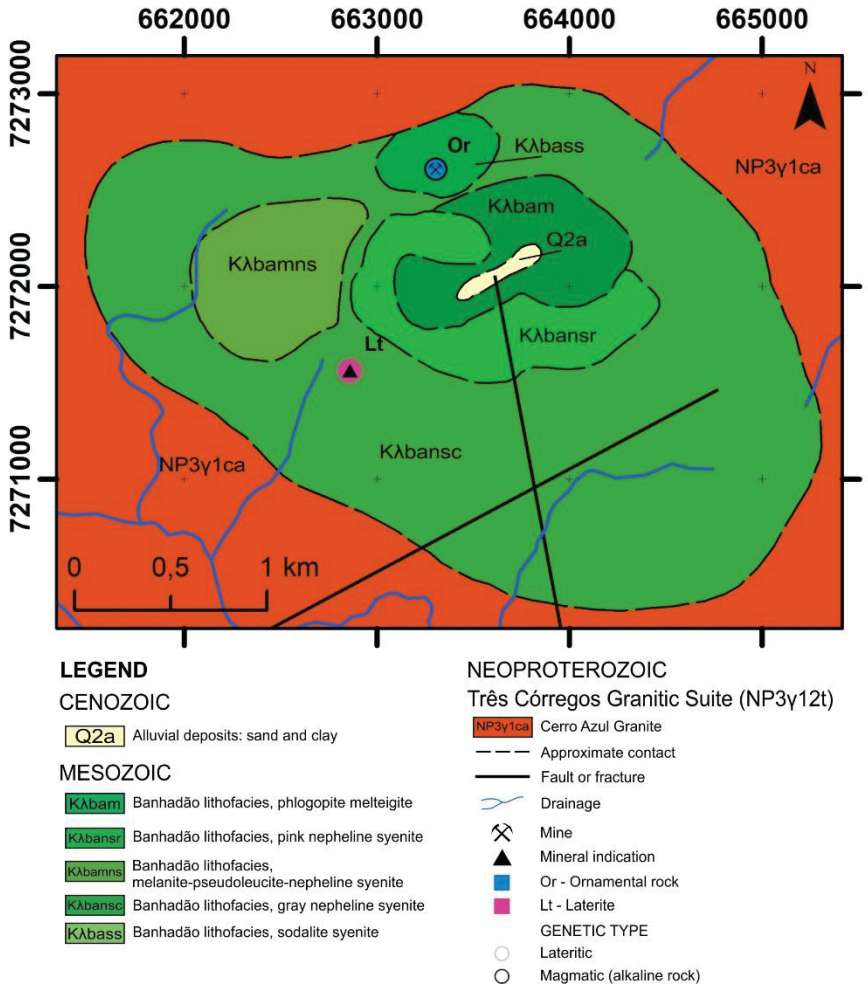

Figure 5. Geological map of the Banhadão Complex. Modified from Ruberti et al. (2012), Brumatti and Almeida (2015).

According to Gomes et al. (2018) the majority of the intrusion is composed of gray or light reddish nepheline syenites, grading from basic to intermediate types. Moreover, incipient fenitization processes are identified along the contact zone with the Três Córregos batholith.

Brumatti et al. (2015) has divided the complex into five lithofacies: phlogopite melteigite, pink nepheline syenite, melanite-pseudoleucite-nepheline syenite, gray nepheline syenite, and sodalite syenite.

It should be noted that there are some inconsistencies regarding CPRM´s geological maps made during different projects contemplating the Banhadão Complex. Firstly, the occurrence of laterite is located in different places in Brumatti and Almeida (2014) (north of Banhadão) and Brumatti and Almeida (2015) and Brumatti et al. (2015) (southwest part). Secondly, the quarternary unit (Q2a) overlapping the Banhadão intrusion is extended in Brumatti and Tomita (2014a,b) maps comparing with Brumatti and Almeida (2014, 2015) and Brumatti et al. (2015). Lastly, these two groups of authors showed slightly different shapes for

Kλbamns and Kλbansc units as well. In this work, the Banhadão geological map provided by Brumatti and Almeida (2015) was chosen because it was the most recent.

The Banhadão Complex was defined ranging 106-110 Ma of age using Ar-Ar method on biotite (Gomes et al. 2018).

Regarding geophysical studies, Ferreira and Algarte (1979) have demonstrated that the Banhadão has a radiometric (total count) anomaly between 500 and 750 cps (counts per second).

2.3.3 Itapirapuã (IT) Nepheline syenite

This complex (24°41'27" S, 49°08'30" W) shows an NW-trending irregular shape at approximately 130 km SSW from Itapeva city (Gomes et al. 2018). It has an approximate outcropped area of 4 km^2 (Brumatti et al. 2015) and it is emplaced into Cerro Azul Granite, which is part of the Neoproterozoic Três Córregos granitic suite (**Figure 6**).

Gomes (1970) reported that Itapirapuã consists mainly of undersaturated medium to coarse syenitic rocks, varying from hypidiomorphic to inequigranular. Mafic syenites, meltegeites, and pulaskites occur in a less frequent distribution in the area while NW-trending decimeter dikes composed of tinguaites crosscut the other alkaline petrographic types and the granitic country rocks (Gomes et al. 2018).

Moreover, the southernmost part of the intrusion is composed of magnetite and it has been the target for iron ore exploitation by Maringá Ferro Liga S/A (Gomes et al. 2018). However, any other references describing the economical potential of Itapirapuã nepheline syenite could be found in the literature.

Itapirapuã Complex has an age interval from 102 to ~106 Ma, according to Ar-Ar determinations on biotite and U-Pb SHRIMP on titanite from melanitic syenitic rocks, respectively (Gomes et al. 2018).

Ferreira and Algarte (1979) have demonstrated that the Itapirapuã has a total count anomaly between 500 and 750 cps.

2.3.4 Barra do Itapirapuã (BIT) Carbonatite

The Barra do Itapirapuã intrusion (24°41'30'' S, 49°13'00'' W) is considered a multiple stockwork (Loureiro and Tavares 1983) forming a complex system where there is an ellipsoidal network of dikes and veins of Fe, Mg and Ca-carbonatites occupying an area around 2 km^2 (**Figure 6**). This intrusion is emplaced in the Neoproterozoic Cerro Azul Granite (Gimenez Filho et al. 2000; Ruberti et al. 2005, 2012; Brumatti et al. 2015). Locating approximately 90

km from the Ribeira (São Paulo state) municipality, Barra do Itapirapuã is situated north to the Itapirapuã river, near the confluence with the Ribeira river (Loureiro and Tavares 1983), and it is intruded along the São Jerônimo-Curiúva lineament, near the Itapirapuã Shear Zone. It is aligned with Banhadão, Mato Preto, and Itapirapuã complexes (Brumatti et al. 2015).

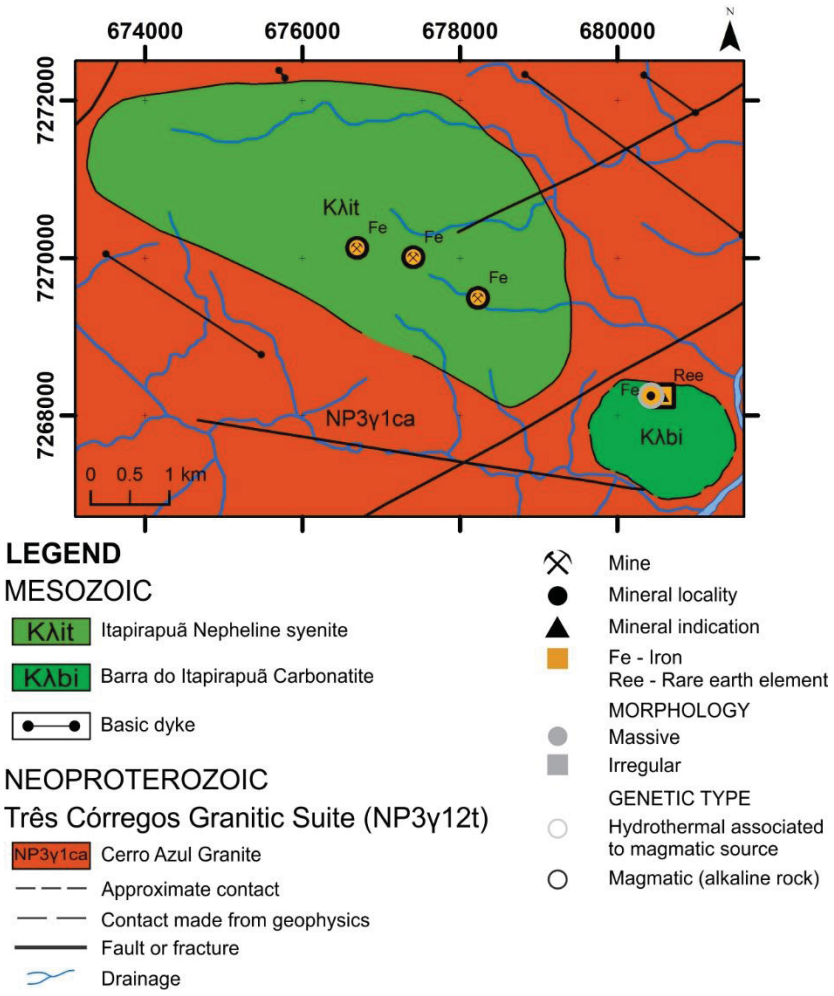

Figure 6. Barra do Itapirapuã carbonatite and Itapirapuã nepheline syenite geological maps (modified from Brumatti and Almeida 2015).

This body was first described by Loureiro and Tavares (1983). After verifying numerous and strong aeromagnetic and aeroradiometric anomalies near the Mato Preto town, Nuclebrás (defunct Brazilian public company) team confirmed the existence of this alkaline complex in the form of a carbonatitic plug in a field trip (alongside Mato Preto) in 1976. The area is located inside the Ribeira Valley and it is described by these authors with difficult access and intense weathering.

Millimeter to centimeter thick carbonatite veins at the surface and decimeter to meter thick dikes at depth prevailed in this borehole validated the stockwork body (Loureiro and Tavares 1983; Ruberti 1998).

In addition to carbonatitic rocks, carbonatitic lamprophyric breccias and veins bearing quartz, fluorite, REE-rich apatite, REE fluorcarbonates, barite, and strontianite are found in the place (Ruberti et al. 2005). As described by Silva et al. (1981), the Barra do Itapirapuã complex shows purple-yellowish fluorite that occurs in fillets on the east limit of carbonatite, associated with quartz, barite, sulfides and rare earth minerals, with an average content of 15%.

The age interpreted for the carbonatite is 129±19 Ma, according to Ruberti et al. (1997), who used the Rb-Sr whole-rock technique.

Ferreira and Algarte (1979) attributed the most significant scintillometric total count anomaly to the intrusion with 5000 cps using the Serra do Mar (CPRM 1978a) and São Paulo-Rio de Janeiro (CPRM 1978b) airborne survey data.

Silva (1984) evaluated the economic potential apatite, rare earth fluorcarbonates, barite, fluorite, galena, sphalerite, niobium, vermiculite, and molybdenum mineralizations in the Barra do Itapirapuã carbonatitic complex. The study estimated a reserve equivalent to 2.1 million tons of complex ores, with apatite and rare earth fluorcarbonates. This author discovered in the region a subeconomic surface of 200 x 40 m composed of vermiculite as well as important evidence of barite, fluorite, Nb, Pb, and Zn (Arioli and Salazar Jr. 2015). Magnetites mineralizations were reported by Loureiro and Tavares (1983) along with strong geochemical anomalies of REE, niobium, thorium, and uranium. In 2012, an economic reserve of around 100 tons of REE oxides was approved to be mined by Vale Fertilizantes S/A (Brumatti et al. 2015).

2.3.5 Barra do Teixeira (BT) Phonolite

The Barra do Teixeira phonolite (**Figure 7**) is located at the coordinates 49º26’ S and 49º41’ W (Sonoki and Garda 1988). This small circular body, located on the Vila Branca Geological Map (Brumatti and Tomita 2014b), is situated between the Teixeira river and the Leandro creek (Brumatti and Tomita 2014a). The area of this body is over 0.25 km^2 and its diameter is less than 700 m.

Vasconcellos (1995) described the Barra do Teixeira petrography which is composed of peralkaline phonolites hosting feldspar phenocrysts surrounded by fibro-radiated zeolites along with fluorite. It is considered a manganese oxide poor small plug (Vasconcellos 1995; Vasconcellos and Gomes 1998). Mostly dikes present in the area showed positive Eu anomalies (Ruberti et al. 2005).

Barra do Teixeira has an age of around 73-78 Ma, dating around the end of the Cretaceous, according to K-Ar isotopic data (Cordani and Hasui 1968; Sonoki and Garda 1988).

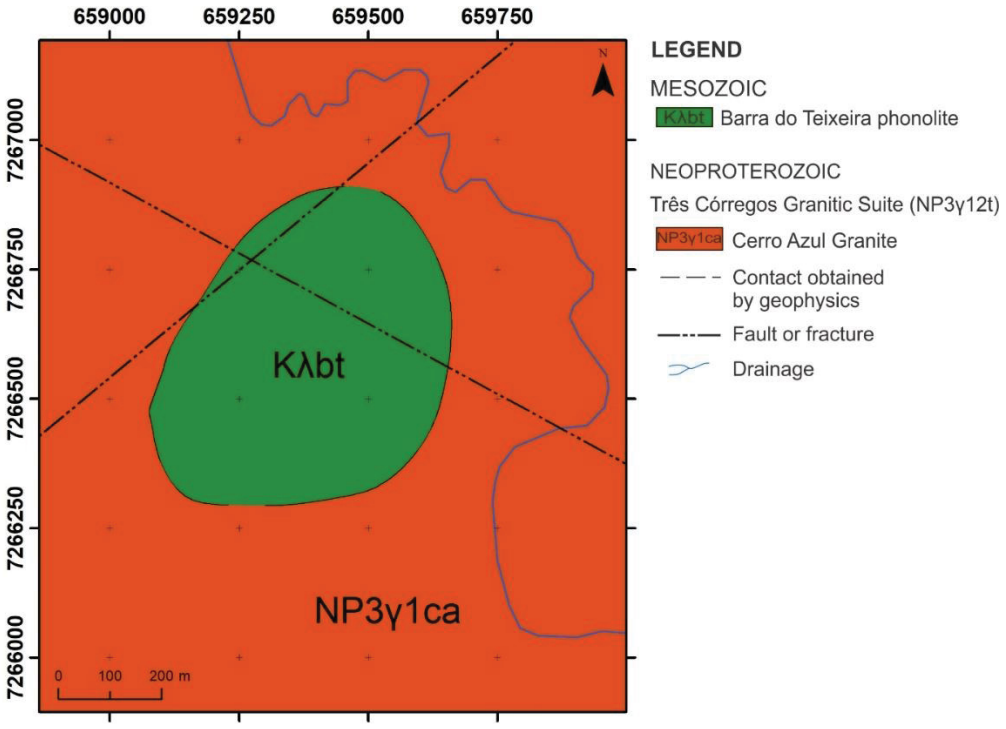

Figure 7. Barra do Teixeira Phonolite geologic map. Modified from Brumatti and Tomita (2014b).

2.3.6 José Fernandes (JF) Gabbro

This suite (24°43'30" S, 48°58'59" W) is located in the rural area of the Adrianópolis town, Paraná State (Chmyz et al. 2011; Almeida 2016) and it is emplaced in the Mesoproterozoic Votuverava Group (Açungui Supergroup) metasedimentary rocks (**Figure 8**, Morais et al. 2012). This intrusion has been cited by numerous authors (Barbosa 1941; Moraes Rego and Almeida 1946; Melcher et al. 1971, 1973; Pieruceti 1973, Pieruceti and Gomes 1975; Chmyz et al. 2011; Almeida 2016; Almeida et al. 2017, 2019)

The José Fernandes intrusion is composed of different gabbroic rocks, including cumulates. Synplutonic alkaline dikes were also intruded into this suite (Almeida 2016; Almeida et al. 2019). Chymz et al. (2011) has divided the suite in nine distinct facies.

Almeida et al. (2019) pointed out that the gabbro formed from batches of alkaline magma with different crustal contributions, based on petrographic, isotopic and geochemical analyses.

Almeida (2016) dated an age of 134.93±0.16 Ma (TIMS U-Pb zircon) for the José Fernandes Gabbro.

Regarding its magnetism, the José Fernandes intrusion exhibits a classic magnetic anomaly where its axis represents the outcropped area of the gabbro (Ferreira and Algarte 1979). Aerogeophysical data from CPRM (2011) showed a significant normal polarity anomaly in the region where José Fernandes outcrops indicating that the body is relatively large and extends to greater depth (Almeida 2016; Almeida et al. 2017).

Chmyz et al. (2011) reported that José Fernandes gabbro could be the source for exploration of ornamental rocks and/or crushed stone.

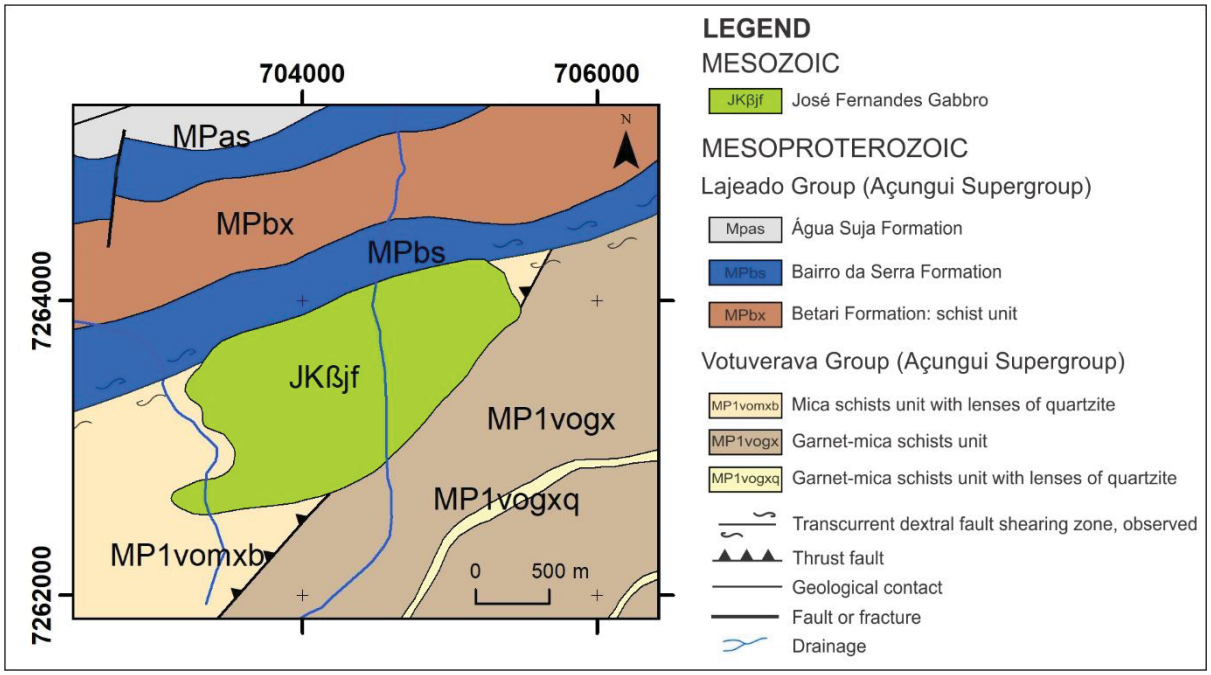

Figure 8. Geological map showing the José Fernandes Gabbro (modified from Morais et al. 2012).

2.3.7 Mato Preto (MP) Complex

The area of the Mato Preto alkaline-carbonatitic suite (24°45' S, 49°12' W**, Figure 9**) is located in the municipality of Cerro Azul, about 110 km from Curitiba, Paraná (Loureiro and Tavares 1983). Circular in shape, this 12 km^2 area (Santos et al. 1990) suite is situated between the Neoproterozoic Três Córregos granite and the Açungui Group (Loureiro and Tavares 1983) near the Morro Agudo Shear Zone (Brumatti and Tomita 2014a). It is part of ultramafic-alkalic-carbonatitic intrusions that border the Paraná Basin (Loureiro and Tavares 1983).

The Mato Preto suite was described in a first attempt by Loureiro and Tavares (1983). The finding was made by Nuclebrás in the same geological expedition that discovered Barra do Itapirapuã near the Mato Preto municipality (see Barra do Itapirapuã for description). The field trip team confirmed the existence of this alkaline complex in the form of a carbonatitic

plug (along with Barra do Itapirapuã) in 1976. Ruberti (1998) described in detail the petrology and geochemistry of Mato Preto (PR) in his habilitation thesis.

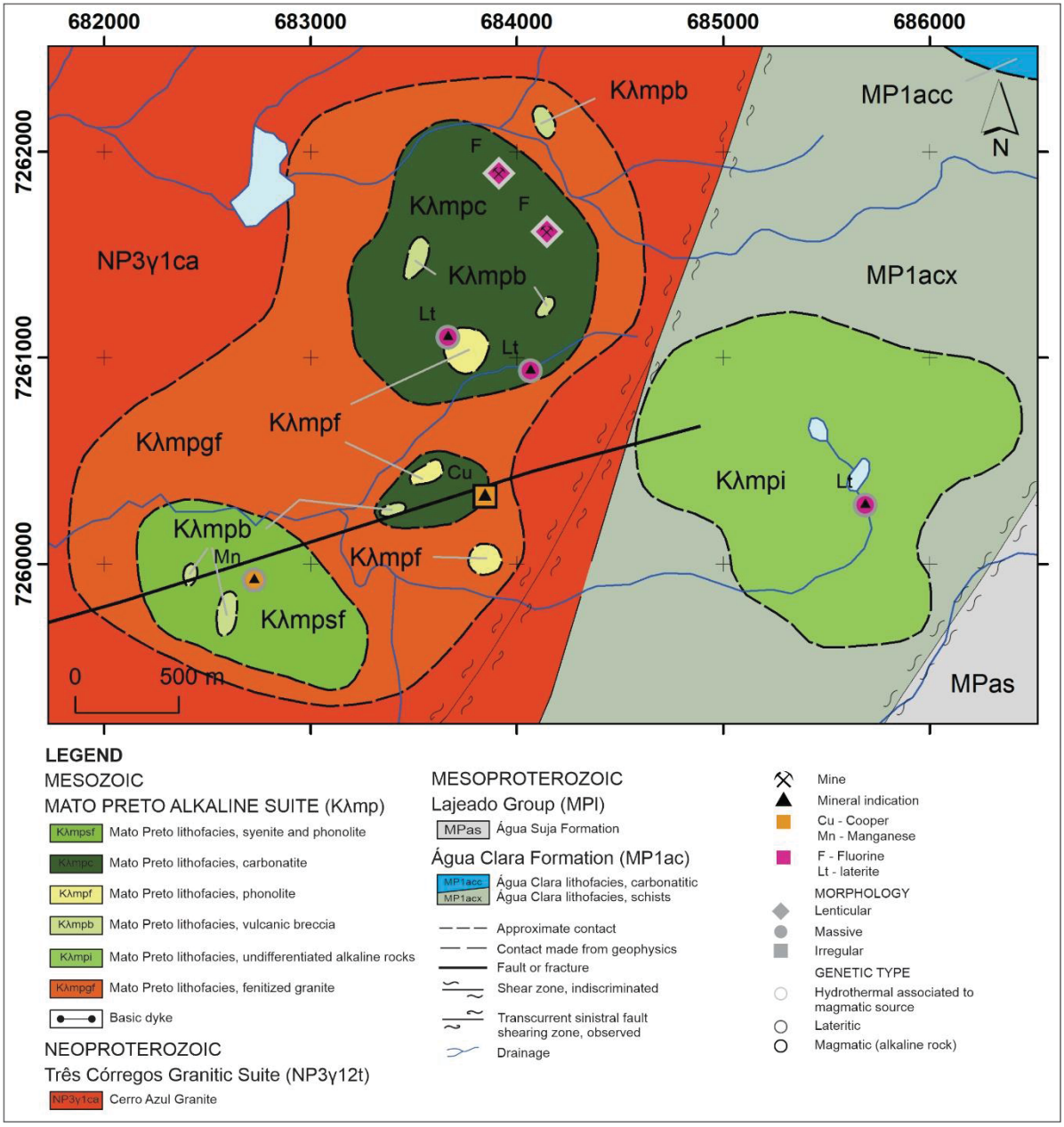

Figure 9. Geological map of Mato Preto alkaline-carbonatitic suite (after Brumatti et al. 2015).

The intensely weathered Mato Preto alkaline-carbonatitic complex (Loureiro and Tavares 1983) encompasses alkalic rocks (e.g. nepheline syenites, phonolites, porphyry phonolites, tinguaites) and ferruginous carbonatites and calciocarbonatites (Comin-Chiaramonti et al. 2001). There is also the existence of tuffs, agglomerates and other silicate rocks, such as ijolites and melteigites. Loureiro and Tavares (1983) reported feldspathic-carbonatite breccias cut by veins, dikes, and lenses of magnetite-calcite-carbonatite strongly radioactive, locally enriched in iron oxides and small magnetite bodies.

The largest volume of carbonatites in the complex is located in the northeastern-central part. Sulfide and fluorite occurrences are associated with those rocks (Loureiro and Tavares 1983). A variety of elements and minerals are related to carbonatite suite in the Mato Preto complex, such as thorium, rare earths, iron, phosphorus, fluorite, magnetite, apatite, pyrite, bornite and in small amounts, uranium, niobium, titanium, and zirconium (Loureiro and Tavares 1983).

Loureiro and Tavares (1983) demonstrated several phases of alkaline magmatism in the formation of the Mato Preto complex as follows:

1) Formation of ijolites and nepheline syenites: characterized by slow cooling.

2) Formation of volcanic tuff and breccias with silicic-carbonatic matrix and clasts of alkaline, granite and fenite rocks: characterized an explosive eruption.

3) Formation of calcitic carbonatites: these rocks outcropped in the south of the region and are composed of pyrochlore, rare earth minerals and magnetite sovites. This lithotype is strongly radioactive and rich in iron, rare earths, thorium and phosphorus.

4) Formation of porphyry phonolites and phonolites: characterized an extrusion.

Loureiro and Tavares (1983) also have divided the suite into two areas according to the carbonatites properties. The first area, called Mato Preto 1, is located in the southern region and two types of carbonatites could be identified there: the former, composed of feldspathic-carbonatitic breccia, poor in iron oxides with almost no radiation while the latter is represented by a more radioactive Fe-bearing carbonate. This rock carries high FeO contents and, more irregularly, rare earth elements, thorium dioxide, and phosphorus pentoxide. U_3O_8 levels in both carbonatites rarely surpass 50 ppm (Loureiro and Tavares 1983).

In Mato Preto 2 (northernmost area of the complex), the carbonatites have higher levels in fluorite and pyrite and lower in iron oxides than in Mato Preto 1. U_3O_8 values of Mato Preto 2 are three times higher than in Mato Preto 1, which has around 12 ppm. Also, the ThO_2 values in Mato Preto 2 exceed in a few amounts the ones found in Mato Preto 1. The U_3O_8/ThO_2 ratio, therefore, is twice higher in Mato Preto 2 carbonatites than in Mato Preto 1 while for the alkaline rocks this figure is over 3 (Loureiro and Tavares 1983).

The Mato Preto (Upper Cretaceous) complex is considered younger than the tholeiitic magmatism event that took place in the Paraná Basin (Gomes et al. 2011). Using K-Ar isotopic ratio, Cordani and Hasui (1968) reported an age of approximately 66 Ma for a phonolite sample from Mato Preto while Sonoki and Garda (1988) outlined an age of 61.9 Ma and 76.4 Ma utilizing the K-Ar method suggesting Late Cretaceous ages.

The Mato Preto carbonatite has a fluorite–barite–galena-REE ore deposit (Jenkins II 1987; Andrade et al. 1999). The Mato Preto fluorite reserves are among the three largest reserves in Brazil computing around 2,800,000 t according to Arioli and Salazar Jr. (2015). The mineralization in the suite is associated with hydrothermal alteration in carbonatite dikes (Santos and Dardenne 1988). One fluorite deposit is an active mine belonging to Mineração Nossa Senhora do Carmo.

Airborne scintillometric survey anomalies in the region are oriented in an NW-direction according to Ferreira and Algarte (1979). These authors registered an anomaly of 3750 cps in the carbonatites of the Mato Preto area related to thorium and uranium minerals.

2.3.8 Tunas (TU) Complex

The Tunas alkaline massif (24°57’ S, 49°06’ W) has an area of 22 km^2 in an NW direction (**Figure 10**), in agreement with the direction of Mesozoic dikes (Brumatti et al. 2015) and it is located 80 km from the city of Curitiba (Algarte 1972) in the Ribeira Road, south to the Ribeira river (Vasconcellos 1995).

The first work about the massif was made by Carvalho and Pinto (1937) - Fuck (1972); Vasconcellos (1995) - who found syenitic rocks cut by trachytic dikes near the city of Tuneiras, located 3 km to the east of Tunas city. This massif has been investigated by Trein et al. (1967) and in a more detailed analysis by Fuck (1972) in the form of geological map and petrographic description. Gomes et al. (1987) had studied the complex regarding its petrological and geochemical aspects. Vasconcellos (1991) and Vasconcellos and Gomes (1992) characterized bodies of distinct volcanic breccias. Vasconcellos (1995) described the geochemistry and petrography of the phonolites in the complex.

The Tunas massif comprises five subvolcanic structures of annular contour (Ruberti et al. 2005) which intruded Precambrian meta-igneous rocks and metasediments of the Votuverava Group and Perau Formation (Brumatti et al. 2015). Along with Banhadão Alkaline suite, Itapirapuã Nepheline syenite, Barra do Itapirapuã Carbonatite, and Mato Preto Alkaline suite, the Tunas Complex intruded the Apiaí Terrane (Brumatti et al. 2015).

This plutonic structure with a felsic nature (Gomes et al. 1987) contemplates in its majority syenites and alkali syenites with subordinate alkali gabbros, syenogabbros, essexites, and syenodiorites. This NW-elongated suite contains 10% of volcanic breccias and small late dikes of syenitic composition are found in the region (Ruberti et al. 2005; Marangoni and Mantovani 2013). The country rock consists mainly of shales, marbles, and metabasites and to a small extent, quartzites, gneisses, and schists to the northeast (Marangoni and Mantovani 2013).

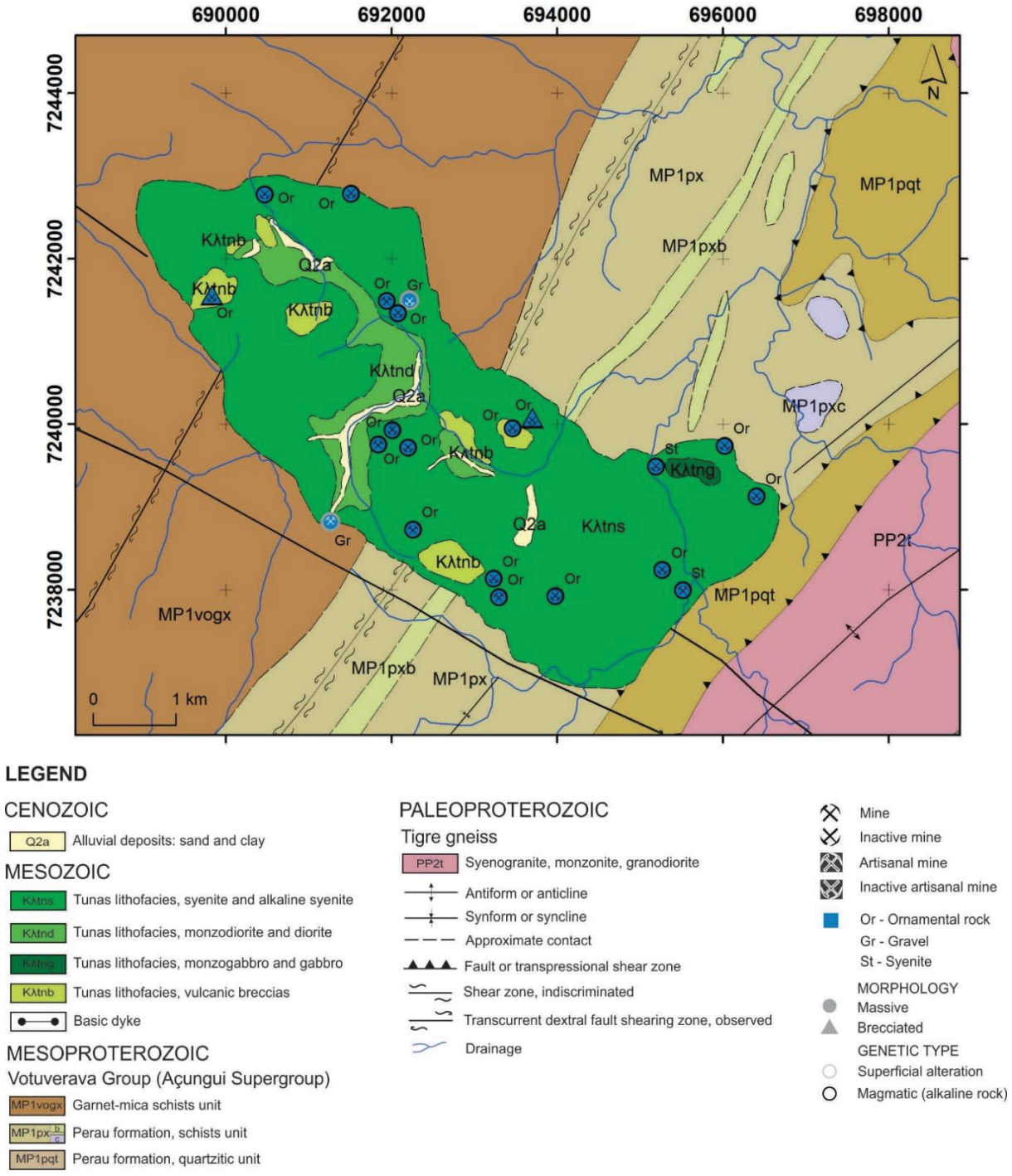

Figure 10. Geological map of the Tunas complex (modified from Brumatti et al. 2015).

Regarding the mineralogy, the Tunas massif hosts feldspars, Ca-clinopyroxene, amphibole, Fe-biotite, olivine, quartz, and/or feldspathoids (nepheline and sodalite) as the main mineral assemblage while Ti-magnetite and apatite composed accessories (Ruberti et al. 2005).

The first ages for the massif were analyzed by Cordani and Hasui (1968) obtaining 110 Ma for two samples and 70 Ma for the others (K-Ar method), suggesting the possibility of this

free-carbonatite intrusion (Loureiro and Tavares 1983) to have occurred in more than one magmatic activity. K-Ar age determination by Gomes et al. (1987) led to an average value of 82 Ma. A similar age was determined by Rugenski (2006), 80.5 Ma, from Rb-Sr isotopic data. Siga Jr. et al. (2007) reported U-Pb syenite's zircon age dating for the Tunas complex around 83 Ma (ID-TIMS) and 85 Ma (SHRIMP). These are interpreted as the ages of crystallization of the suite. Gomes et al. (1987) interpreted the high $^{87}Sr/^{86}Sr$ initial ratios (0.7078-0.7081) in Tunas' dikes as caused by crustal contamination to the massif.

According to the data from the geological campaign, soil sampling, and scintillometry, Silva (1984) did not detect any evidence of economical important mineralizations such as fluorite, phosphates, and metallic minerals on the Tunas massif. The syenites and associated rocks are suitable only for extraction as ornamental rocks. Active and abandoned mines of ornamental rocks were found in the region (Brumatti et al. 2015). The area also contains secondary deposits of clays which may be useful for the ceramic industry (Silva 1984). Brumatti et al. (2015) has reported that an authorization for research in the National Department of Mineral Production (DNPM) was given in the area to explore bauxite.

Soil and stream sediment geochemistry data in the Tunas alkaline suite show the contrast of values between this suite and the country rock, as well as the decrescent variation of the REE concentration in the NW-SE direction (Brumatti et al. 2015).

Ferreira and Algarte (1979) using the Serra do Mar Sul aerogeophysical survey (CPRM 1978a) characterized the Tunas magnetic anomaly with a maximum intensity of 1000 nT and a minimum of -600 nT. This dipole anomaly was displayed by Rugenski (2006) with an interval between 800 nT and -300 nT for the same dataset.

Rugenski (2006) states that the Tunas alkaline complex did not show a gravimetric response. This author infers some reasons such as low contrast between Tunas and country rocks, low depth of the intrusion, gravimeter malfunction during the acquisition, and/or unbalanced barometers. Therefore, this author has created 2.5D models from three NW-oriented magnetic profiles that cross through the massif from the Serra do Mar Sul project (CPRM 1978a). The response from the models suggested a body with a depth around 3 km and a width of approximately 1 km, suggesting that Tunas does not have a geometry favorable to the existence of a deep root (Rugenski 2006; Marangoni and Mantovani 2013).

3 THEORETICAL FRAMEWORK

This chapter will outline in a more detailed way the theory behind the magnetic and radiometric methods used in this thesis.

3.1 MAGNETOMETRY

3.1.1 Concepts

The magnetic method measures spatial variations in the magnetic field of Earth (Dentith and Mudge 2014). These variations are often diagnostic of mineral structures as well as regional ones. It should be noted that magnetometry is the most versatile of geophysical prospecting techniques despite the fact that lacks uniqueness of interpretation given the dipole characteristic of its anomalies (Telford et al. 1990).

As noted by Isles and Rankin (2013), aeromagnetic surveys measure the strength (scalar quantity) of the local Earth's field. The amount of this strength is given by the Earth's core field, called in the literature as the International Geomagnetic Reference Field (IGRF), fields associated with the magnetism in crustal rocks and the magnetic field created in the lower ionosphere due to interaction with solar winds (Hinze et al. 2013), which is commonly referred to as diurnal variations. Those three fields comprise the Total Magnetic Intensity (TMI). However, TMI images are commonly described in the literature as the difference between the measured field (with corrections of diurnal variations applied) and the IGRF. It was chosen to follow this incorrect, but commonly used, abbreviation because of its broad use in the literature and geophysical industry. It must be stressed that TMI can also be described as IGRF residual (Isles and Rankin 2013), residual magnetic anomaly (Sheriff 2002), total-field (magnetic) anomaly (Blakely 1995; Reeves 2005), anomalous magnetic field - AMF (Reeves 2005; Ramos et al. 2014).

The TMI is given by the magnetism of rocks, which is mainly controlled by the physical property called magnetic susceptibility (Dentith and Mudge 2014), that determines the degree to which a body has been magnetized (Telford et al. 1990). Magnetic data give information on geological features at depths varying from the Earth's surface to the Curie point isotherm, which lies around 15 km of depth (Isles and Rankin 2013).

The aim of magnetic data interpretation is generally to find magnetic anomalies, its depth, dimensions, and magnetization (Sheriff 2002). It may give a consistent picture of the distribution of magnetization of the crust and it is not disturbed by lakes, waterways or soils that may cover the bedrock (Airo 2015).

3.1.2 Radially averaged power spectrum (RAPS)

During the last five decades, spectral analysis has been used in a variety of geologic applications, such as modeling based on the inversion of power-density spectrum (García-Abdeslem and Ness 1994) and magnetic characterization of basins (Moro et al. 2018, Pesce et al. 2019).

The radially averaged power spectrum (RAPS), developed by Spector and Grant (1970), consists of power spectrum analysis to aeromagnetic map interpretation using Fourier techniques where the influences of horizontal size, depth, thickness, and depth extent of the blocks on the shape of the power spectrum are evaluated. These authors created a model of a crustal magnetic layer using an ensemble of vertical prisms. This is a technique to estimate the average depth of a large collection of magnetic sources from their statistical properties (Blakely 1995).

While the energy spectrum is a two-dimensional function of the energy relative to wavenumber and direction, the RAPS is a function of wavenumber alone and is measured by averaging the energy for all directions for the same wavenumber.

When considering a grid that is large enough to include many sources, the log spectrum of this data can be interpreted to determine the statistical depth to the tops of the sources using the following relationship (Geosoft 2010):

$$log\ E(r) = 4\pi hr \quad (1)$$

where log E(r) = log energy spectrum;

h = depth to the top of the sources;

$r = (u^2 + v^2)^{1/2}$, where u and v are wavenumbers in the x and y directions, respectively, measured in radians per meter if x and y are in given meters.

The depth to the tops of an ensemble of sources is estimated by measuring the slope of the energy (power) spectrum and dividing it by 4π (Cowan and Cowan 1993) according to the equation below:

$$h = -s/4\pi \quad (2)$$

where h is the depth to the top of the sources and s is the slope of one of the components of the sources.

An energy spectrum for magnetic data may exhibit three depth ensembles: a deep source component, a middle source component and, a shallow source component. Also, a white noise component is present on the spectrum (Cowan and Cowan 1993).

3.1.3 Enhancement of data

Improvement of data could be done by steps that involve filtering or noise rejection (Sheriff 2002). Usually, enhancements in gravity and magnetic data consist of first-order derivatives of these data in order to locate edges and/or centers of causative sources or to gain some information about their magnetization (Nabighian et al. 2005; Castro et al. 2018).

The filters used for the processing of the magnetic data in this work were: reduction-to-pole, derivative-based filters, e.g. vertical derivative, Analytic Signal (AS), Total Horizontal derivative (THDR), phase-based filters (e.g. tilt angle), vertical integral of the analytic signal (VIAS) and analytic signal of the integral vertical (ASVI).

According to Hidalgo-Gato and Barbosa (2015), derivative-based filters are not suited to enhance anomalies produced by shallow and deep bodies simultaneously due to its poor performance. Another drawback of these filters is that they do not work properly in the presence of noise or low-quality data.

As for phase-based filters, their use is more common for enhancement of anomalies produced by both shallow and deep sources (Hidalgo-Gato and Barbosa 2015), which present short- and long-wavelength spectral contents, respectively.

3.1.3.1 Reduction-to-pole (RTP)

Developed by Baranov (1957) and Baranov and Naudy (1964), this technique transforms the TMI data measured at any Earth's field inclination to the TMI data as if the survey was conducted at the north magnetic pole, i.e. its magnetic inclination (I) is equal to 90º (Isles and Rankin 2013). Thus, the dipolar character of a given anomaly turns to monopolar, such as in gravimetric surveys, because RTP converts anomalies, which may be laterally displaced, to be located over their respective sources and also alter their shape so that symmetrical sources cause symmetrical anomalies while asymmetry in the data will be representative of source geometric or magnetic properties (Blakely 1995, Holden et al. 2016).

The use of this transform often assumes that all the bodies are magnetized by induction, which can lead to misleading results if there is a significant remanent magnetization that is not parallel to the induced field (Nabighian et al. 2005).

The equation for the reduction-to-pole in the frequency domain (Grant and Dodds 1972) is given by

$$RTP\ Operator\ L(\theta) = \frac{1}{[\sin(I) + icos(I)\cos(D-\theta)]^2} \tag{3}$$

where

θ is the wavenumber direction;

I is the magnetic inclination;

D is the magnetic declination.

3.1.3.2 Vertical derivative

The vertical derivative or Z-derivative has been used for decades to delineate features in gravity and magnetic field data due to accentuate shallower anomalies. An example of this filter is the second vertical derivative which was used as a powerful tool for interpretation (Evjen 1936; Vacquier et al. 1951). However, it was only in the 1980's decade that a stable calculation of the first vertical derivative was proposed by Nabighian (1984).

According to Isles and Rankin (2013), the first vertical derivative is the main high-pass filter for aeromagnetic survey data. It is worth noting that this filter does not have a directional bias, which is an important aspect to improve the structural and spatial resolution in the imagery.

3.1.3.3 Analytic Signal (AS)

This transformation - abbreviated as AS or AnSig, and also called total gradient - was first described in the 2D realm by Nabighian (1972, 1974). It turned out to be a popular technique for locating the edges and depth of magnetic bodies. The amplitude of the analytic signal is equal to the total gradient, being independent of the magnetization direction (Nabighian 1972).

Roest et al. (1992) extended this technique for the three-dimensional case, being a method that is dependent on the direction of the inducing field, unlike its 2D case (Haney et al. 2003; Li 2006a). This transform is cited as 3-D analytic signal, analytic signal amplitude (ASA), envelope, or total gradient amplitude (TGA) (Sheriff 2002; Ferreira et al. 2013; Isles and Rankin 2013). In this work, the term total gradient (TG) will refer to the 2-D analytic signal while ASA will be adopted for its three-dimensional case.

The ASA could map edge locations at low field inclinations and in the presence of remanent magnetization in an effective way (Isles and Rankin 2013). This filter inserts the anomalies peaks directly above thin bodies and along the edges of larger geologic features if there is a magnetic difference between them and their surroundings (Mitchinson et al. 2017).

The equation for the 3D case is given by

$$ASA(x,y) = \sqrt{\left(\frac{\partial M}{\partial x}\right)^2 + \left(\frac{\partial M}{\partial y}\right)^2 + \left(\frac{\partial M}{\partial z}\right)^2} \quad (4)$$

where M is the magnetic anomaly.

3.1.3.4 Total horizontal derivative (THDR)

This technique developed by Cordell and Grauch (1985), also called pseudogravity horizontal gradient magnitude (PSG-hgm) by Pilkington and Tschirhart (2017), is calculated by combining the X and Y derivatives.

The edges or boundaries of magnetic sources are represented by the highest values of the THDR (Mitchinson et al. 2017). Even though it lacks some resolution, the THDR is a stable filter and it is sensitive to magnetization direction and source-dip effects (Grauch and Cordell 1987). This filter is expressed by

$$THDR = \sqrt{\left(\frac{\partial M}{\partial x}\right)^2 + \left(\frac{\partial M}{\partial y}\right)^2} \quad (5)$$

3.1.3.5 Tilt angle (TI)

The tilt angle filter, abbreviated as TI, TILT, or tilt derivative (TDR), was designed by (Miller and Singh 1994) and it is sensitive to dip and magnetization effects. According to Li (2006b), TI is related to the methods: horizontal tilt angle (TDX, Cooper and Cowan 2006), and theta map (TH, Wijns et al. 2005). The tilt angle treats larger and smaller anomalies with equal weighs, being positive above the causative source and negative outside of it while its edges are delimited by the zero degrees contour (Mitchinson et al. 2017).

The tilt angle is given by

$$TI(x,y) = tan^{-1}\left[\frac{\partial M}{\partial z} \Big/ \sqrt{\left(\frac{\partial M}{\partial x}\right)^2 + \left(\frac{\partial M}{\partial y}\right)^2}\right] \quad (6)$$

3.1.3.6 Analytic signal of the vertical integral (ASVI) and Vertical integral of the analytic signal (VIAS)

These techniques were introduced by Paine et al. (2001) and consist of transforming the TMI data into measures weakly dependent on the magnetization direction by calculating the total gradient of the vertical integration (ASVI) of the TMI or vertically integrating its total gradient (VIAS). These quantities are treated as if they were reduced to the pole allowing the

3D magnetic susceptibility algorithm inversion developed by Li and Oldenburg (1996) to be performed. Li et al. (2010) pointed out that the data transformed by the ASVI or VIAS method are not true magnetic anomalies since the inversion algorithm used considers only induced magnetization. Although there is this inconsistency, both ASVI and VIAS lead to interpretable results (Leão-Santos et al. 2015; Li 2017) being appropriate for isolated or multiple sources as well (Pilkington and Beiki 2013).

One drawback of the VIAS method is that it can cause significant amplification of low-frequency components of data while the ASVI technique attenuates this amplification caused by the vertical integral (Paine et al. 2001). However, both techniques permit modeling when the TMI data seems to have strong remanent magnetization or there is no clear information about the influence of remanence in the area of interest. It is worth noting that the ASVI or VIAS transform will not yield the true source geometry with high levels of confidence. It will be more common that they produce similar bodies which broader and deeper limits than the true sources (Paine et al. 2001).

The analytic signal can be vertically integrated as follows

$$VIAS(x,z) = \int_{z}^{\infty} AS(x,z)dz \qquad (7)$$

$$= \int_{z}^{\infty} dz/(x^2+z^2)$$

$$= \begin{cases} [sgn(x)\pi/2 - \tan(z/x)]/x & \text{if } x \neq 0 \\ 1/z & \text{if } x = 0 \end{cases}$$

3.1.4 Euler deconvolution

Euler deconvolution is a useful semi-automatic technique to locate gravity and magnetic sources and estimate its depth-to-the top. It was first developed by Thompson (1982) for the 2D case and later adapted for three-dimensional situations (Reid et al. 1990).

It is worth noting that information about the direction of the magnetism is not required. Therefore, areas with remanent magnetism will not implicate difficulties for this method (Dentith and Mudge 2014). Nevertheless, Euler deconvolution needs input from the interpreter called structural index (SI) that characterizes the geometry of the source and it is related to how fast the amplitude of the response declines with distance from the causative body (Dentith and Mudge 2014). The structural index given for each type of source geometry is given in **Table 2** while the expression for Euler 3D deconvolution is given by

$$(x-x_0)\,\partial T/\partial x + (y-y_0)\,\partial T/\partial y + (z-z_0)\,\partial T/\partial z = N(B-T) \qquad (8)$$

where

x_0, y_0, z_0 is the position of a magnetic source;

x, y, z is the position of the detected total field T;

B is the regional value of the total field;

N is the structural index, which measures the rate of change with distance of a field.

Table 2. Structural index (SI) value for magnetic sources corresponding to the geometry of the causative body.

Source	SI
Contact / Step	0
Sill / Dike	1
Cylinder / Pipe	2
Sphere / Barrel / Ordnance	3

3.1.5 Structural magnetic-framework

2D analysis from magnetic lineaments, discontinuities, magnetic sources, and their limits have been performed to assess geological unit trends and it plays an important role in identifying and delimiting main magnetic structures. Many recent studies have used this texture analysis from aeromagnetic data (Holden et al. 2012; Moro et al. 2018; Pereira and Ferreira 2018). According to Isles and Rankin (2013), this technique helps in structural problems ranging from basin to prospect scales. However, these authors pointed out that the degree of this contribution is controlled by several factors such as the magnetic signature of the geology, survey line spacing and survey height, and level of structural information achieved from the input of other datasets.

Structural magnetic lineaments maps, in general, are created over filtered gridded data to reveal features at distinct crustal depths. In this work, grayscale of the first Z-derivative was used to trace magnetic lineaments. Grayscale images permit easier identification of high-frequency (fine-scale detail) features for the human eye rather than colored presentations, which are better suited for low-frequency details (Isles and Rankin 2013).

3.1.6 Inverse modeling and magnetic susceptibility

Inverse modeling or inversion is the determination of a possible model done by computer algorithms, with little to no human intervention, according to observed data. Inversion is not a unique process, i.e. there is an infinite number of possibilities, and therefore, it is the role of the interpreter to choose the best result (Sheriff 2002; Dentith and Mudge 2014). 3D magnetic inversion has received much attention in recent years due to its vital role in determining the geometries of mineralized environments.

In this work, magnetic susceptibilities inversions were performed. Magnetic susceptibility (χ) can be expressed as:

$$M = \chi \boldsymbol{H} \quad (9)$$

where M is magnetization or magnetic moment per unit volume and H is the magnetized field strength. It can also be described as the degree measurement to which a substance may be magnetized (Sheriff 2002). This measure is inversely proportional to the absolute temperature (Sheriff 2002). Magnetic susceptibility is dimensionless in the International System (SI) and centimeter–gram–second (emu-cgs) systems but differs in magnitude by 4π. Susceptibility in SI units (SIu) is equal to 4π times emu-cgs (CGSu) susceptibility. **Figure 11** illustrates magnetic susceptibilities for common rocks and minerals.

The majority of inversions consider that the magnetization direction is parallel to Earth's induced field and there is no significant effect of self-demagnetization as well (Li 2017).

3.2 GAMMA-RAY SPECTROMETRY

3.2.1 Concepts

The gamma-ray spectrometric or radiometric method is used in the identification of natural radioactive isotopes of potassium (K), equivalent thorium (eTh), and equivalent uranium (eU) in rocks. This passive geophysical method has penetration depth of a maximum half a meter from the surface (Dentith and Mudge 2014; Airo 2015).

The principal aim of this technique is to locate anomalies of K, eTh, and eU that could represent differences in lithotype units, weathering, and regolith effects, as well as the presence of mineralization (Dickson and Scott 1997). These elements are the only ones that are not artificially created and that can produce enough high-energy and intense gamma rays by radioactive decay to be measured in surveys (Minty 1997).

The 'e' before Th and U stands for equivalent. This is due to the fact that these elements concentrations are collected in the ^{214}Bi and ^{208}Tl channels, respectively, considering that there is a radioactive equilibrium for its daughter products in the decay series of U and Th (Grant 1998).

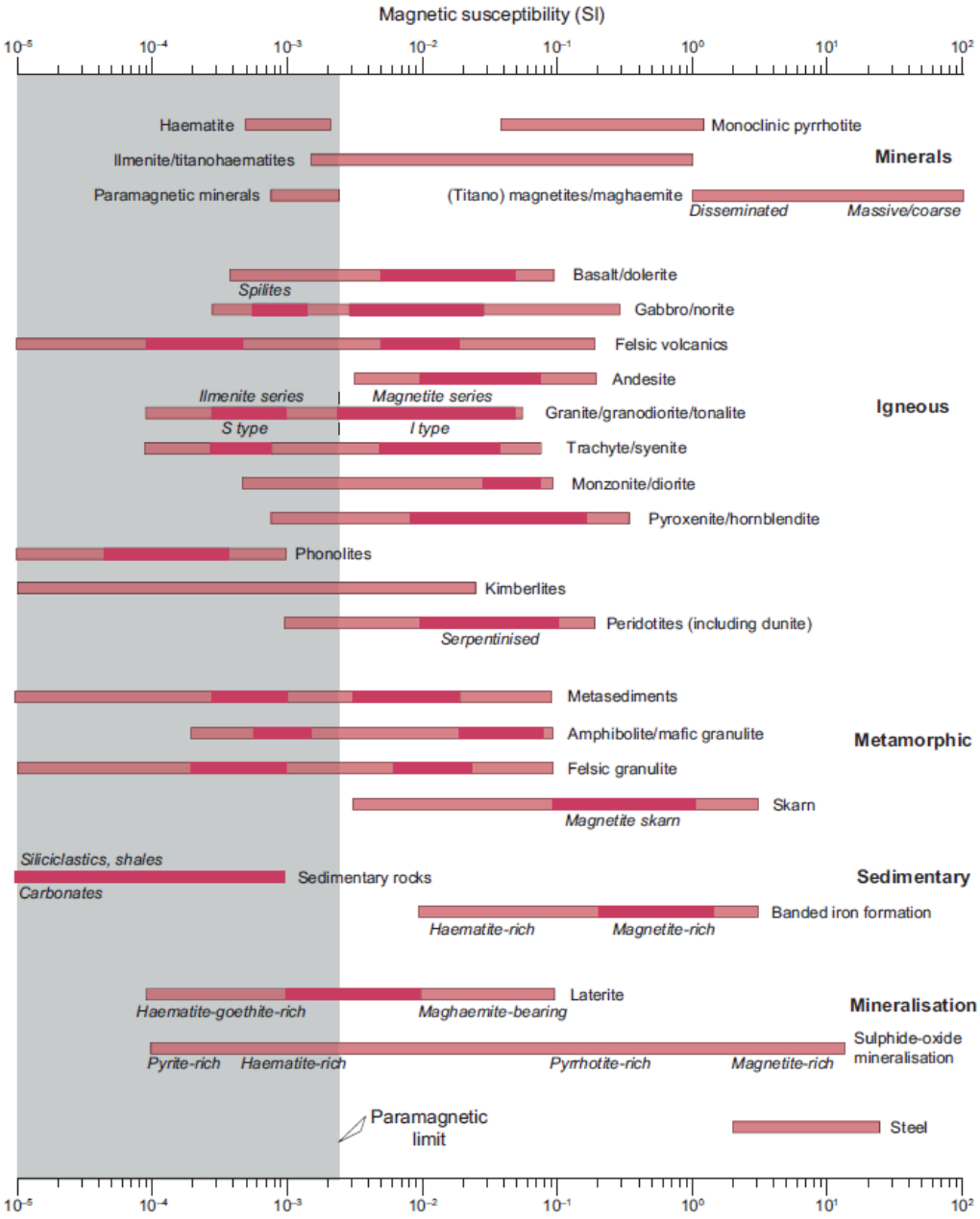

Figure 11. Magnetic susceptibility values for rocks and minerals. Dark red represents the most common intervals while the gray area represents the paramagnetic domain (Clark 1997; Dentith and Mudge 2014).

In the following, a summary of each radioelement geochemistry is provided. Average concentrations of K, eTh, and eU for common rocks and igneous types carried out by Killeen (1979) and by Galbraith and Saunders (1983) are also provided. The data compiled by these authors are illustrated in **Table 3** and **Table 4**.

Table 3. Average concentrations of radioelements and in rock types (after Killeen 1979). Values in parentheses represent the minimum and maximum abundance found for each rock analyzed by this author.

Rock type	K (%)	eU (ppm)	eTh (ppm)
Acid extrusives	3.1 (1.0 - 6.2)	4.1 (0.8 - 16.4)	11.9 (1.1 - 41.0)
Acid intrusives	3.4 (0.1 - 7.6)	4.5 (0.1 - 30.0)	25.7 (0.1 - 253.1)
Intermediate extrusives	1.1 (1.1 - 2.5)	1.1 (0.2 - 2.6)	2.4 (0.4 - 6.4)
Intermediate intrusives	2.1 (0.1 - 6.2)	3.2 (0.1 - 23.4)	12.2 (0.4 - 106.0)
Basic extrusives	0.7 (0.06 - 2.4)	0.8 (0.03 - 3.3)	2.2 (0.05 - 8.8)
Basic intrusives	0.8 (0.01 - 2.6)	0.8 (0.01 - 5.7)	2.3 (0.03 - 15.0)
Ultrabasic	0.3 (0.0 - 0.8)	0.3 (0.0 - 1.6)	1.4 (0.0 - 7.5)
Alkali feldspathoidal intermediate extrusives	6.5 (2.0 - 9.0)	29.7 (1.9 - 62.0)	133.9 (9.5 - 265.0)
Alkali feldspathoidal intermediate intrusives	4.2 (1.0 - 9.9)	55.8 (0.3 - 720.0)	132.6 (0.4 - 880.0)
Alkali feldspathoidal basic extrusives	1.9 (0.2 - 6.9)	2.4 (0.5 - 12.0)	8.2 (2.1 - 60.0)
Alkali feldspathoidal basic intrusives	1.8 (0.3 - 4.8)	2.3 (0.4 - 5.4)	8.4 (2.8 - 19.6)
Chemical sedimentary	0.6 (0.02 - 8.4)	3.6 (0.03 - 26.7)	14.9 (0.03 - 132.0)
Carbonates	0.3 (0.01 - 3.5)	2 (0.03 - 18.0)	1.3 (0.03 - 10.8)
Detrital Sedimentary	1.5 (0.01 - 9.7)	4.8 (0.1 - 80.0)	12.4 (0.2 - 362.0)
Metamorphosed igneous	2.5 (0.1 - 6.1)	4 (0.1 - 148.5)	14.8 (0.1 - 104.2)
Metarmorphosed sedimentary	2.1 (0.01 - 5.3)	3 (0.1 - 53.4)	12 (0.1 - 91.4)

Table 4. Average concentrations of radioelements and their ratios in igneous rocks (Galbraith and Saunders 1983). Values in parentheses represent mean radioelement levels for members of the calc-alkalic series.

Rock type	K (%)	eU (ppm)	eTh (ppm)	K/eU (10^4)	eTh/eU	eTh/K (10^{-4})
Alkaline - utrabasic	1.77	0.5	0.6	5.10	3.57	0.73
Alkaline - basic	3.36	2.3	2.5	3.94	2.30	0.83
Alkaline - basic - intermediate	4.27	3.2	6.2	3.67	5.53	1.47
Alkaline - intermediate	4.40	3.5	10.3	1.48	3.53	2.37
Alkaline - intermediate - acidic	4.82	2.8	15.7	2.31	7.12	3.27
Alkaline - acidic	5.52	5.3	22.6	1.84	7.12	4.11
Alkaline - hyperacidic	7.81	4.0	43.0	1.96	11.10	5.80
Ultrabasic	0.32 (0.58)	0.1 (0.1)	1.1 (0.1)	3.56 (5.85)	11.78 (1.00)	3.31 (0.17)
Basic	1.46 (1.84)	1.4 (1.4)	2.8 (4.5)	1.38 (1.84)	2.68 (3.48)	2.22 (2.80)
Basic – intermediate	2.31 (1.86)	2.0 (2.0)	6.4 (5.5)	1.57 (1.67)	4.19 (3.80)	2.93 (3.16)
Intermediate	2.73 (2.85)	3.0 (3.0)	10.6 (11.1)	1.30 (1.60)	5.32 (5.05)	4.08 (3.92)
Intermediate – acidic	3.21 (3.42)	4.2 (5.0)	15.5 (17.7)	0.95 (1.16)	4.66 (5.00)	5.02 (5.12)
Acidic	3.66 (3.83)	6.0 (5.8)	22.2 (26.2)	1.34 (1.49)	7.84 (7.07)	6.14 (6.83)
Hyperacidic	4.25 (3.85)	8.6 (7.2)	41.3 (18.0)	0.70 (1.05)	6.45 (2.81)	9.69 (4.44)
Calcic - intermediate - acidic	0.98	3.2	15.7	0.30	4.95	20.03
Calcic - acidic	1.26	0.9	20.5	1.40	22.78	16.27
Calcic - hyperacidic	2.80	9.3	40.0	0.30	4.30	14.29

3.2.2 Potassium (K)

Potassium is an alkali element that has an average value of 2% in the crust, being the most abundant when comparing to thorium and uranium. However, only 0.012% of this element occurs as a radioactive isotope, the ^{40}K (Minty 1997; Dentith and Mudge 2014).

Alkali feldspars, micas, and illites are the main minerals containing potassium, while this substance is not presented in mafic minerals. The concentrations of K are minimal for peridotites and dunites and increase for mafic basalts and are the highest for felsic rocks (Dickson and Scott 1997).

3.2.3 Equivalent uranium (eU)

With an average of approximately 3 ppm in the crust, this element comprises valence states U^{4+} and U^{6+} (Dickson and Scott 1997). The uranium has two isotopes that occur naturally, ^{238}U and ^{235}U, and turn into lead (Pb) as its stable isotope daughter at the end of the decay series (Minty 1997). However, only the ^{238}U is useful for gamma-ray spectrometric surveys since the ^{235}U comprises less than 1% of naturally occurring uranium (Dentith and Mudge 2014).

Uranium may be available in rocks as silicate and oxide minerals, as well as xenotime, monazite, and zircon. Only the latter two minerals do not destabilize on weathering (Dickson and Scott 1997).

3.2.4 Equivalent thorium (eTh)

This large ionic radii element appears as the radioisotope ^{232}Th, with valence state Th^{4+}, while its stable isotope at the end of the decay series is lead-208 (Minty 1997, Dentith and Mudge 2014). Like uranium, this substance is not susceptible to substitute other elements in silicate minerals (Dentith and Mudge 2014).

Minerals that can host Th are monazite, zircon (both are major Th-bearing minerals and stable on weathering), allanite, and xenotime. Also, this element can be present in trace amounts in other minerals (Dickson and Scott 1997). Thorium is primarily a stable substance due to its low solubility, except in the presence of acid solutions and organic compounds (Langmuir and Herman 1980; Choppin 1988).

Extremely alkalic rocks, carbonatites, and kimberlites could be presented in radiometric images enriched in eU and eTh or even with high ratios of eTh/eU for the former two rocks (Dentith and Mudge 2014).

3.2.5 Ratio maps

Radioelements concentration ratios have been applied for the detection of slight differences in the gamma-ray spectrometric data and for mineral exploration (e.g. Darnley 1972). The ratios of K, eU, and eTh may be used to minimize the distortion in the data due to

changes in lithotypes as well as act as an attenuator for environmental artifacts, which are produced by the presence of soil moisture, vegetation, or non-radioactive cover (Minty 2011).

One aim of creating ratio maps is to find anomalous signatures where there is enrichment and/or depletion of one or more radioelements in relation to others or to locate zones of alteration (Dentith and Mudge 2014). For example, the ratio K/(eTh + eU) could be created to analyze the variation of potassium in relation to eTh and eU.

Another example of a ratio map is the relation K*eU/eTh, called F-parameter (Efimov 1978; Gnojek and Prichystal 1985). It can evaluate the respective abundance of potassium in relation to the eU/eTh. This parameter, which is more statistically stable than the eTh/eU, may also help to distinguish non-altered rock and altered ones, where the former have values of up to 1.2 or 1.3 while altered rocks may show 2 to 5 (Gnojek and Prichystal 1985).

In addition to the traditional ratios widely used in the literature - e.g. eU/eTh, eU/K, eTh/K (IAEA 1991) –, other gridded ratios created to assess radioelements associations are as follows: K/eU, K/eTh, K/(eU+eTh), eU/(K+eTh), eU/(K+eU+eTh), eTh/(K+eU), (eTh+eU)/K, (K*K)/(eU*eTh), (eU*eU)/eTh, and (eTh*eTh)/K (Dentith and Mudge 2014).

3.2.6 Thorium-normalized potassium (KD), thorium-normalized uranium (UD) and DRAD

These normalizations, described in detail by Saunders et al. (1987, 1993, 1994), were used in reconnaissance of petroleum accumulations and by Pires (1995) to identify areas related to hydrothermalism in gold deposits of central Brazil. It was developed to suppress the undesired effects of variations in lithotypes, soils, and vegetation. This technique consists of the equations as follows:

$$K_i = (\text{mean of the grid } K_s \,/\, \text{mean of the grid } eTh_s) * eTh_s \quad (10)$$

and

$$eU_i = (\text{mean of the grid } eU_s \,/\, \text{mean of the grid } eTh_s) * eTh_s \quad (11)$$

where K_i and eU_i are the ideal thorium-defined potassium and ideal thorium-defined uranium values, respectively. K_s, eU_s, and eTh_s are the points measured for potassium, equivalent uranium, and equivalent thorium, respectively.

The thorium-normalized radioelement is given by:

$$\text{KD}\% = (K_s - K_i) \,/\, K_i \text{ for potassium} \quad (12)$$

and

$$UD\% = (eU_s - eU_i) \,/\, eU_i \text{ for uranium} \quad (13)$$

where *KD* and *UD* are deviations of the real values from the calculated ideal ones for each point measured.

Saunders et al. (1993) also combined KD% and UD% to the term called DRAD:

$$DRAD = (UD\% - KD\%) \quad (14)$$

where positive values of this variable may be related to favorable indications of petroleum.

3.2.7 Ternary maps

A ternary image can be classified as a color composite image created by the modulation of red, green, and blue colors of the monitor according to the relative abundance of K, eTh, and eU. It is a method of enhancing multiple channels in one image, being the most used procedure to display gamma-ray spectrometry data (Dentith and Mudge 2014). Two advantages of displaying ternary maps are the chance to discriminate chemical signatures of the surface and to separate lithotypes based on the difference of colors (Dentith and Mudge 2014).

The standard in the literature and industry is to show K as red, eTh as green and eU as blue, since the equivalent uranium is the noisiest channel and blue intensity variations are the least noticeable for the human eye (IAEA 2003). White color represents a relative abundance of the three radioactive elements while black depicts a significant lack in all of them. Furthermore, yellow, magenta, and cyan colors could be used as an alternative for the RGB system in ternary maps.

3.2.8 Profiles

Profile plots have been used to visualize relations between the radioelements and other signatures of both magnetic and radiometric data. Representing stacked or multiple profiles in association with lithotypes is a powerful tool to correlate mapped geology and to identify anomalies that may represent mineralized environments (IAEA 2003).

Profiles are useful to display more reliable data, i.e. with full spatial resolution, than a grid. This is due to the use of filters along flight lines for the grid interpolation to avoid aliasing problems (Horsfall 1997).

4 MATERIAL AND METHODS

4.1 AEROGEOPHYSICAL DATA CHARACTERISTICS

Magnetic and gamma-ray spectrometric data from Paraná-Santa Catarina (PR-SC) Project were used (CPRM 2011). The PR-SC magnetic and radiometric survey was flown between 2009 and 2011, covering an area over 65,562 km^2 in the Paraná and Santa Catarina states, Brazil. North-south oriented flight lines were spaced 500 m apart. The geophysical data were acquired at a terrain clearance of 100 m (with some areas over 300 m for security reasons, CPRM 2011). A Scintrex CS-3 high-sensitivity cesium vapor magnetometer sensor and Exploranium GR-820 airborne gamma spectrometer (which records 256 channels of summed data) were used for data collecting and the sampling rate for each sensor was 0.1 s and 1 s, respectively.

CPRM (2011) applied the following steps for the correction of magnetic data from the Paraná-Santa Catarina project: parallax error correction, removal of diurnal variations, leveling, microleveling, and subtraction of the International Geomagnetic Reference Field (IGRF).

Gamma-spectrometric data were corrected by CPRM (2011) following the procedures specified by the International Atomic Energy Agency (IAEA 1991) as follows: dead-time correction, filtering, parallax error, calculation of effective height above ground level (AGL), removal of aircraft and cosmic background, removal of atmospheric radon background, stripping, attenuation correction and conversion to apparent radioelement concentrations.

The average flight height of each line of the entire airborne survey data was analyzed, in a similar way described by Silva (1994) in which it was demonstrated the average survey height of the Serra do Mar Sul aerogeophysical project (CPRM 1978a). A detailed description of the computer routine applied is given in **Appendix 1**. Due to the large quantity of data, the use of charts is considered a faster visualization technique to check divergent values, when they are compared to the total mean of flight height, rather than data presented in tables. This technique also may be used to evaluate the relation between line spacing and survey height where the former could not exceed five times the latter due to excessive production of undersampling artifacts (Isles and Rankin 2013).

4.2 COORDINATES OF THE STUDY AREA AND GRIDDING OF DATA

The study area was delimited by coordinates 655,000 – 720,000 (X-axis) and 7,280,000 – 7,230,000 (Y-axis), comprising partial areas from the geological maps of Cerro Azul (Brumatti and Almeida 2014) and Apiaí (Morais et al. 2012) (**Figure 12**). These

1:100,000-scale maps were used to discuss the geophysical data in association with the mapped geology.

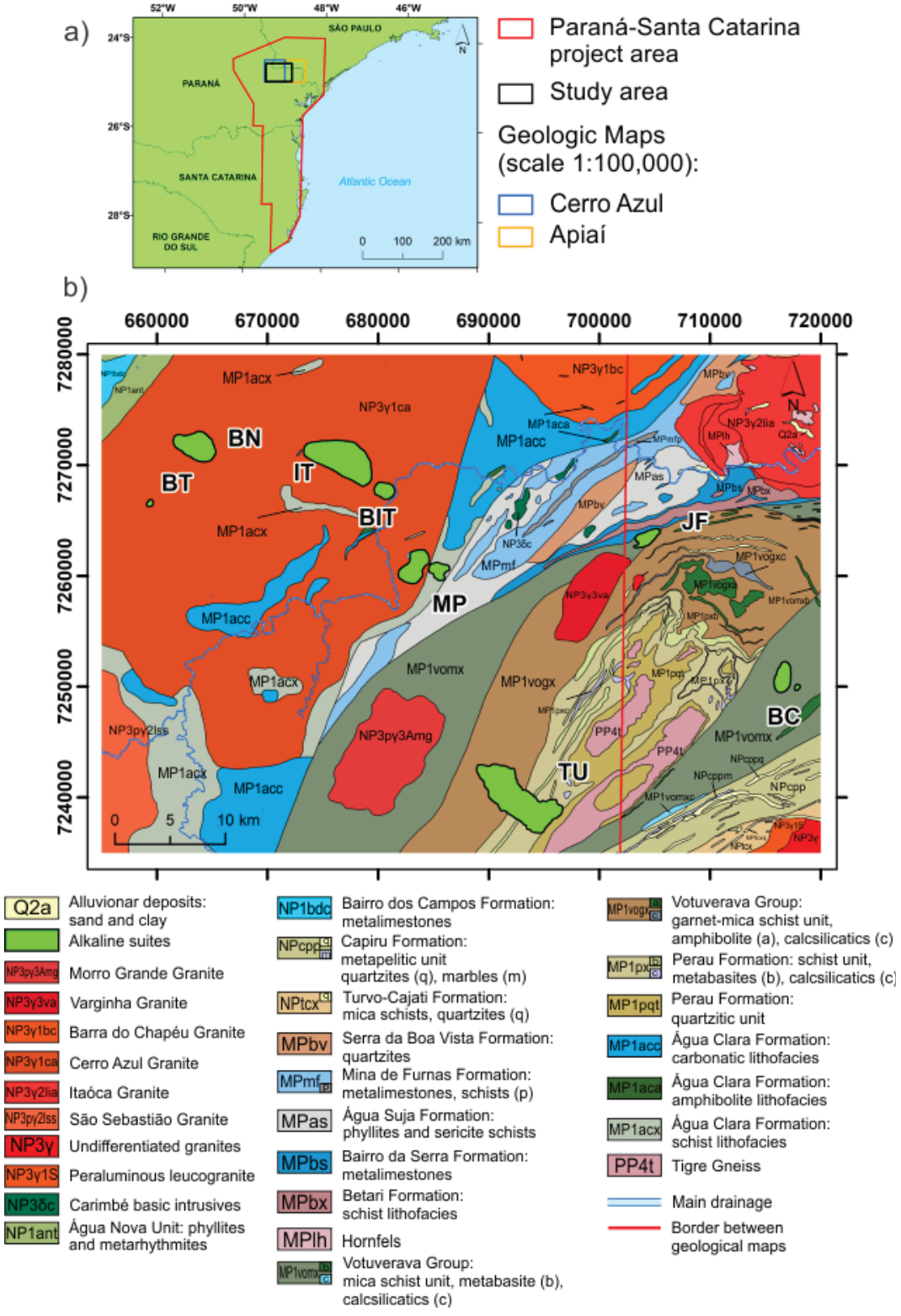

Figure 12. Image of the study area inside the Paraná-Santa Catarina airborne survey and in the Cerro Azul (Brumatti and Almeida 2014) and the Apiaí (Morais et al. 2012) geologic maps (a). Simplified geological map for the study area (b). Alkaline complexes: Bairro da Cruz (BC), Barra do Itapirapuã (BIT), Banhadão (BN), Barra do Teixeira (BT), Itapirapuã (IT), José Fernandes (JF), Mato Preto (MP), and Tunas (TU).

The coordinate system of the airborne survey was the World Geodetic System (WGS) 84 UTM Zone 22S and, therefore, all the geological and geophysical images were created in this work adopted this coordinate system. According to the Brazilian Institute of Geography and Statistics (IBGE 2019), this system is compatible with SIRGAS2000, which is the official geodetic reference for Brazil.

The technique chosen for gridding was the minimum curvature, described by Briggs (1974) and Swain (1976). It uses two-dimensional splines to represent the surface, where the splines fit the flight line data to a grid surface. This method requires a grid cell size to a minimum of about one-fifth of the line separation (Luyendyk 1997) and it is a better option than the bi-directional gridding if there is no dominant geological trend perpendicular to the flight-line direction (IAEA 2003), which is the case for the majority of the suites (NW-SE oriented) in this work. The RANGRID algorithm from the Oasis Montaj software was used to generate the gridded images.

Therefore, all the magnetic and radiometric data were interpolated onto a 100 m grid cell-size, which represents 1/5 of the spacing between lines. This value is inside the established interval in the literature for grid cell size, i.e. 1/5 to 1/3 (Isles and Rankin 2013). According to Billings and Richards (2000), the central consideration in the flight-lines is whether the cell size is fine enough to prevent aliasing of signal in the gridded image.

4.3 MAGNETIC DATA PROCESSING

All the magnetic processing steps were performed in the Oasis Montaj suite. TMI data for the study area was gridded and it was reduced to the pole according to the parameters calculated for the date of acquisition (**Table 5**).

Table 5. Parameters used for the reduction to pole for the study area and for inverse modeled igneous rocks presented in this work.

Region	Magnetic inclination	Magnetic declination	Amplitude correction inclination
Study area	-34.49	-18.91	-55.51
Bairro da Cruz	-34.96	-19.02	-55.04
José Fernandes	-34.73	-18.79	-55.27
Tunas	-34.87	-18.86	-55.13

Semi-quantitative analyses involved the estimation of depths for the study area from the radially averaged power spectrum (RAPS) and standard Euler 3D deconvolution solutions. The steps to generate the RAPS and to calculate the average depth of each source component (Cowan and Cowan 1993) were performed according to Sigismondi (2019) in which a RAPS .pcs file is created in the Oasis montaj software and exported to a worksheet to generate the graph of the logarithm of the spectral density (energy) averaged for all the grid

elements for given wavenumbers. Then, each line segment with a constant slope in the spectrum was attributed to a determined depth interval following the procedure of Cowan and Cowan (1993). For the Euler 3D solutions, it was assigned a structural index (SI) equal to 1 (relative to dikes), a maximum depth tolerance of 5%, and a window size (grid points) of 20 times the grid cell size. Those parameters showed a better result comprising a reasonable number of solutions in the study area rather than other parameters tested, such as SI equal to 0 (contact type) and lower grid cell sizes.

Depth estimates from the tilt angle were also performed on the RTP-TMI data. This method described in Blakely et al. (2016) determines the depth below flight elevation of the zero contours (edges of causative sources) from the arctangent of vertical derivative divided by total horizontal derivative (THDR) of the anomaly.

Regarding structural magnetic analysis, the first vertical derivative of RTP-TMI was generated to highlight high-frequency details and to trace lineaments that were associated with the known geology. The delineation of structural features in the study area was done on this filter due to its capacity of enhancing shallow features and it does not have a bias of direction.

The complexes that showed a significant magnetic response, i.e. Bairro da Cruz, José Fernandes, and Tunas, were 3D unconstrained inverse modeled to obtain an estimate of the distribution of their magnetic susceptibilities and depth of emplacement. Inversions were applied in the TMI, RTP-TMI, VIAS-TMI, and ASVI-TMI data. The RTP parameters for each body modeled were described in **Table 5** while inclinations and declinations used in both VIAS and ASVI filters are +90 and 0, respectively. This is due to the fact that these two filters simulate an RTP response of TMI data and can be used for modeling when the influence of remanent magnetism is unknown. The parameters used for the inversions in the VOXI environment of the Oasis Montaj software were illustrated in **Appendix 2**.

4.4 GAMMA-RAY SPECTROMETRIC PROCESSING

Radiometric basic grids (potassium, equivalent thorium, and uranium) were corrected following the procedure of Ferreira et al. (2009) where each radioactive element received a constant to keep its minimum value to 0.01 and, therefore, avoiding divisions by values equal or below to zero when ratioing (Weihermann et al. 2016). The constants added to the K, eTh, and eU grids were 1.05%, 1.22 ppm, and 2.39 ppm, respectively.

Fourteen ratios maps were created following the procedure of Grant (1998), where instead of calculating the ratios from line data and then gridding them, divisions were

performed onto the gridded data. The ratios generated were: K/eU, K/eTh, K/(eU+eTh), K*(eTh/eU) - this ratio is called the F-parameter, eU/eTh, eU/K, eU/(K+eTh), eU/(K+eU+eTh), eTh/K, eTh/(K+eU), (eTh+eU)/K, (K*K)/(eU*eTh), (eU*eU)/eTh, and (eTh*eTh)/K. In addition, the parameters thorium-normalized potassium (KD), thorium-normalized uranium (UD), and DRAD were also implemented to evaluate the concentration of K and eU when they are normalized in relation to eTh. Equal-area distribution was used for zone color ranges in the interpretation of ratios and other parameter images. A ternary R-K, G-eTh, B-eU image was also generated for the study area.

The minimum, average and maximum levels of K, eTh, and, eU of each intrusion in the study area were determined from the gridded data and plotted in box-plot charts while radioelements concentrations for each sampled data point inside complexes' boundaries (according to the geological maps previously described in this work) were illustrated in normalized ternary diagrams created in the TriPlot 4.1 software and later refined in the Origin program to identify trends in K, eTh, and eU concentrations. In contrast to the grids corrections, negative sampled data points were attributed null values to avoid miscalculating relative concentrations of K, eTh, and eU in the diagrams.

4.5 PROFILES PROCESSING

For the study area, stacked profiles containing the variables K, eU, eTh, TMI, RTP-TMI, and Digital Terrain Model (DTM, World Geodetic System 1984) from the survey N-S flight lines were plotted along the mapped lithotypes for each intrusion to assess their absolute and relative levels. No correction of negative or zero values for the radioactive elements was applied. This derives from the fact that quantities below or equal to zero may be a valid representation of the radiometric dataset, which is characterized by a Poisson distribution and, therefore, supports data that lie outside the expected interval of values, even after all the treatments carried after the acquisition phase. The correction of negative values in profiles will bias subsequent statistical analysis, and thus must never be set to zero (Grant 1998).

5 RESULTS AND DISCUSSION

Article title: Magnetic and radiometric signatures of alkaline rocks and gabbros from the Ponta Grossa Arch, southeastern Paraná Basin, Brazil.

Authors: Vinicius Antunes Ferreira da Silva[1*], Francisco José Fonseca Ferreira[1]

[1]Federal University of Paraná, Department of Geology, Laboratory for Research in Applied Geophysics, Curitiba, Paraná, Brazil. Emails: vinicius.anp@gmail.com, francisco.lpga@gmail.com

*Corresponding author.

5.1 ABSTRACT

The Ponta Grossa Arch, placed in southern Brazil, is the locality of alkaline, carbonatitic-alkalic and gabbroic intrusions, called Ponta Grossa Arch Alkaline Province. Alkaline rocks have been recognized and detailed in different scales by airborne geophysics contributing to mapping and mineral exploration. The aim of this study was to investigate the magnetic and radiometric characteristics of some rocks from this province using airborne survey data. The bodies contemplated in this work are: Bairro da Cruz, Banhadão, Barra do Itapirapuã, Mato Preto and Tunas complexes, Barra do Teixeira Phonolite, Itapirapuã Nepheline syenite, and José Fernandes Gabbro. We applied the radially averaged power spectrum, Euler 3D deconvolution, and tilt angle to estimate depths of magnetic sources. A structural framework was interpreted from vertical derivative image alongside the application of magnetic susceptibility 3D inverse modeling for Bairro da Cruz, José Fernandes, and Tunas. Gamma-ray spectrometric methods involved analyses of basic maps (K, eU, eTh), ternary map (RGB), 14 ratio maps, thorium-normalized parameters, and sampled data points radioelement concentrations. Stacked profiles from flight lines comprising radiometric and magnetic data were generated for each suite. It was found that the area had mostly shallow sources, averaging a depth of 500 m. Significant dipolar anomalies with normal polarity are associated with Bairro da Cruz, José Fernandes, and Tunas intrusions. The 3D models showed low magnetic susceptibilities values. Gamma-ray spectrometric results allowed us to verify that the majority of the complexes were mainly enriched in eTh over eU and K. Carbonatite bodies showed the highest contents of eTh and eU. These findings were consistent with geophysical responses of alkaline bodies and impact the understanding of geophysical signatures, especially radiometric ones, of alkaline provinces in Brazil.

Keywords: airborne gamma-ray spectrometry; aeromagnetics; Ponta Grossa Arch Alkaline Province; alkalines; carbonatites; gabbros.

5.2 INTRODUCTION

The Ponta Grossa Arch (PGA) is an uplifted domain located in the southeastern Paraná Basin and its Precambrian basement (**Figure 13**). The arch hosts alkaline and carbonatitic-alkalic intrusions. These complexes were studied by Almeida (1983) who labeled them as the Ponta Grossa Arch Alkaline Province (PGAAP). Most of this province is situated between the southern parts of the Guapiara (Ferreira et al. 1981) and the São Jerônimo-Curiúva (Vieira 1973; Ferreira 1982) lineaments.

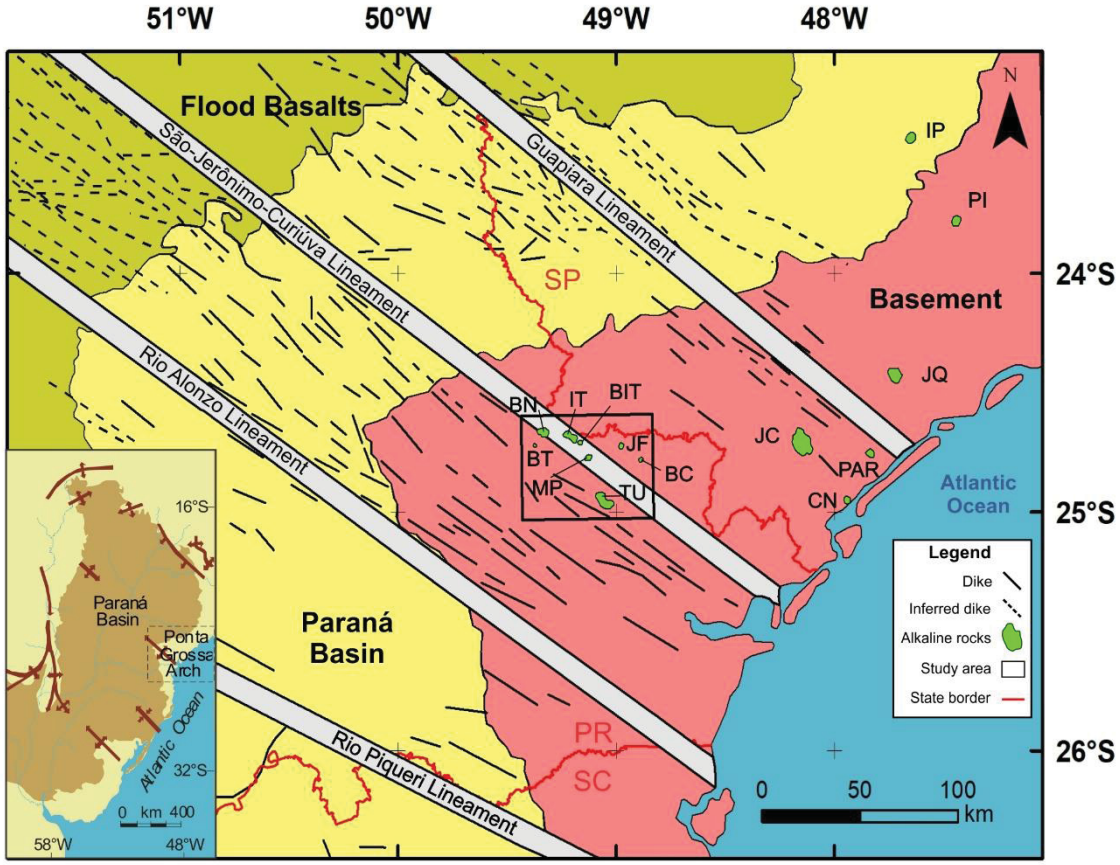

Figure 13. Sketch map of the Ponta Grossa Arch Alkaline Province (modified from Ruberti et al. 2005; Gomes et al. 2018). Alkaline complexes: Bairro da Cruz (BC), Barra do Itapirapuã (BIT), Banhadão (BN), Barra do Teixeira (BT), Cananéia (CN), Ipanema (IP), Itapirapuã (IT), Jacupiranga (JC), José Fernandes (JF), Juquiá (JQ), Mato Preto (MP), Pariquera-Açu (PAR), Piedade (PI), and Tunas (TU). States: São Paulo (SP), Paraná (PR), and Santa Catarina (SC).

Alkaline intrusions have been recognized and detailed in different scales by airborne magnetics and gamma-ray spectrometric surveys. These surveys contribute to a variety of geological and geophysical interpretation and modeling applications, such as geological mapping and mineral exploration (Airo et al. 2014), as well as the discovery of uranium deposits in alkaline igneous complexes (e.g. Cercado Mine in Poços de Caldas, Forman and Angeiras 1981). For example, aeromagnetic maps aid the interpreter in verifying anomalies

that coincide with outcropping alkaline intrusions, or even those with no surface manifestation, as well as to verify possible structural control on such intrusions (Marangoni and Mantovani 2013; Louro et al. 2019). Aeromagnetic maps may also reveal typical magnetic features such as circular anomalies for carbonatitic-alkaline bodies which coincide with their radiometric responses (Airo 2015). As for radiometrics, alkaline rocks tend to enrich in equivalent thorium (eTh), which forms complex ions with sulfides, carbonates, and phosphates (Airo 2015). Furthermore, carbonatitic-alkalic complexes may show potential for rare earth elements (REE), niobium, and vermiculite mineralizations which are resources with economic importance for Brazil (Gomes and Comin-Chiaramonti 2005). Deposits of phosphate, niobium, and vermiculite may be formed in alkaline rocks which are affected by supergene processes and also by the residual concentration of minerals during weathering phase (Gomes and Comin-Chiaramonti 2005).

The PGAAP was studied by Ulbrich and Gomes (1981), Almeida (1983) and several authors, including Comin-Chiaramonti and Gomes (2005), Gomes et al. (2011), and Gomes and Comin-Chiaramonti (2017), who did an extensive review about the Mesozoic-Cenozoic alkaline magmatism in the Brazilian platform. The area has also been studied by Marangoni and Mantovani (2013), who characterized state-of-the-art potential field (magnetic and gravimetric) signatures in the PGAAP and other alkaline provinces in Brazil. However, these authors have not reported geophysical signatures of all the bodies from the PGAAP, describing only Ipanema (IP), Jacupiranga (JC), Juquiá (JQ), Pariquera-Açu (PAR), and Tunas (TU). In addition, all the works compiled by Marangoni and Mantovani (2013) used previous and lower-resolution aerogeophysical data (i.e. flight lines spaced with 1 km or more) than the 2011 airborne survey contracted by the Geological Survey of Brazil - CPRM (CPRM 2011).

Although a variety of geophysical studies were applied in Brazilian alkaline rocks, not all the provinces have been studied in detail by different geophysical methods (Marangoni and Mantovani 2013). Little attention has been paid to the use of gamma-ray spectrometric data along with the magnetic one. The aim of this study is to define what are the airborne magnetic and radiometric signatures of eight bodies in the PGAAP, namely: Bairro da Cruz, Banhadão, Itapirapuã, Barra do Itapirapuã, Barra do Teixeira, José Fernandes, Mato Preto, and Tunas. High-resolution aeromagnetics (HRAM), and radiometric datasets were analyzed to assess the pattern of anomalies over the study area and then comparing them with other previous studies.

5.3 GEOLOGICAL CONTEXT

The Brazilian and South American platforms have been through magmatic activity comprising alkaline and alkaline-carbonatitic complexes starting in the Permian-Triassic and lasting until the Oligocene period. The majority of these complexes in Brazil are of Late Cretaceous age (Gomes and Comin-Chiaramonti 2005).

Alkaline province, according to Almeida (1983), is a term used to define areas of occurrence of clusters of alkaline bodies, with specific rock associations and ages, and are grouped mainly based on their geological setting and recognizable tectonic features (Riccomini et al. 2005; Gomes and Comin-Chiaramonti 2005). Although there is no clear consensus about the definition of alkaline rocks, they may be classified as situated above the X - Y and X - Z lines in the Total Alkalis-Silica - TAS ($Na_2O + K_2O$ vs SiO_2) graph (Gill 2010). They can vary from ultramafic to felsic and are deficient in silica and/or alumina with respect to alkalis (Na_2O, K_2O, and CaO) (Fitton and Upton 1987).

According to Riccomini et al. (2005), in the context of the Paraná Basin, seven alkalines provinces could be recognized in its borders due to tectonic and geological-geophysical evidence. These provinces are Alto Paraguay, Ponta Grossa Arch, Valle Chico, Misiones, Central Paraguay, Amambay, and Rio Apa (Gomes and Comin-Chiaramonti 2005).

The PGAAP resides in the Ponta Grossa Arch, which is an uplifted megastructure that extends for about 600 km in a northwest-southeast trending and its hinge line dips toward NW, the inner part of the Paraná Basin (Piccirillo and Melfi 1988; Piccirillo et al. 1990). It comprises several northwest-trending tholeiitic dike swarms (Ussami et al. 1994) and also four significant magnetic lineaments in the same direction. According to Raposo and Ernesto (1995), the arch is delimited by the Guapiara lineament in the northeast, by the Piqueri or Rio Piqueri in the southeast while the arch's central region contains the São Jerônimo-Curiúva and Rio Alonzo lineaments. These structures have lengths around 600 km and have a width between 20 and 100 km. They may be related to the arch uplift and conditioned the alkaline and tholeiitic magmatism distribution (Ferreira et al. 1984).

Almeida (1983) pointed out thirteen intrusions for the Ponta Grossa Arch, named: Banhadão, Barra do Itapirapuã, Barra do Rio Ponta Grossa, Barra do Teixeira, Cananéia, Itanhaém, Itapirapuã, Jacupiranga, Juquiá, Mar Pequeno (Sabaúma, SP), Mato Preto, Sete Quedas, and Tunas. Later, two more bodies were added to this province: Pariquera-Açu and Registro (Ferreira and Algarte 1979; Ferreira et al. 1987; Mantovani et al. 2005).

The following paragraphs are a brief description of the igneous rocks studied in this work. This information is also summarized in **Table 6**. The bodies are presented in the

geologic maps of Cerro Azul (Brumatti and Almeida 2014) and Apiaí (Morais et al. 2012). The alkaline suites were illustrated in the Results and Discussion section (**5.5.6 Profile analysis**).

Table 6. Summary of the main characteristics of the igneous rocks in the study area.

Rock name	Main lithotypes	Main classification	Coordinates	Age (Ma)	Carbonatites and REE reported
Bairro da Cruz (BC) Complex	Olivine-gabbros and phonolites	Alkaline, basic, intrusive/volcanic	24º52' S, 49º23' W	230±17[a], Upper Triassic	No
Banhadão (BN) Complex	Nepheline syenites and phonolites	Alkaline, basic, intrusive	24º39' S, 49º23'W	106-110[b], Lower Cretaceous	No
Itapirapuã (IT) Nepheline syenite	Undersaturated syenites	Alkaline, basic, intrusive	24°41'27" S, 49°08'30" W	102-106[c], Lower Cretaceous	No
Barra do Itapirapuã (BIT) Carbonatite	Carbonatites (plug)	Alkaline - carbonatite, intrusive	24°41'30'' S, 49°13'00'' W	129±19[d], Lower Cretaceous	Yes
Barra do Teixeira (BT) Phonolite	Peralkaline phonolites (plug)	Alkaline, basic, volcanic	49º26' S, 49º41' W	73-78[d,e], Upper Cretaceous	No
José Fernandes (JF) Gabbro	Variety of gabbros	Basic, intrusive	24°43'30" S, 48°58'59" W	134.93±0.16[f], Lower Cretaceous	No
Mato Preto (MP) Complex	Nepheline syenites, phonolites, and carbonatites	Alkaline (carbonatites), basic, intrusive	24°45' S, 49°12' W	62-76[d,e] Paleocene to Upper Cretaceous	Yes
Tunas (TU) Complex	Syenites and alkali syenites	Alkaline, felsic, intrusive	24°57' S, 49°06' W	70-85[d,g,h,i] Upper Cretaceous	No

References: [a] Hama et al. (1977), [b] Gomes et al. (2018), [c] Ruberti et al. (1997), [d] Cordani and Hasui (1968), [e] Sonoki and Garda (1988), [f] Almeida (2016), [g] Gomes et al. (1987), [h] Rugenski (2006), [i] Siga Jr. et al. (2007).

The Bairro da Cruz Complex is located on the Bocaiúva do Sul municipality, Paraná State. This complex is a small volcanic center of approximately 1 km^2 area showing an oval shape and irregular contours. It is comprised of coarse (olivine-gabbros) and fine (phonolites) varieties, as well as possible basic alkaline affinity rocks at more saturated terms in the central part and the western border of Bairro da Cruz complex. The country rocks are mainly comprised of amphibole-schists and calc-silicate rocks (Hama et al. 1977). In addition, numerous small dikes (maximum of 1 m of width) cut these gabbroic rocks in the area (Hama et al. 1977; Almeida 2016). K/Ar dating in pyroxene-amphibole resulted in an age of 230±17 Ma for the Bairro da Cruz Complex (Hama et al. 1977). These authors suggest that this

intrusion alongside the José Fernandes gabbro represents a previous basic-alkaline magmatism that occurred before the wide basaltic extrusion in the Paraná Basin.

The Banhadão alkaline intrusion is located at 20 km NE of Cerro Azul town, Paraná State. It has an area of 8 km^2 approximately (Gomes et al. 2018) and it was emplaced into the Neoproterozoic Três Córregos granitic suite (Hama et al. 1977; Brumatti et al. 2015). Algarte (1972) and Kaefer and Algarte (1972) demonstrated that the intrusion is composed of nepheline and phonolite syenites. Among the syenites, there are the following varieties: foyaite, nepheline-sodalite-syenlte, muniongite, ijolite, alkali-syenlte, and others (Hama et al. 1977). Brumatti et al. (2015) has divided the complex into five lithofacies: phlogopite melteigite, pink nepheline syenite, melanite-pseudoleucite-nepheline syenite, gray nepheline syenite, and sodalite syenite. Banhadão was defined ranging 106-110 Ma of age using Ar-Ar method on biotite (Gomes et al. 2018).

The Itapirapuã Complex shows an NW-trending irregular shape and it has an approximate outcropped area of 4 km^2 (Brumatti et al. 2015). This intrusion is emplaced into Cerro Azul Granite. Gomes (1970) reported that Itapirapuã consists mainly of undersaturated syenitic medium to coarse rocks variable in texture from hypidiomorphic to inequigranular. Mafic syenites, meltegeites, and pulaskites occur in a less frequent distribution in the area while NW-trending decimeter tinguaites dikes crosscut the other alkaline petrographic types and the granitic country rocks (Gomes et al. 2018). Itapirapuã is situated in an age interval of 102 and ~106 Ma, according to Ar-Ar determinations on biotite and U-Pb SHRIMP on titanite from melanitic syenitic rocks, respectively (Gomes et al. 2018).

The Barra do Itapirapuã intrusion is considered a multiple stockwork (Loureiro and Tavares 1983) forming a complex system where there is an ellipsoidal network of dikes and veins of Fe, Mg and Ca-carbonatites occupying an area around 2 km^2. This intrusion is emplaced in the Neoproterozoic Cerro Azul Granite (Brumatti et al. 2015) and it is located inside the Ribeira Valley being described by Loureiro and Tavares (1983) as showing difficult access and intense weathering. In addition to carbonatitic rocks, carbonatitic lamprophyric breccias and veins bearing quartz, fluorite, REE-rich apatite, REE fluorcarbonates, barite, and strontianite were found in the place (Ruberti et al. 2005). The age interpreted for the carbonatite is 129±19 Ma, according to Ruberti et al. (1997), who used the Rb-Sr whole-rock technique.

The Barra do Teixeira phonolite represents a small circular body with 0.25 km^2 of area, located on the Vila Branca Geological Map (Brumatti and Tomita 2014). Vasconcellos (1995) described the Barra do Teixeira as composed of peralkaline phonolites hosting feldspar phenocrysts surrounded by fibro-radiated zeolites along with fluorite. It is considered a MgO

poor small plug (Vasconcellos 1995; Vasconcellos and Gomes 1998). Barra do Teixeira has an age of around 73-78 Ma, dating approximately at the end of the Cretaceous, according to K-Ar isotopic data (Cordani and Hasui 1968; Sonoki and Garda 1988).

The José Fernandes gabbro is placed located in Adrianópolis town, Paraná State (Chmyz et al. 2011; Almeida 2016). It is emplaced in the Mesoproterozoic Votuverava Group (Morais et al. 2012). Different types of gabbroic rocks, including cumulates, composed the José Fernandes intrusion. This suite is also intruded by synplutonic alkaline dikes (Almeida 2016; Almeida et al. 2019). Almeida et al. (2019) pointed out that the gabbro formed from batches of alkaline magma with different crustal contributions, based on petrographic, isotopic, and geochemical analyses. Almeida (2016) dated an age of 134.93±0.16 Ma (TIMS U-Pb zircon) for this complex.

The Mato Preto alkaline-carbonatitic suite is located in the municipality of Cerro Azul, Paraná (Loureiro and Tavares 1983). Circular in shape, this 12 km^2 area suite (Santos et al. 1990), is situated between the Neoproterozoic Três Córregos granite and the Açungui Group (Loureiro and Tavares 1983). This intensely weathered suite (Loureiro and Tavares 1983) contains alkalic rocks (e.g. nepheline syenites, phonolites, porphyry phonolites, tinguaites) which hosts ferruginous carbonatites and calciocarbonatites (Comin-Chiaramonti et al. 2001). There is also the existence of tuffs, agglomerates, and other silicate rocks, such as ijolites and melteigites. A variety of elements and minerals are related to carbonatite suite in the Mato Preto complex, such as thorium, rare earths, iron, phosphorus, fluorite, magnetite, apatite, pyrite, bornite and in small amounts, uranium, niobium, titanium, and zirconium (Loureiro and Tavares 1983). Cordani and Hasui (1968), using K-Ar isotopic ratio, reported an age of approximately 66 Ma for a phonolite sample from Mato Preto while Sonoki and Garda (1988) outlined an age of 61.9 Ma and 76.4 Ma utilizing K-Ar, suggesting Late Cretaceous ages.

The Tunas alkaline massif has an area of 22 km^2 in an NW direction, according to the direction of Mesozoic dikes (Brumatti et al. 2015) and it is located 80 km from the city of Curitiba in the Ribeira Road, south to the Ribeira river (Algarte 1972; Vasconcellos 1995). This plutonic structure with a felsic nature (Gomes et al. 1987) contemplates in its majority syenites and alkali syenites with subordinate alkali gabbros, syenogabbros, essexites, and syenodiorites. This NW-elongated suite contains 10% of volcanic breccias and small late dikes of syenitic composition were also found in the region (Ruberti et al. 2005; Marangoni and Mantovani 2013). The country rock consists mainly of shales, marbles, and metabasites and to a small extent, quartzites, gneisses, and schists to the northeast (Marangoni and Mantovani 2013). The first ages for the massif were analyzed by Cordani and Hasui (1968) obtaining 110 Ma for two samples and 70 Ma for the others (K-Ar method), suggesting the possibility of this free-carbonatite intrusion (Loureiro and Tavares 1983) to have occurred in more than one

magmatic activity. K-Ar age determination by Gomes et al. (1987) led to an average value of 82 Ma. A similar age was determined by Rugenski (2006), 80.5 Ma, from Rb-Sr isotopic data. Siga Jr. et al. (2007) reported U-Pb syenite's zircon age dating for the Tunas complex around 83 Ma (ID-TIMS) and 85 Ma (SHRIMP).

5.4 MATERIALS AND METHODS

The study area was delimited by coordinates 24º35'10.60" - 25º01'46.66" S and 48º49"10.74" - 49º28'09.04" W, comprising partial regions from the geological maps of Cerro Azul (Brumatti and Almeida 2014) and Apiaí (Morais et al. 2012) (**Figure 14**). These 1:100,000-scale maps were used to discuss the geophysical data in association with the mapped geology.

Magnetic and gamma-ray spectrometric data were provided by CPRM (2011) from the Paraná-Santa Catarina Project (PR-SC). This airborne survey was flown between 2009 and 2011, covering an area over 65,562 km^2 in the Paraná and Santa Catarina states, Brazil. North-south oriented flight lines were spaced 500 m apart. The data were acquired at a terrain clearance of 100 m (CPRM 2011). A Scintrex CS-3 high-sensitivity cesium vapor magnetometer sensor and Exploranium GR-820 airborne gamma spectrometer were used for data collecting and the sampling rate for each sensor was 0.1 s and 1 s, respectively. The coordinate system of the airborne survey was the World Geodetic System (WGS) 84 UTM Zone 22S and, therefore, all the geological and geophysical images were created in this work adopted this coordinate system.

All the magnetic and radiometric data were interpolated onto a 100 m grid cell-size, which represents 1/5 of the spacing between lines, using the minimum curvature algorithm (Briggs 1974; Swain 1976). All the gridding and magnetic and radiometric processing were performed in the Oasis Montaj suite.

The total magnetic intensity (already IGRF-corrected and microleveled) data was gridded and it was reduced to the pole (RTP, Baranov 1957; Baranov and Naudy 1964) according to the parameters calculated for the date of acquisition (**Table 7**).

Table 7. Parameters used for the reduction to the pole for the study area and inverse modeled igneous rocks in this study.

Region	Magnetic inclination	Magnetic declination	Amplitude correction inclination
Study area	-34.49	-18.91	-55.51
Bairro da Cruz	-34.96	-19.02	-55.04
José Fernandes	-34.73	-18.79	-55.27
Tunas	-34.87	-18.86	-55.13

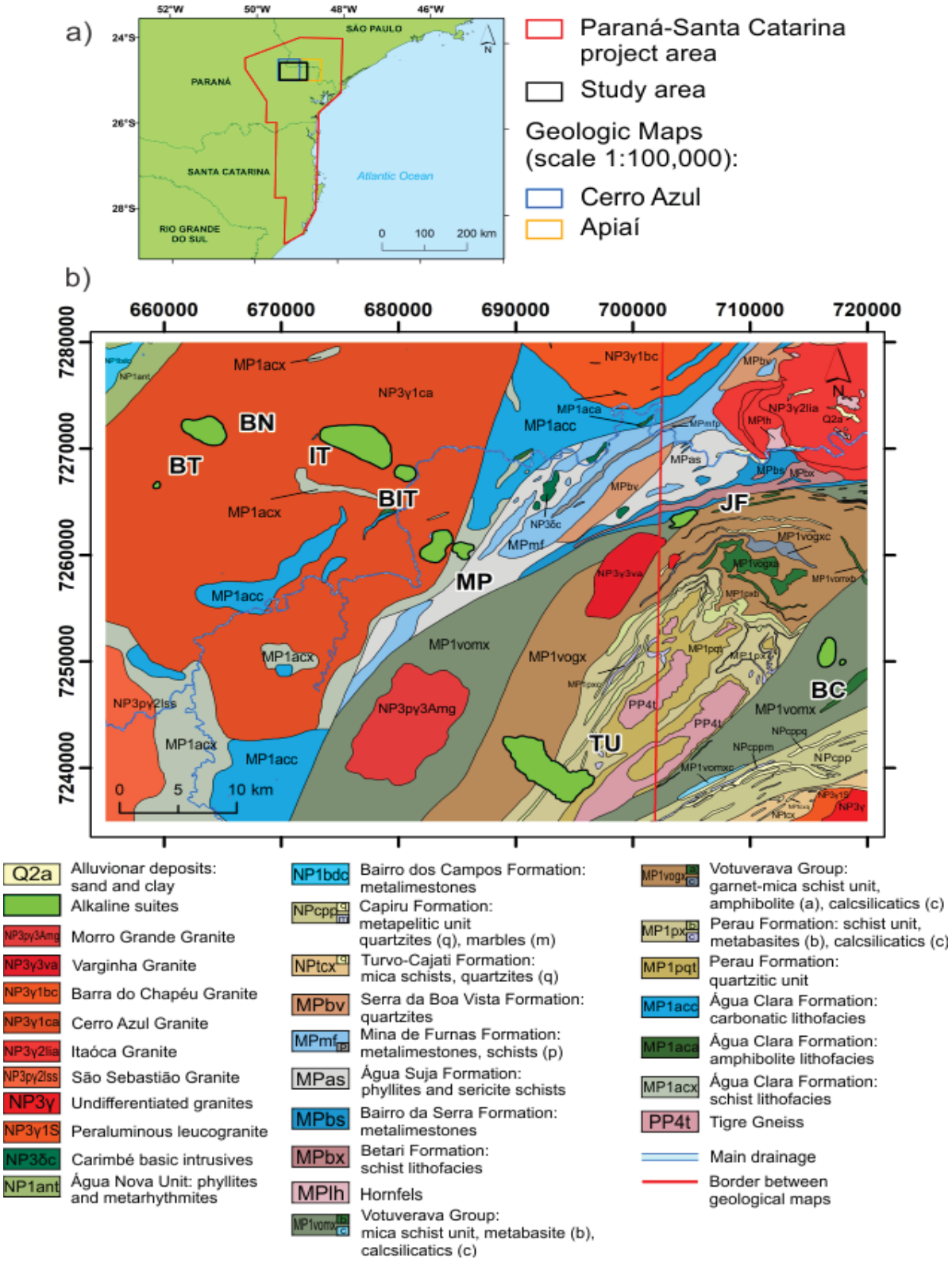

Figure 14. Image of the study area inside the Paraná-Santa Catarina airborne survey and in the Cerro Azul (Brumatti and Almeida 2014) and the Apiaí (Morais et al. 2012) geologic maps (a). Simplified geological map for the study area (b). Alkaline complexes: Bairro da Cruz (BC), Barra do Itapirapuã (BIT), Banhadão (BN), Barra do Teixeira (BT), Itapirapuã (IT), José Fernandes (JF), Mato Preto (MP), and Tunas (TU).

Semiquantitative analyses involved the estimation of depths for the study area from the radially averaged power spectrum (RAPS, Spector and Grant 1970), Euler 3D deconvolution (Reid et al. 1990), and tilt angle (Miller and Singh 1994). The steps to generate the RAPS and to calculate the average depth of each source component were performed according to the procedure of Cowan and Cowan (1993), where each line segment with a constant slope of the power spectrum was attributed to a determined depth. Then, this slope is divided by 4π to find the depth to the top of the magnetic sources according to the equation $h = -s/4\pi$ (Cowan and Cowan 1993), where h is the depth to the top of the sources and s is the slope of one of the components of the sources. An energy spectrum for magnetic data may exhibit three or four parts: a deep source component, a middle source component, a shallow source component, and a white noise component. With respect to the Euler 3D solutions, it was assigned a structural index (SI) equal to 1 (relative to dikes), a maximum depth tolerance of 5%, and a window size (grid points) of 20 times the grid cell size. These parameters showed a better result comprising a reasonable number of solutions in the study area rather than other parameters tested, such as SI equal to 0 (contact type) and lower grid cell-sizes. Depth estimates from the tilt angle were also performed on the RTP-TMI data. This method described in Blakely et al. (2016) determines the depth below flight elevation of the zero contours (edges of causative sources) from the arctangent of vertical derivative divided by total horizontal derivative of the anomaly.

Structural magnetic analysis was also performed. The vertical derivative of RTP-TMI grid was generated to highlight high-frequency details and to trace lineaments that later were associated with the known geology. The delineation of structural features in the study area was done on this filter due to its capacity of enhancing shallow features and it does not have a bias of direction (Isles and Rankin 2013). 2D analysis from magnetic lineaments, discontinuities, magnetic sources, and their limits have been performed to assess geological unit trends and it plays an important role in identifying and delimiting main magnetic structures. Many recent studies have used this texture analysis from aeromagnetic data (Holden et al. 2012; Moro et al. 2018; Pereira and Ferreira 2018).

Moreover, the analytic signal of the vertical integration (ASVI) and vertical integral of analytic signal (VIAS) were gridded for use in 3D inversions. These techniques were introduced by Paine et al. (2001) and consist of transforming the TMI data into measures weakly dependent on the magnetization direction by calculating the total gradient of the vertical integration of the TMI (ASVI) or vertically integrating its total gradient (VIAS). These quantities are treated as if they were reduced to the pole allowing the 3D magnetic susceptibility algorithm inversion developed by Li and Oldenburg (1996) to be performed. Li et al. (2010) pointed out that the data transformed by this method are not true magnetic

anomalies while the inversion algorithm used considers only induced magnetization. Although there is this inconsistency, both ASVI and VIAS lead to interpretable results (Leão-Santos et al. 2015; Li 2017) being appropriate for isolated or multiple sources as well (Pilkington and Beiki 2013).

The complexes that showed a significant magnetic response, i.e. Bairro da Cruz, José Fernandes, and Tunas, were 3D unconstrained inverse modeled to obtain an estimate of the distribution of their magnetic susceptibilities and depth of emplacement. Inversions were applied in the TMI, RTP-TMI, VIAS-TMI, and ASVI-TMI grids. The RTP parameters for each modeled body were described in **Table 7**, while the parameters used for the inversions were illustrated in **Appendix 2**.

In terms of radiometric processing, basic grids (K, eTh, and eU) were corrected following the procedure of Ferreira et al. (2009) where each radioactive element received a constant to keep its minimum value to 0.01 and, therefore, avoiding divisions by values equal or below to zero when ratioing (Weihermann et al. 2016). The constants added to the K, eTh, and eU grids were 1.05%, 1.22 ppm, and 2.39 ppm, respectively.

Fourteen ratios maps were created following the procedure of Grant (1998), where instead of calculating the ratios from line data and then gridding them, divisions were performed from the gridded data. The ratios generated were: K/eU, K/eTh, K/(eU+eTh), F=K*(eTh/eU) (F-parameter, Efimov 1978; Gnojek and Prichystal 1985), eU/eTh, eU/K, eU/(K+eTh), eU/(K+eU+eTh), eTh/K, eTh/(K+eU), (eTh+eU)/K, (K*K)/(eU*eTh), (eU*eU)/eTh, and (eTh*eTh)/K. In addition, the parameters thorium-normalized potassium (KD), thorium-normalized uranium (UD) and DRAD (Saunders et al. 1987, 1993, 1994), were also implemented to evaluate the concentration of potassium and eU when they are normalized in relation to eTh. Equal-area distribution was used for zone color ranges in the analysis of ratios and other parameters images. A ternary R-K, G-eTh, B-eU image was also generated for the study area.

The minimum, average and maximum levels of K, eTh, and eU of each intrusion in the study area were determined from the gridded data and plotted in box-plot charts while radioelements concentrations for each sampled data point inside complexes' boundaries (according to the geological maps previously described in this work) were illustrated in normalized ternary diagrams created in the TriPlot software and later refined in the Origin suite to identify trends in K, eTh, and eU concentrations. In contrast to the grids corrections, negative sampled data points were attributed null values to avoid miscalculating relative concentrations of K, eTh, and eU in the diagrams.

Stacked profiles containing the variables K, eU, eTh, TMI, RTP-TMI, and Digital Terrain Model (DTM) from the PR-SC airborne survey flight lines were plotted along the mapped lithotypes for each intrusion to assess their absolute and relative levels. Profiles are useful to display more reliable data, i.e. with full spatial resolution, than a grid. This is due to the use of filters along flight lines for the grid interpolation to avoid aliasing problems (Horsfall 1997). No correction of negative or zero values for the radioelements was applied. This derives from the fact that quantities below or equal to zero may be a valid representation of the radiometric dataset, which is characterized by statistics and, therefore, supports data that lie outside the expected interval of values, even after all the treatments carried after the acquisition phase (Grant 1998).

5.5 RESULTS AND DISCUSSIONS

5.5.1 Magnetic field of the study area

Magnetic field values in the study area presented an amplitude of approximately 1000 nT (**Figure 15**). No significant representation of classical dipolar anomalies was observed for IT, BIT, BN, BT, and MP igneous rocks even when TMI data was interpolated in a rectangular area around the location of the intrusions. This behavior can be explained by the common lack of strong magnetization of these types of rocks (Airo 2015). It should be noted that the Barra do Itapirapuã and the Mato Preto complexes did not produce circular magnetic anomalies or any distinctive magnetic signature, unlike other alkaline-carbonatitic complexes cited in the literature (e.g. IIvaara, Sokli, Airo 2015).

The dipolar anomaly of the Bairro da Cruz Complex could be attributed to the presence of coarse olivine-gabbros (Hama et al. 1977), which is one of the most ferromagnetic igneous rocks (Clark 1999). The same could be said about the José Fernandes Gabbro, an intrusion with a strong magnetic response that was even detected in lower quality airborne survey datasets (Ferreira and Algarte 1979).

High anomalies are located in the eastern part of the study area and to less extent southeast and the north of the Banhadão and Itapirapuã suites. The shape and NW-direction of anomalies in the southwestern part (**Figure 15b**) infer that the source bodies are comprised of dikes, which are widely presented in the Ponta Grossa Arch (Raposo and Ernesto 1995; Brumatti and Almeida 2014).

5.5.2 Estimate of depths

The radially averaged power spectrum (RAPS) from TMI grid was generated to assess the depth to the top of magnetic sources (**Figure 16**). This graph showed that three lines over

the power spectrum (blue line) could be identified. Each gradient of these lines represents a component of deep, middle, and shallow sources. Deep sources are situated at 1.70 km depth, the middle sources at 0.60 km and shallow ones are approximately at 0.50 km. Deep sources have wavelengths over 30 km, almost ten- and thirty-fold higher than the values of middle and shallow sources, respectively. Smaller wavelengths were considered noises and were not considered for depth estimates over the power spectrum.

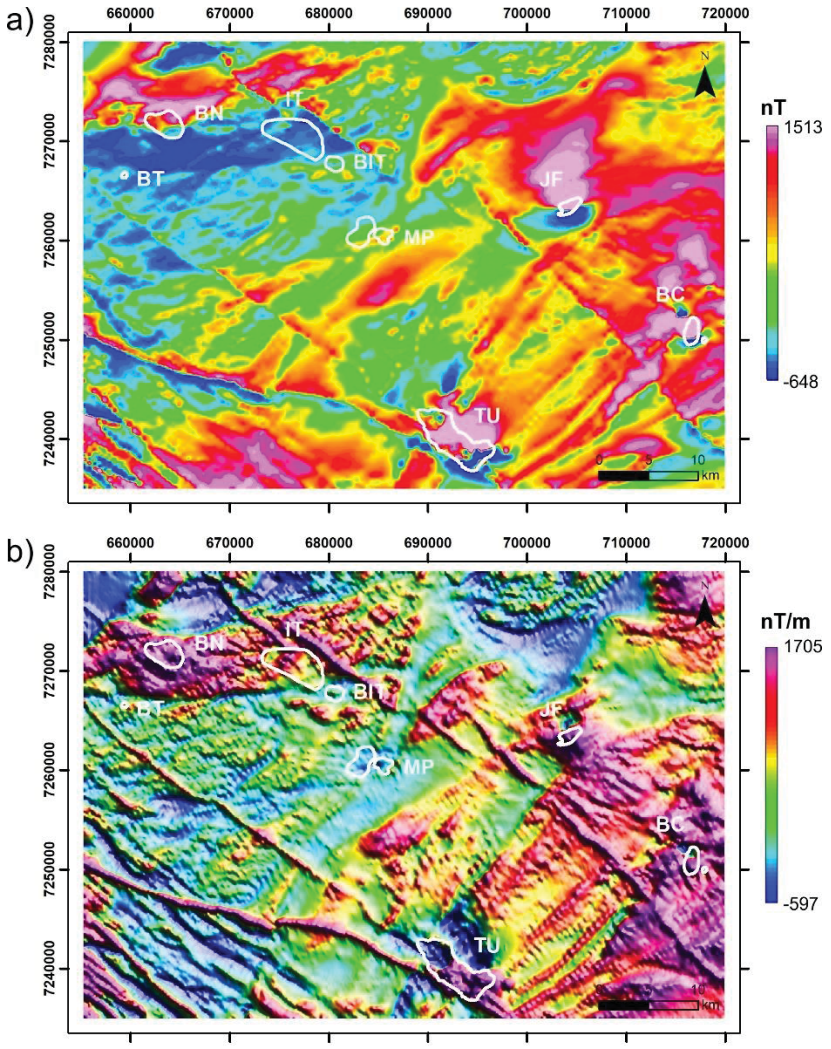

Figure 15. TMI map data from study area (a) and its reduction to the pole (b) with hue-saturation-value (HSV) model colour shaded (45° declination and inclination). Thick white lines represent the alkaline complexes: Bairro da Cruz (BC), Barra do Itapirapuã (BIT), Banhadão (BN), Barra do Teixeira (BT), Itapirapuã (IT), José Fernandes (JF), Mato Preto (MP), and Tunas (TU).

The quantity of noise in the data could be attributed to the interference of dikes mapped by Brumatti and Almeida (2014) presented in the southwestern part. The dikes could be considered a part of shallow structures and even middle ones, given that there are no huge intervals between the depth of each type of source. Shallow and middle depths were interpreted as small-scale fractures along with the dikes while deep sources may suggest

large alkaline bodies as well as their country rocks, e.g. Cerro Azul Granite, which is the country rock of 5 of 8 bodies studied in this work (Banhadão, Barra do Teixeira, Barra do Itapirapuã, Itapirapuã, and half of the Mato Preto suite).

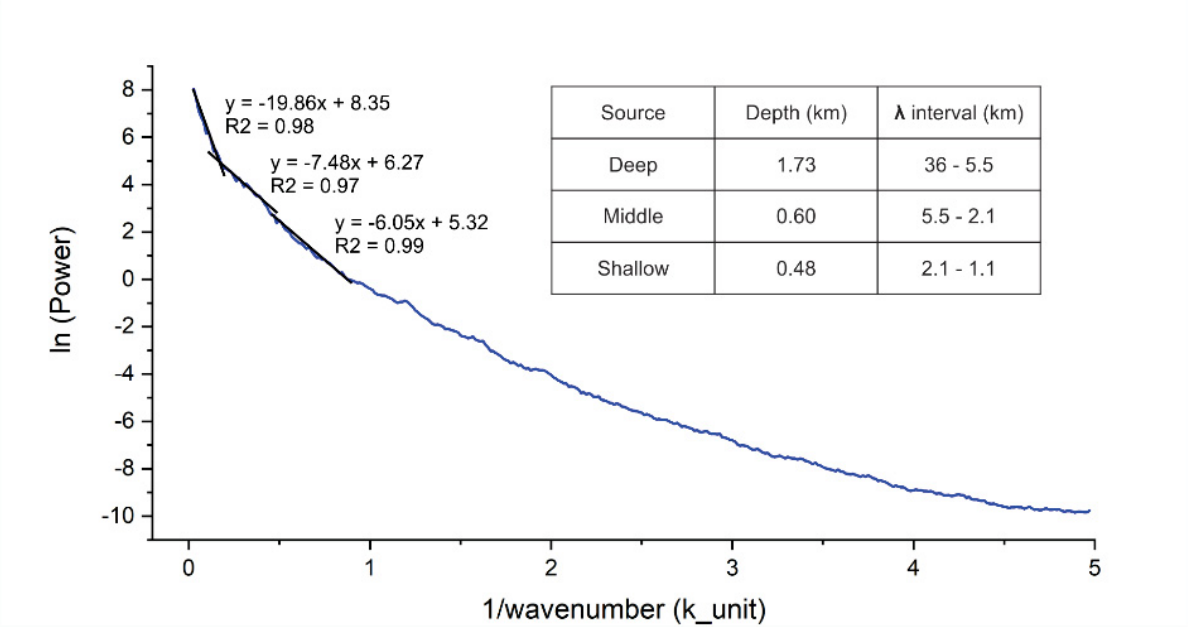

Source	Depth (km)	λ interval (km)
Deep	1.73	36 - 5.5
Middle	0.60	5.5 - 2.1
Shallow	0.48	2.1 - 1.1

Figure 16. RAPS obtained from the study area TMI data showing different segments (black lines) representing depth to the top of sources. “ln” stands for natural logarithm while the "k_unit" in the graph means kilo unit, which is ground unit times 1000 (e.g. 1 kilometer = 1000 meters). The equations refer to the linear trendline of each component along with the coefficient of determination (R2).

Another result to estimate depth sources can be seen in **Figure 17** and **Figure 18**, using the standard Euler deconvolution and the tilt angle techniques, respectively. The depths were divided according to the type of sources characterized in the power spectrum. The majority of Euler solutions showed depths to the top around 0 to 400 m (**Figure 17**). It is worth noting that middle and deep sources are NE-oriented in general while the shallow structures are defined in an NW direction. The tilt derivative method (**Figure 18**) outlined the edges of the causative sources and displayed that those are comprised almost entirely by shallow depths. Both methods demonstrated that the causative sources over the intrusions are mainly at depths up to 400 m.

5.5.3 2D magnetic lineaments analysis

The first vertical derivative (**Figure 19a**) was used to delineate lineaments (**Figure 19b**) over the study area. It can be seen that broader and deeper anomalies are comprised in a type of corridor with a trend around N50E between the Mato Preto and José Fernandes intrusions. The lineaments that bound this corridor are considered first-order since they commonly separate magnetic domains (Curto et al. 2014).

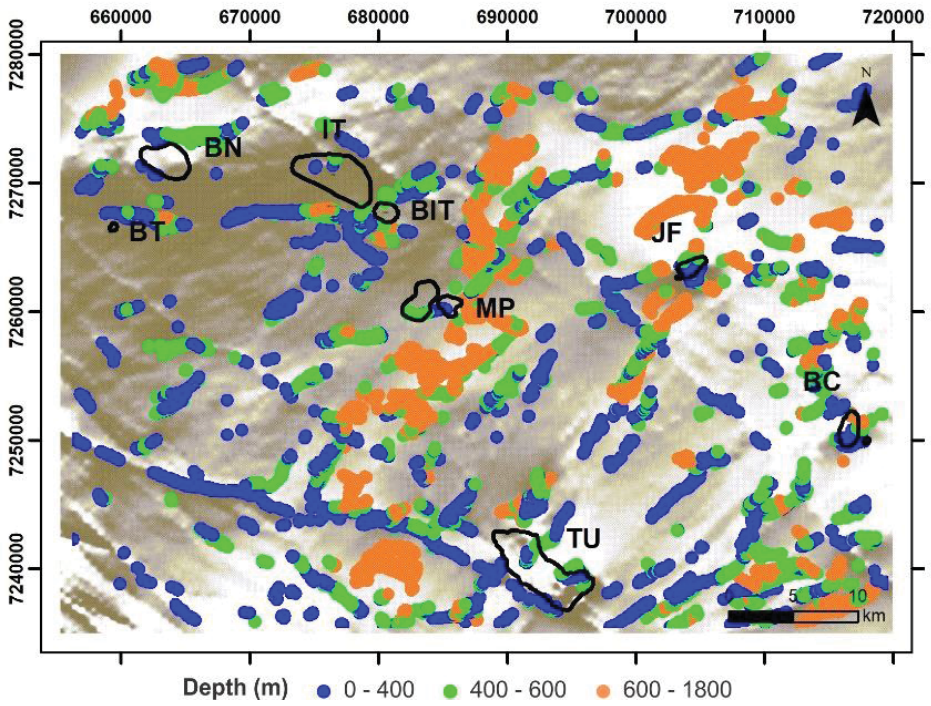

Figure 17. Standard 3D Euler deconvolution solutions over the TMI grid using structural index 1, maximum depth tolerance of 5%, and squared window of 20 times the grid cell size of 100 m.

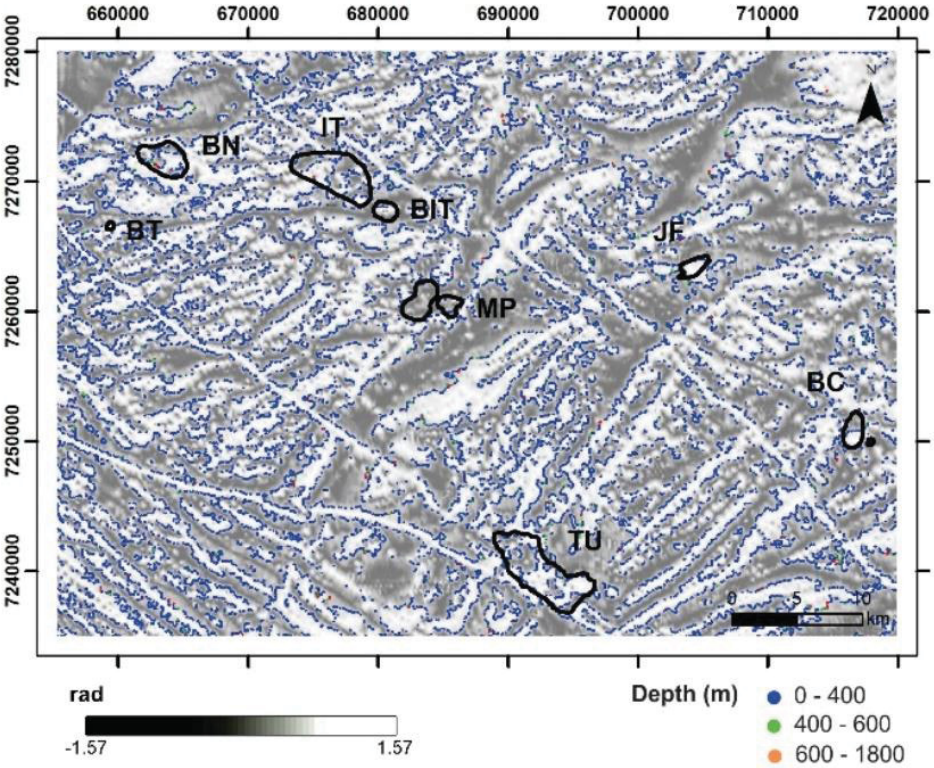

Figure 18. Source delimitation and depths estimated from the tilt angle. Depths (colored circles) are located over the zero contours of the tilt derivative of RTP-TMI grid (in grayscale).

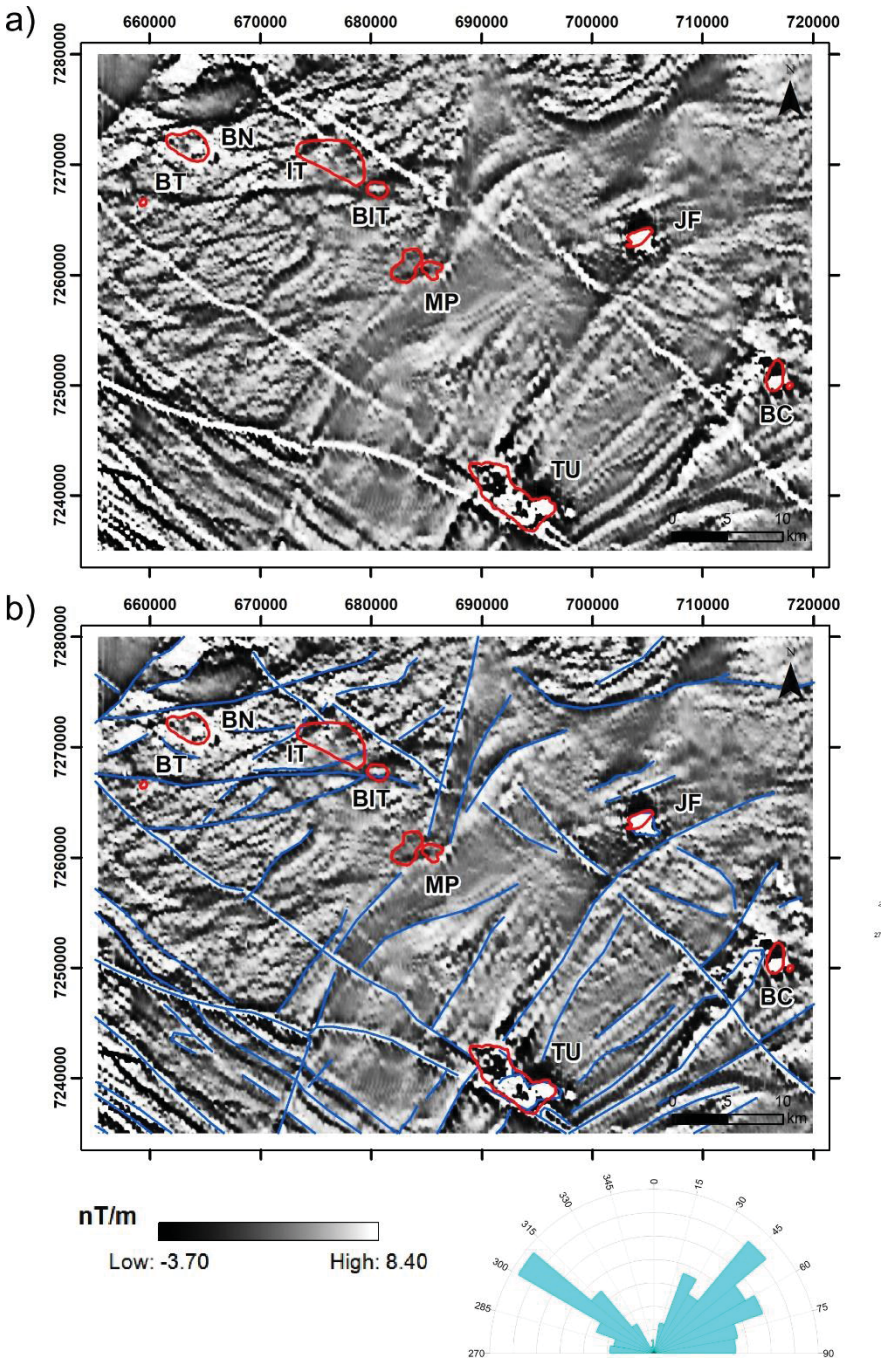

Figure 19. First vertical derivative (1st VD) of the RTP-TMI data (a) where prominent lineaments (blue) were interpreted (b). The rose diagram shows the orientation of magnetic lineaments.

Extensive magnetic lineaments (i.e. over 20 km) are presented with orientation N30E and N30-45W. In addition, there are smaller lineaments with length around 10 km in the east-west direction placed in the northwest region.

Three principal lineaments with strong vertical derivative intensities with a preferred direction of N20-40W and length over 30 km could be observed. The first is located north to the Itapirapuã and extends to the south of Bairro da Cruz. The second and third are located to the south of Barra do Teixeira and converge on the Tunas intrusion. These principal

lineaments and the ones located in a similar direction and with 5 km or more length were considered second-order while third-order were those with an east-west direction and commonly do not extend more than 10 km.

A concentrated distribution of N30-40W-oriented lineaments, located in the southwestern portion, could be attributed to dikes responses, as they were mapped in the same region according to the Cerro Azul geological sheet from Brumatti and Almeida (2014).

5.5.4 Inverse modeling

In this section, the intrusions that presented a significant magnetic response were inversely modeled to assess their magnetic susceptibilities and depths. TMI, RTP-TMI, ASVI-TMI, and VIAS-TMI grids for Bairro da Cruz, José Fernandes, and Tunas were illustrated to compare the magnetic susceptibility model with each grid. Profiles for these igneous rocks were reduced to the pole (**Figure 20**) to evaluate the influence of remanent magnetism before inversion. Positions of RTP-TMI profiles' peaks in comparison with TMI ones may suggest that the induced field is the principal type of magnetism and that remanent magnetism does not significantly affect the magnetization direction. It is known that diabase dikes in the area can carry remanence and therefore could influence the response for the igneous bodies. However, Raposo and Ernesto (1995) demonstrated that the vast majority of dikes in the Ponta Grossa Arch have remanent magnetization with normal polarity. Furthermore, TMI grids of Bairro da Cruz (**Figure 21a**), José Fernandes (**Figure 23a**), and Tunas (**Figure 25a**) showed positive anomalies in their north lobes while the negatives concentrated over their southern portions. This is in good agreement with induced magnetic responses for bodies located in the earth's southern hemisphere that are not significantly affected by remanence (Louro et al. 2017).

5.5.4.1 Bairro da Cruz Complex

It is known from the literature that TMI airborne magnetic data for BC is situated between -250 nT and 500 nT (Ferreira and Algarte 1979) and configures a normal dipole anomaly (Almeida 2016). **Figure 21a** illustrates magnetic values around -530 nT for the negative lobe of BC anomaly and over 1260 nT in the positive one. This represents an important increase of over two times in the amplitude interval reported by Ferreira and Algarte (1979). It may be reasonable to suppose that lower values found for BC are due to the lower resolution of the airborne survey acquired (CPRM 1978), which consisted in space between flight lines of 1 km and flight height of 150 m.

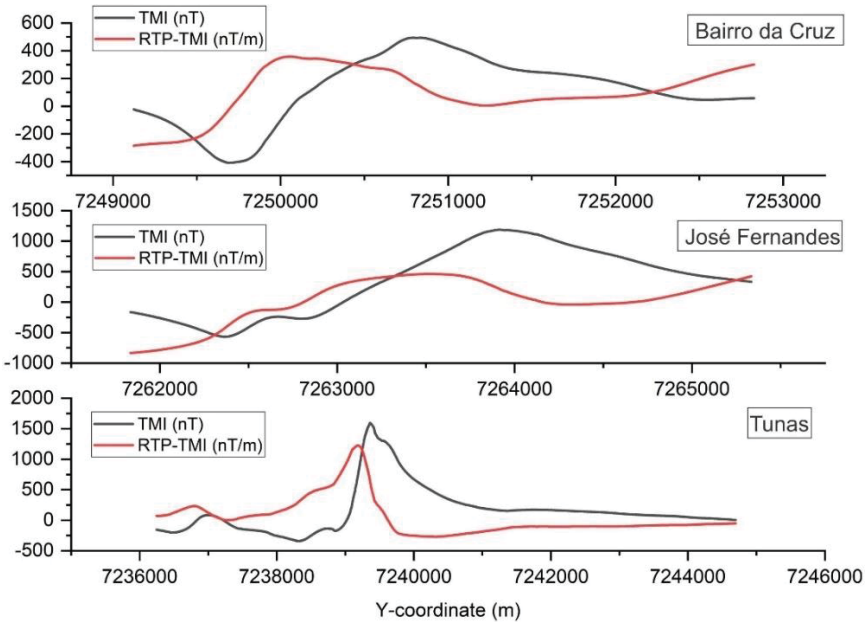

Figure 20. TMI and RTP-TMI profiles for Bairro da Cruz, José Fernandes, and Tunas intrusions. Flight line numbers of the PR-SC project used to create the profiles: L12845:915 (Bairro da Cruz), L12595:697 (José Fernandes), and L12405:686 (Tunas). These flight lines are the same as illustrated on the **Figure 29**, **Figure 34**, and **Figure 38** profiles.

As indicated in **Figure 21b**, the reduced to the pole anomaly was not located in the center of the outcropped Bairro da Cruz borders. Better results were found for the ASVI and VIAS of TMI data (**Figure 21c,d**). No significant differences were found between these two methods. Moreover, none of the grids resulted in an appropriate response for the eastern body of Bairro da Cruz. All the enhancements methods applied practically showed scarce differences in this area. A possible explanation for this might be that this body has a different composition than its western counterpart and, therefore, lacks any magnetic contrast to its country rock. It is important to bear in mind that in the geological map presented by Hama et al. (1977) there is no eastern part for the Bairro da Cruz intrusion while the Apiaí Geological Map (Morais et al. 2012) lacks any information about this mapped rock related to its petrography or composition.

Inversions are displayed in **Figure 22**. In general, the contrast of apparent magnetic susceptibility values was similar, with the RTP-TMI showing the highest maximum between the models. Nevertheless, this model along with the TMI one created several bodies and no significant correlation was found with the outcropped surface. The ASVI-TMI and VIAS-TMI inversions displayed ellipse-shaped features with magnetic susceptibility distribution more elongated in the Z-axis. All the models have illustrated susceptibilities inside the range for gabbros (i.e. 3.10^{-4} to 0.3 SIu), according to the classification of Clark (1997). Negative values of magnetic susceptibility were situated above -1, which can be explained by diamagnetic minerals (e.g. quartz) in the meta-arenites and quartzites present in the country rock of Bairro

da Cruz, Mica schists unit. However, phonolite magnetic susceptibilities (10^{-5} to 10^{-3} SIu, see Clark 1997) were not successfully represented in the modeling of **Figure 22**. One possible explanation for this is that the Bairro da Cruz is a small body and, therefore, it was not appropriated sampled in the airborne survey. Another reason is that the phonolites are weakly magnetic (Clark and Emerson 1991), thus ensuring a poor distribution of magnetic susceptibility for this rock type.

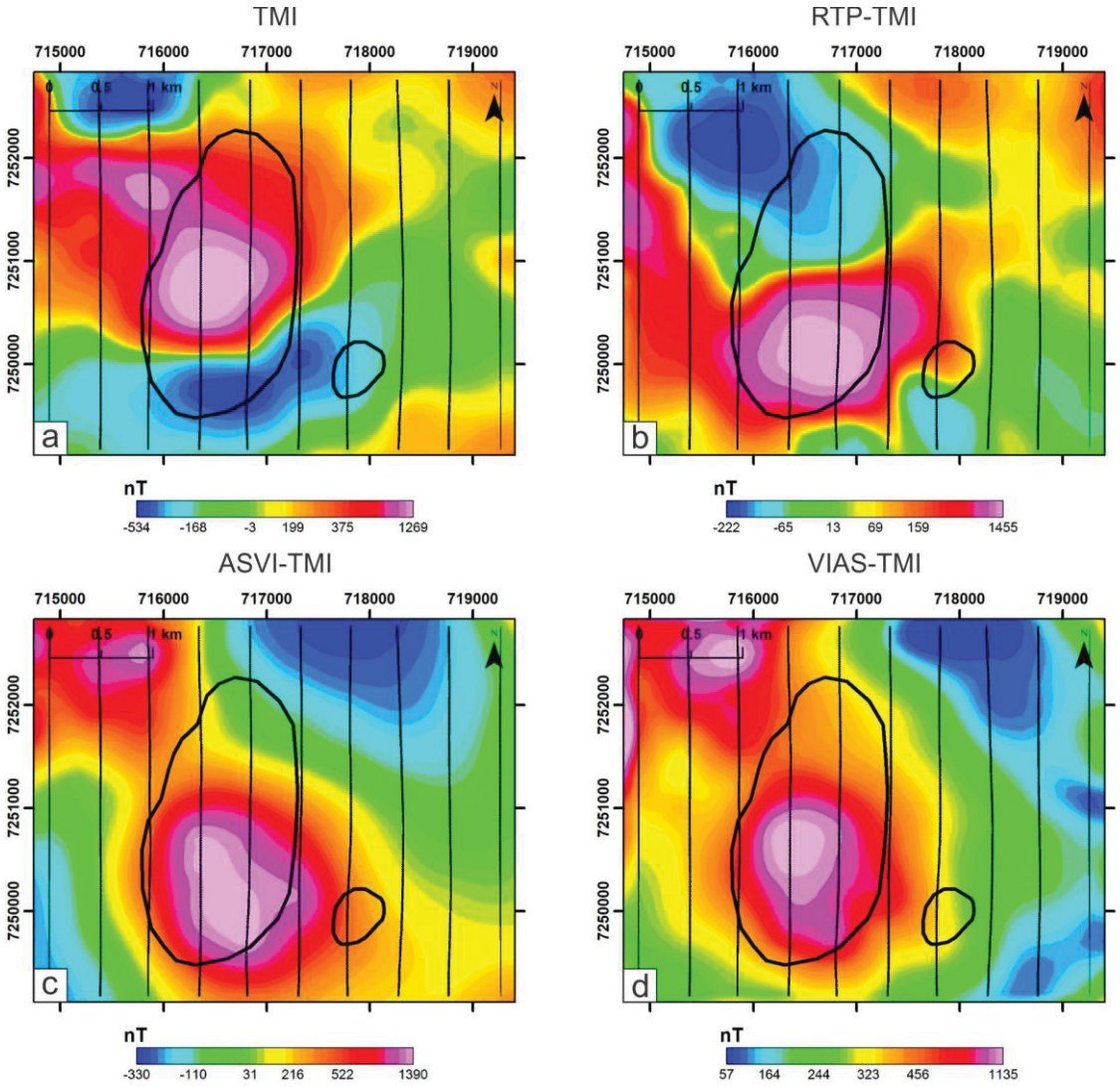

Figure 21. Grids used for the inverse modeling of Bairro da Cruz Complex (black polygons): a) Total magnetic intensity (TMI), b) TMI reduced-to-pole (RTP-TMI), c) Analytic signal of the vertical integral of TMI (ASVI-TMI) and d) Vertical integral of the analytic signal of TMI (VIAS-TMI). N-S oriented black lines are the airborne survey flight lines.

Altitudes for all the susceptibility models were situated between 650 and -1650 m. In summary, these results suggest that the Bairro da Cruz could have a thickness of around 2 km reaching a depth of more than 1 km below the Mean Sea Level (MSL).

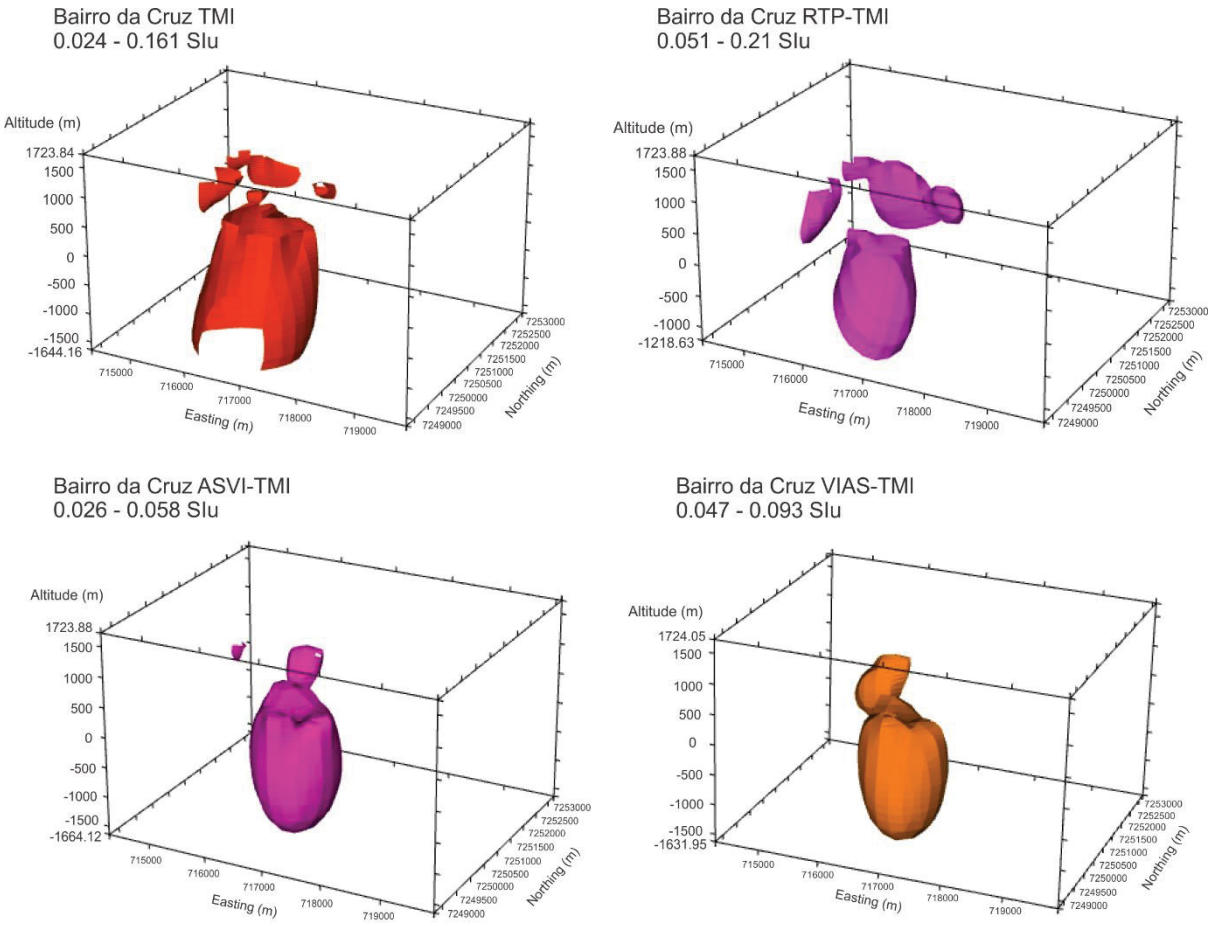

Figure 22. Contrast of apparent magnetic susceptibility distribution in 3D models for each type of Bairro da Cruz gridded data described in **Figure 21**. Models were cut in an arbitrary threshold value (displayed on the image) to create a better representation with the surface geology. Minimum values for each model: -0.111 (TMI), -0.125 (RTP-TMI), -0.046 (ASVI-TMI) and -0.058 SIu (VIAS-TMI). The maximum values of magnetic susceptibility were not modified. Altitudes are GPS altitudes and zero values correspond to the Mean Sea Level (MSL).

5.5.4.2 José Fernandes Gabbro

The results obtained from the gridded magnetic data of José Fernandes are summarized in **Figure 23**. From the data, it can be seen that a magnetic dipole with normal polarity is presented for the José Fernandes gabbro (**Figure 23a**). This result reflects those of Ferreira and Algarte (1979) and Almeida (2016), who also found a similar anomaly for this body. The reduced to the pole data (**Figure 23b**) displayed amplitudes around 1600 nT while it has positioned the center of the anomaly in the western portion of the geological body while the ASVI-TMI and VIAS-TMI (**Figure 23c**,**d**) created two strong anomalies located near the center of the José Fernandes gabbro. None of the models observed displayed anomalies with the same NE-trend observed for the JF in the geological map of Morais et al. (2012).

The magnetic susceptibility inversion models for this gabbro (**Figure 24**) illustrated values between 0 and 0.250 SIu which is consistent with gabbros results from Clark (1997). JF is emplaced in metasedimentary rocks (Morais et al. 2012) and, thus, values of magnetic susceptibility below or close to zero could be attributed to those rock types. Susceptibility models were situated between 550 and -1430 m of altitude, thus, suggesting thickness for the causative sources around 800 and 1000 m. A note of caution is due here since there is no magnetic data available which could support better approximations for the distribution of susceptibility.

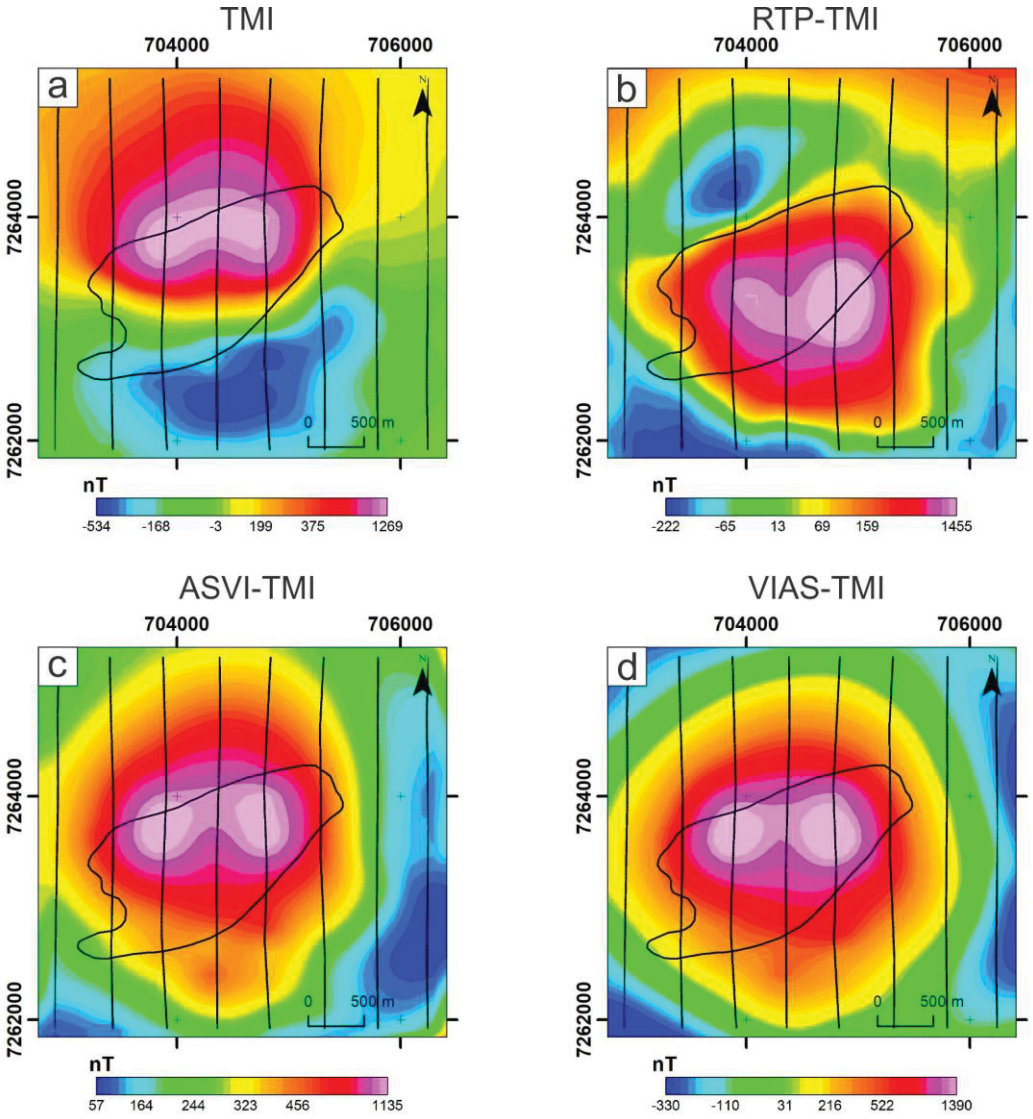

Figure 23. Grids used for the inverse modeling of José Fernandes Gabbro (black polygon): a) Total magnetic intensity (TMI), b) TMI reduced-to-pole (RTP-TMI), c) Analytic signal of the vertical integral of TMI (ASVI-TMI) and d) Vertical integral of the analytic signal of TMI (VIAS-TMI). N-S oriented black lines are the airborne survey flight lines.

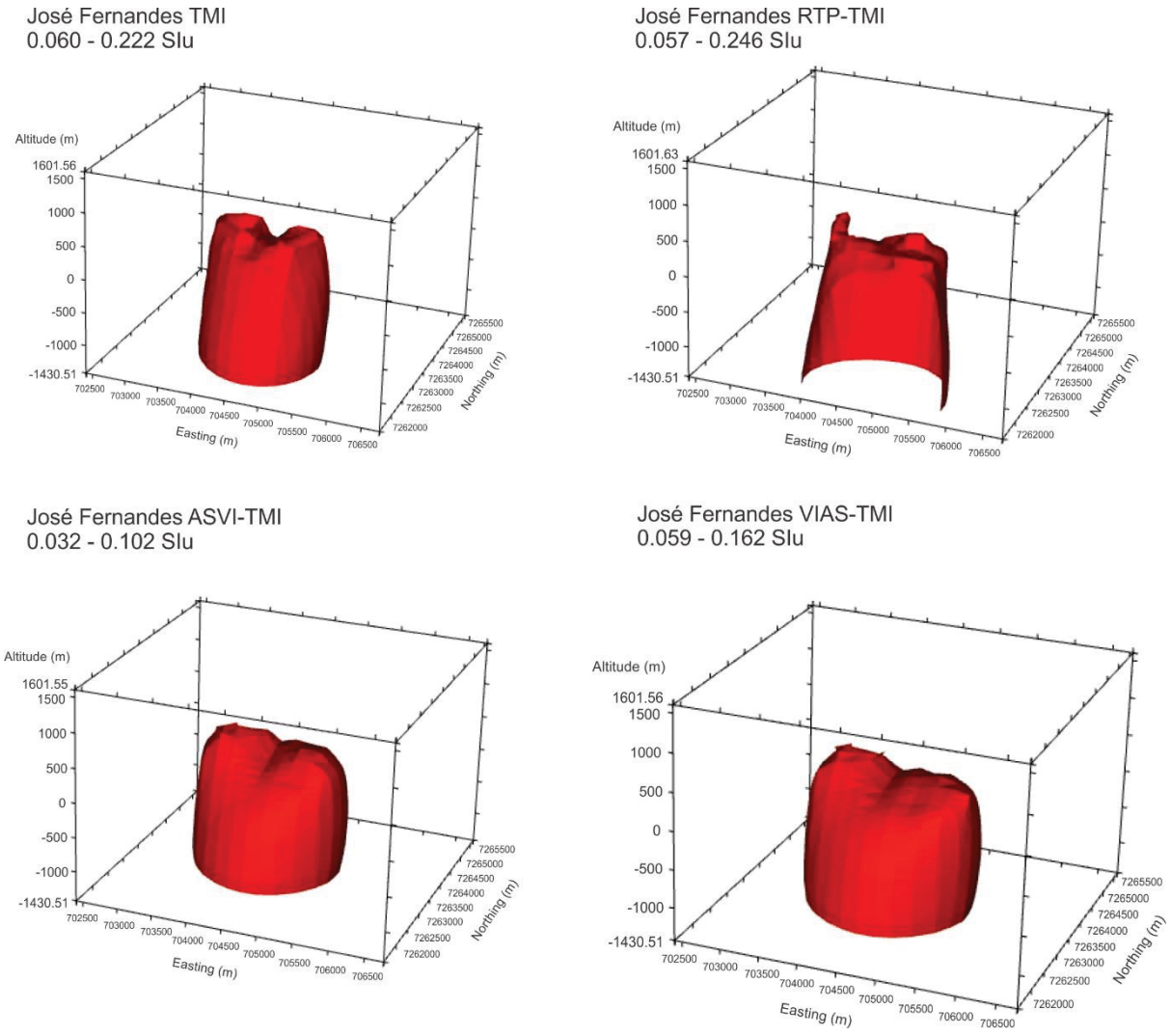

Figure 24. Contrast of apparent magnetic susceptibility distribution in 3D models for each type of José Fernandes gridded data described in **Figure 23**. Models were cut in an arbitrary threshold value (displayed on the image) to create a better representation with the surface geology. Minimum values for each model: -0.108 (TMI), -0.136 (RTP-TMI), -0.039 (ASVI-TMI) and -0.074 SIu (VIAS-TMI). The maximum values of magnetic susceptibility were not modified. Altitudes are GPS altitudes and zero values correspond to the Mean Sea Level (MSL).

5.5.4.3 Tunas Complex

The magnetic response of the Tunas Complex is illustrated in **Figure 25**. It can be observed from the total magnetic intensity data (**Figure 25a**) that positive values are situated in the north and low values in the south. However, it is in the southeastern portion of this alkaline complex that a dipole anomaly with more than 1 km of extension could be visualized. TMI values were situated in the -650 and 1510 nT interval, which is higher than the ones reported by Ferreira and Algarte (1979) and Rugenski (2006), i.e. -600 to 1000 nT, -300 to 800 nT, respectively. A possible explanation for this might be that these authors have processed the data from the Serra do Mar airborne survey (CPRM 1978), which has different flight lines directions (i.e. NW) and is undersampled comparing to the Paraná-Santa Catarina

project. RTP, ASVI, and VIAS applied to the TMI data (**Figure 25b**,**c**,**d**) have positioned a strong anomaly over the southeastern area of Tunas massif with maximum values around 1600 nT and up to 3000 nT for the VIAS-TMI image (**Figure 25d**). This result may be explained by the fact that the VIAS technique may have caused significant amplification of low-frequency components of data, which is a drawback of this method pointed out by Paine et al. (2001).

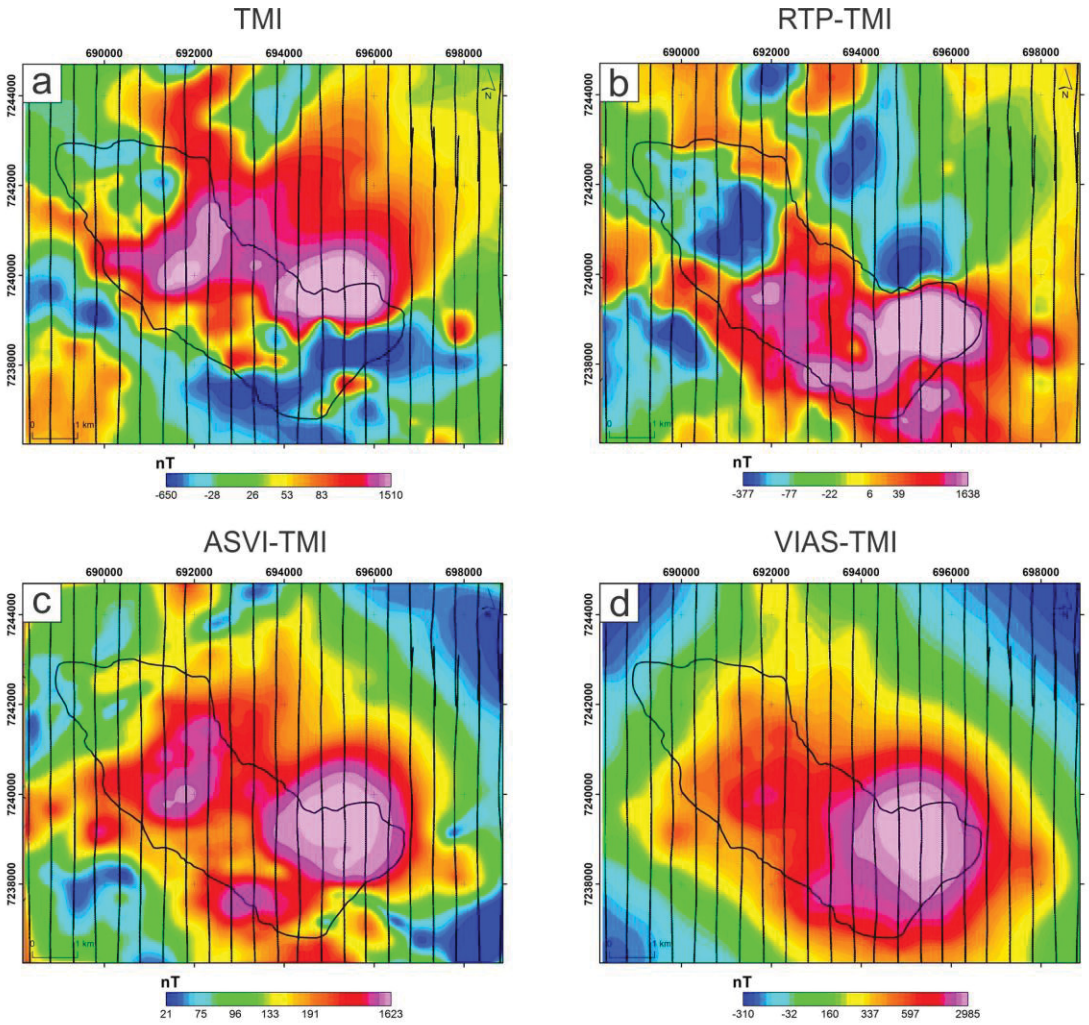

Figure 25. Grids used for the inverse modeling of Tunas Complex (black polygon): a) Total magnetic intensity (TMI), b) TMI reduced-to-pole (RTP-TMI), c) Analytic signal of the vertical integral of TMI (ASVI-TMI) and d) Vertical integral of the analytic signal of TMI (VIAS-TMI). N-S oriented black lines are the airborne survey flight lines.

Distribution models of contrast of apparent magnetic susceptibility (**Figure 26**) demonstrated an NW-trend. This finding is consistent with that of Brumatti et al. (2015) who mapped Tunas. However, our results were not very encouraging since they created a significant quantity of bodies for the TMI and RTP-TMI data while ASVI and VIAS enhancements do not correspond to the outcropped geology of a single intrusion. The values were situated over 0.02 to 0.2 SIu. Comparison of these results with studies related to other alkaline complexes in Brazil suggest similarities, such as Jacupiranga (0.001 to 0.161 SIu, Alva-Valdivia and López-Loera 2011), Juquiá (0.048 SIu, Rugenski 2006), Araxá (maximum

of 0.234 SIu, Pereira et al. 2010), and Catalão I (0.17 SIu, Mantovani et al. 2016). The exception is the VIAS-TMI data which displayed quantities between 0.04 and 1.91 SIu. This is a rather unexpected result suggesting that the VIAS method (**Figure 25**) had amplified the low frequencies components from the magnetic field, a limitation of this technique reported by Paine et al. (2001).

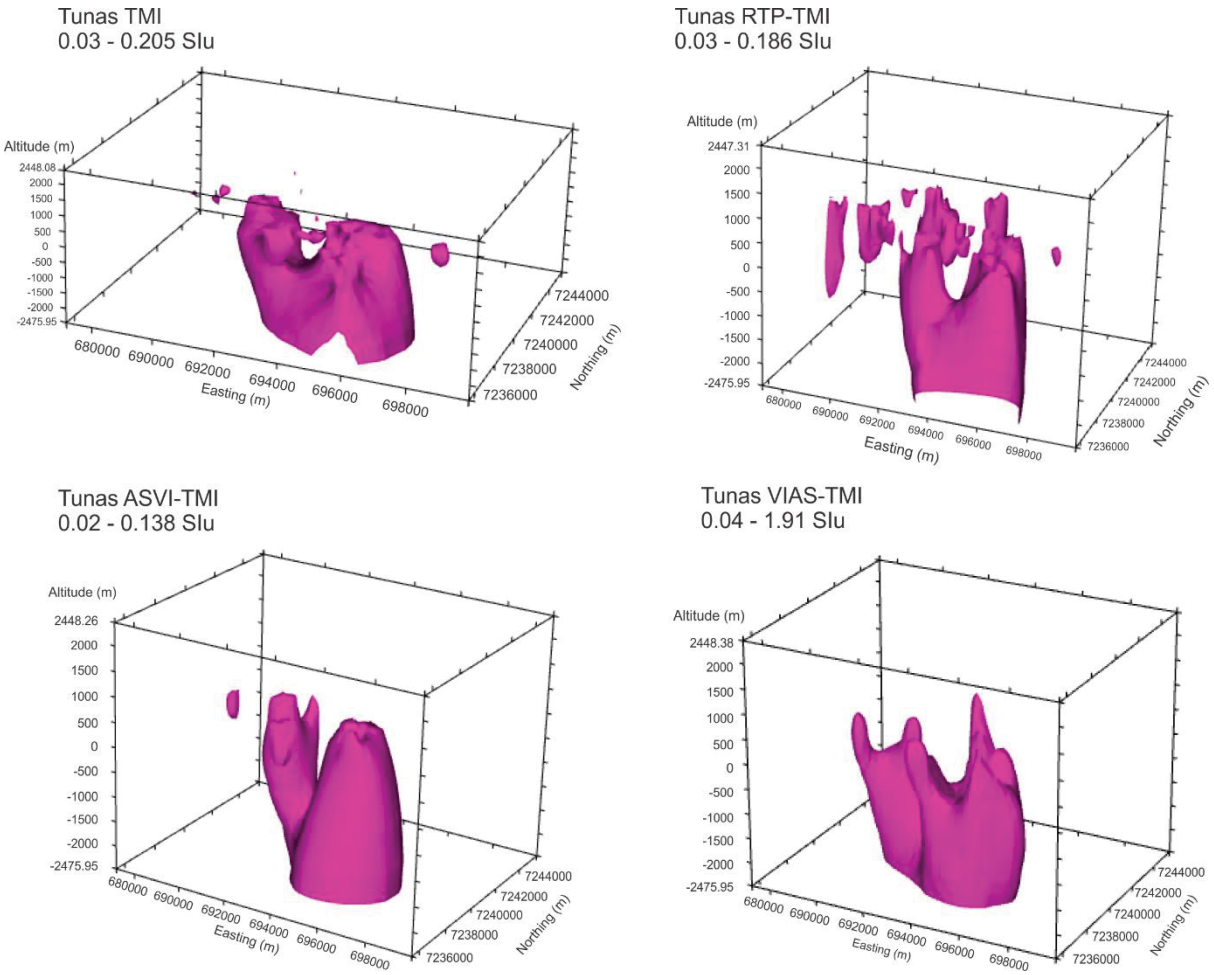

Figure 26. Contrast of apparent magnetic susceptibility distribution in 3D models for each type of Tunas Complex gridded data described in **Figure 25**. Models were cut in an arbitrary threshold value (displayed on the image) to create a better representation with the surface geology. Minimum values for each model: -0.088 (TMI), -0.195 (RTP-TMI), -0.05 (ASVI-TMI) and -0.16 SIu (VIAS-TMI). The maximum values of magnetic susceptibility were not modified. Altitudes are GPS altitudes and zero values correspond to the Mean Sea Level (MSL).

The largest axis of Tunas models had 6000 m while its minor had 2500 m. The contrast of apparent magnetic susceptibility models had altitudes between 1000 and -2500 m. This result is similar to that of Rugenski (2006), who reported a depth of around 3000 m for the bottom of this body using 2.5D modeling.

Overall, the small size in width and length and narrow depths from the magnetic responses and models of Bairro da Cruz, José Fernandes, and Tunas igneous rocks may suggest that they do not have deep crustal roots.

5.5.5 Radiometric analysis

Figure 27 provides an overview of K (%), eTh (ppm), and eU (ppm) concentrations for each intrusion according to the gridded data of the Paraná-Santa Catarina project. Even though percentages are compared against parts per million (ppm), it was decided to follow this procedure given is the standard in the literature and if potassium was converted to ppm (1% = 10,000 ppm), then all the potassium data would be displayed as incredibly high, which would lead to misinterpretations.

What stands out in the boxplot diagrams is that eTh is the most abundant radioactive element for all suites, sometimes extrapolating values of 50 ppm. In addition, practically all the minimum, maximum and mean quantities of equivalent uranium are higher than potassium ones. This radioelement has its highest concentration on the Mato Preto suite (i.e. 5.07%). Also, this intrusion has the highest average of potassium values (i.e. 2.27%). Overall, eU and K have really low concentrations in comparison with eTh. For example, there is a 20-fold increase in this radioelement averaged concentration compared to eU in the Barra do Itapirapuã intrusion. This figure for the Mato Preto suite showed an increase of ten times for eTh in relation to eU.

Bairro da Cruz showed average values for the three radioelements near the range described by Killeen (1979) for alkali feldspathoidal basic extrusives rocks. K and eU concentrations of this body have displayed more proximity to alkaline - ultrabasic rocks values of Galbraith and Saunders (1983) while eTh showed concentrations closer to alkaline - basic types.

The radioelements levels for the Barra do Teixeira phonolite are very similar to the Bairro da Cruz Complex. Nevertheless, the average concentrations were near to the average specified by Killeen (1979) for alkali feldspathoidal basic extrusive bodies rather than Bairro da Cruz. For the Galbraith and Saunders (1983) classification, potassium (1.04%), equivalent uranium (1.80 ppm), and equivalent thorium (8.62 ppm) average concentrations for Barra do Teixeira may be included in the alkaline - basic type although its eTh concentrations were situated 6 ppm above in relation to the mean eTh value (2.5 ppm) proposed by these authors.

K and eU average concentrations of Banhadão and Itapirapuã complexes were consistent with Killeen (1979) ranges for alkali feldspathoidal basic intrusives while Banhadão and Itapirapuã eTh concentrations are near the maximum value proposed by this author. For Galbraith and Saunders (1983) classification, the results displayed an association towards an alkaline basic to intermediate rock for K and eU while eTh mean values demonstrated to be far for the average defined for these authors to this rock type by a margin around 20 ppm.

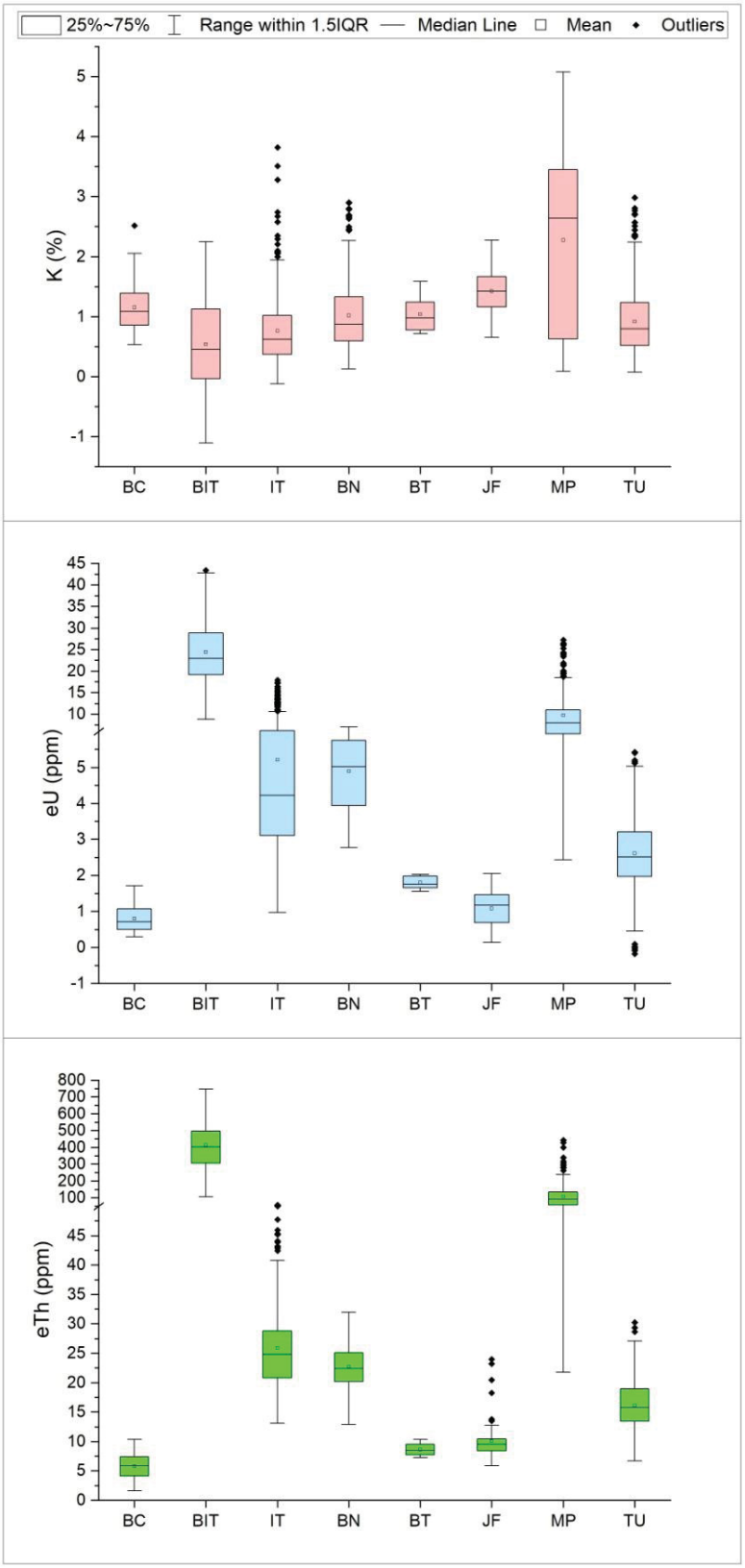

Figure 27. Box-and-whisker plots of radiometric data from the airborne geophysical survey. IQR stands for interquartile range. Alkaline complexes: Bairro da Cruz (BC), Barra do Itapirapuã (BIT), Banhadão (BN), Barra do Teixeira (BT), Itapirapuã (IT), José Fernandes (JF), Mato Preto (MP), and Tunas (TU). Note that the eU and eTh plots have a scale break to improve readability since there are large differences between the high and low values of the data.

Barra do Itapirapuã displayed mean concentrations of K, eU, and eTh as follows: 0.54%, 24.37 ppm, and 413.24 ppm, respectively. The higher values for eTh and eU, in particular eTh, support evidence from previous studies (Ford et al. 1988; Verplanck and Gosen 2011), which demonstrated that high values of both elements, especially eTh, is frequent in carbonatites and REE-bearing alkaline intrusions. For instance, Ford et al. (1988) reported values for the Allan Lake carbonatite, located in Canada, ranging from 1.4 - 3.5%, 0.5 - 3.8 ppm, and 14.5 - 119.4 ppm for K, eU, and eTh, respectively.

A similar figure of Barra do Itapirapuã is revealed for the Mato Preto Complex. With K concentrations situated in intervals of 0.08 to 5.07%, eU in 2.43 - 27.23 ppm and eTh in 21.76 - 443.49 ppm, this alkalic-carbonatitic suite showed the highest values of eTh, except for Barra do Itapirapuã. A possible suggestion for this is that while Barra do Itapirapuã is comprised in its majority of carbonatites, and thus frequent displaying large eTh values, Mato Preto has alkaline lithotypes in its configuration, lowering the average concentrations for this radioelement.

The José Fernandes gabbro, a basic intrusive rock, displayed average contents of K (%) and eU (ppm) around 1. This figure for eTh is 10 ppm. The K and eU concentrations are situated near the mean values of Killeen (1979) and Galbraith and Saunders (1983) for basic intrusives and basic rocks, respectively. Equivalent thorium levels of José Fernandes are situated above 8 ppm from the average concentration defined by both classifications, even though it is situated in the interval defined by Killeen (1979).

Radioelements for the Tunas Complex showed average levels below 3 for K (%) and eU (ppm) and over 15 ppm for eTh. This complex may be situated in the intermediate intrusives (Killeen 1979) or the alkaline-intermediate to acidic igneous groups (Galbraith and Saunders 1983).

Overall, the bodies showed some discrepancy for both classification systems at least in one radioelement. Whereas K and eU levels for a complex were consistent with one of the rock types defined by Killeen (1979) or Galbraith and Saunders (1983), eTh for the same complex demonstrated to be higher than the average for these authors. These findings may somewhat limit the creation of a generic system to characterize each complex. This is due to the fact that they are composed of different alkaline lithofacies in the majority of the cases and, therefore, display different radioelements levels according to their lithofacies composition.

Table 8 displays the responses for radiometric ratios and parameters previously stated in this work. The responses were based on relative values of the intrusions around each of its country rock according to the images for each parameter presented in **Appendix 3**. Pink to

red colors in the gridded images were attributed to high values, the majority of yellow and green colors were considered medium values and blue color was considered low.

Table 8. Gamma-ray spectrometric and magnetic responses of igneous rocks in the study area. The blue stands for relatively low values while yellow and red represents medium and high values, respectively. The letter D in the TMI row represents that the body showed a dipole anomaly response. Igneous rocks: Bairro da Cruz (BC), Barra do Itapirapuã (BIT), Banhadão (BN), Barra do Teixeira (BT), Itapirapuã (IT), José Fernandes (JF), Mato Preto (MP), and Tunas (TU).

	Igneous rocks							
Variable	BC	BN	IT	BIT	BT	JF	MP	TU
K								
eTh								
eU								
K/eTh								
K/eU								
K/(eU+eTh)								
(K^2)/(eU*eTh)								
F=K*(eU/eTh)								
eU/K								
eU/(K+eTh)								
eU/(K+eU+eTh)								
eU/eTh								
(eU^2)/eTh								
eTh/K								
(eTh^2)/K								
(eTh+eU)/K								
eTh/(K+eU)								
KD								
UD								
DRAD								
Color in RGB	Black	Cyan	Cyan	Cyan	Black	Black	White	Cyan
TMI		D				D		D

It can be seen from **Table 8** that high concentrations of eTh and eU are presented for Banhadão, Itapirapuã, Barra do Itapirapuã, Mato Preto, and Tunas complexes while the other bodies have displayed medium to low values for these radioelements. Mato Preto is the unique of the complexes studied that revealed higher potassium values. However, the thorium-normalized potassium (KD) for this body displayed low responses, suggesting that soil and/or vegetation may have influenced concentrations of K.

F-parameter alongside ratios with K variable in the numerator showed responses that lack any pattern to characterize both alkaline complexes and gabbros. Overall, these parameters presented low to medium values but do not show a significant correlation for the bodies in the study area.

Ratios with eU term in numerator revealed high responses in general. eU/K and (eU^2)/eTh ratios allowed to differentiate between the gabbros (Bairro da Cruz and José Fernandes) and the other alkaline complexes. The responses for the alkalic rocks are high whereas the gabbros showed medium to low values. No significant pattern was found in thorium-normalized uranium (UD) and DRAD parameters that allowed a clear distinction between the bodies.

Equivalent thorium term in numerator ratios showed high responses for all the bodies, except Bairro da Cruz, Barra do Teixeira, and José Fernandes, which displayed medium to low values. This is coherent with previous findings from this work where eTh is the most abundant element for all the igneous suites.

RGB colors for each suite comprised cyan and black overall. The cyan color suggests that eU and eTh are presented in the rock while there is some lack of K. Black color indicates the absence of radioelements. Only the Mato Preto suite displayed higher values for all radioactive elements.

Figure 28 reveals ternary diagrams of relative (normalized to 100%) K, eTh, and eU concentrations for each complex studied in this work. The data points comprised of sampled data from the gamma-ray spectrometer of the PR-SC project. All the igneous rocks have relative quantities of eTh above 60% with the majority of sampled points situated between 70 and 90%. Almost none of the complexes reached 20% K concentrations, except Bairro da Cruz, which has few points above this threshold. The majority of intrusions were situated between 0 and 25% of eU relative concentrations while Itapirapuã is the unique body to reach levels around 40%. It is worth noting that this intrusion, unlike its neighbors, has its sampled data grouped along the eTh edge. The Itapirapuã Complex showed a distribution with almost 100% of eTh and decreased along this edge to 60% while eU increased in the opposite direction and K percentages remained relatively stable. Barra do Itapirapuã, on the other hand, demonstrated a higher data density with 62 points situated around 0 to 1% of K and 90 to 100% of eTh.

5.5.6 Profile analysis

For this section, profiles along flight lines for each igneous suite were displayed showing the K, eTh, eU, TMI, RTP-TMI, and DTM responses in the N-S direction.

5.5.6.1 Bairro da Cruz Complex

It can be seen that the radioelements levels from the Mica schists unit (Morais et al. 2012) start decreasing (K and eU) or remain stable (eTh) when entering in the BC Complex

(**Figure 29**). In this igneous intrusion, K and eTh increased its concentrations towards the body central part. For the latter, its figure reached around 7 ppm when there was also a maximum of K concentration (i.e. 1.7%) and remained constant until drops to over 5 ppm after 500 m approximately. eU has displayed some high and low peaks, but, in general, remained virtually stable. In the central part, where equivalent thorium kept constant, that radioelement reached its lowest values inside the igneous suite.

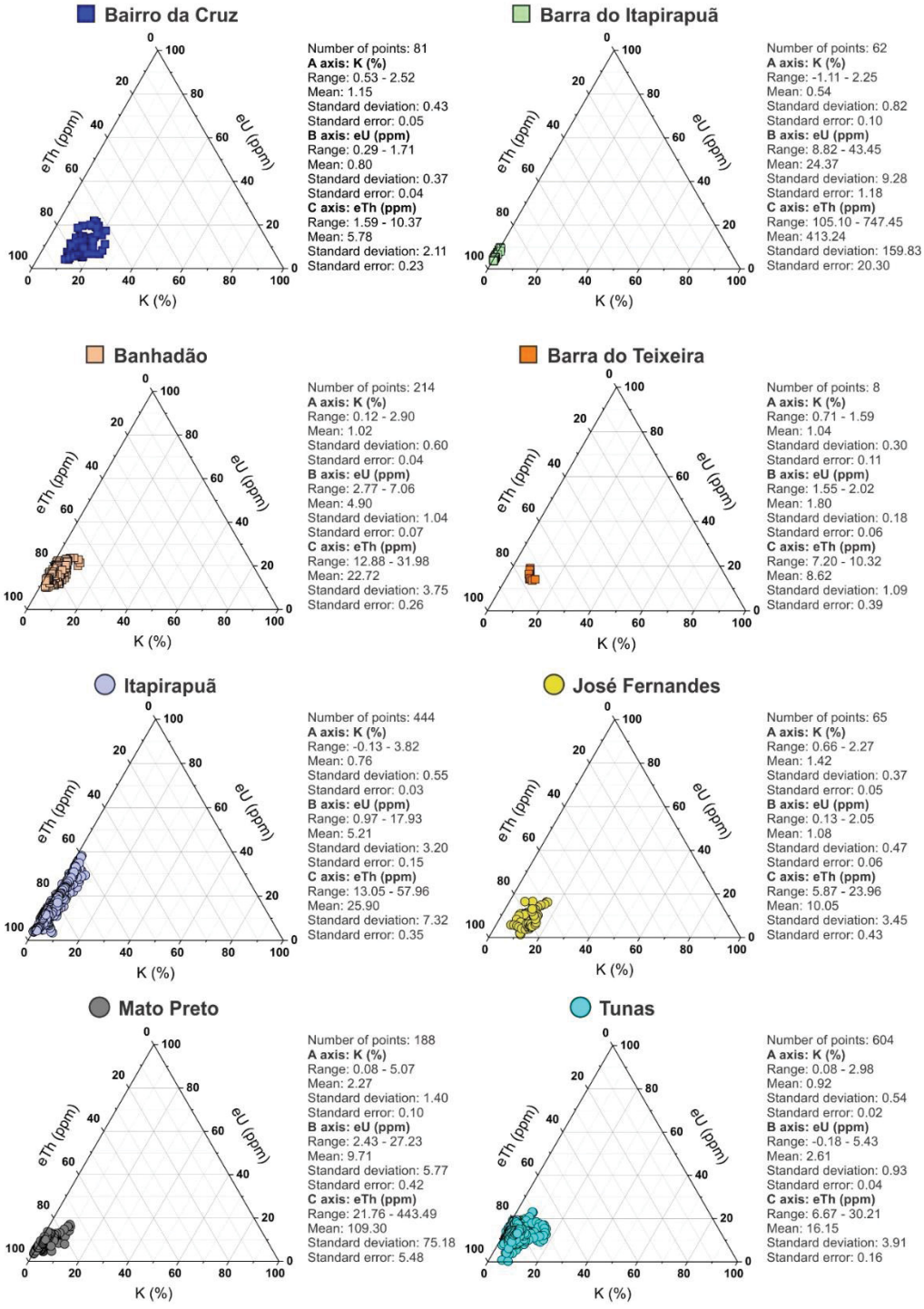

Figure 28. Relative radioelement concentrations for each intrusion displayed in ternary diagrams. Data points are sampled data from the airborne survey.

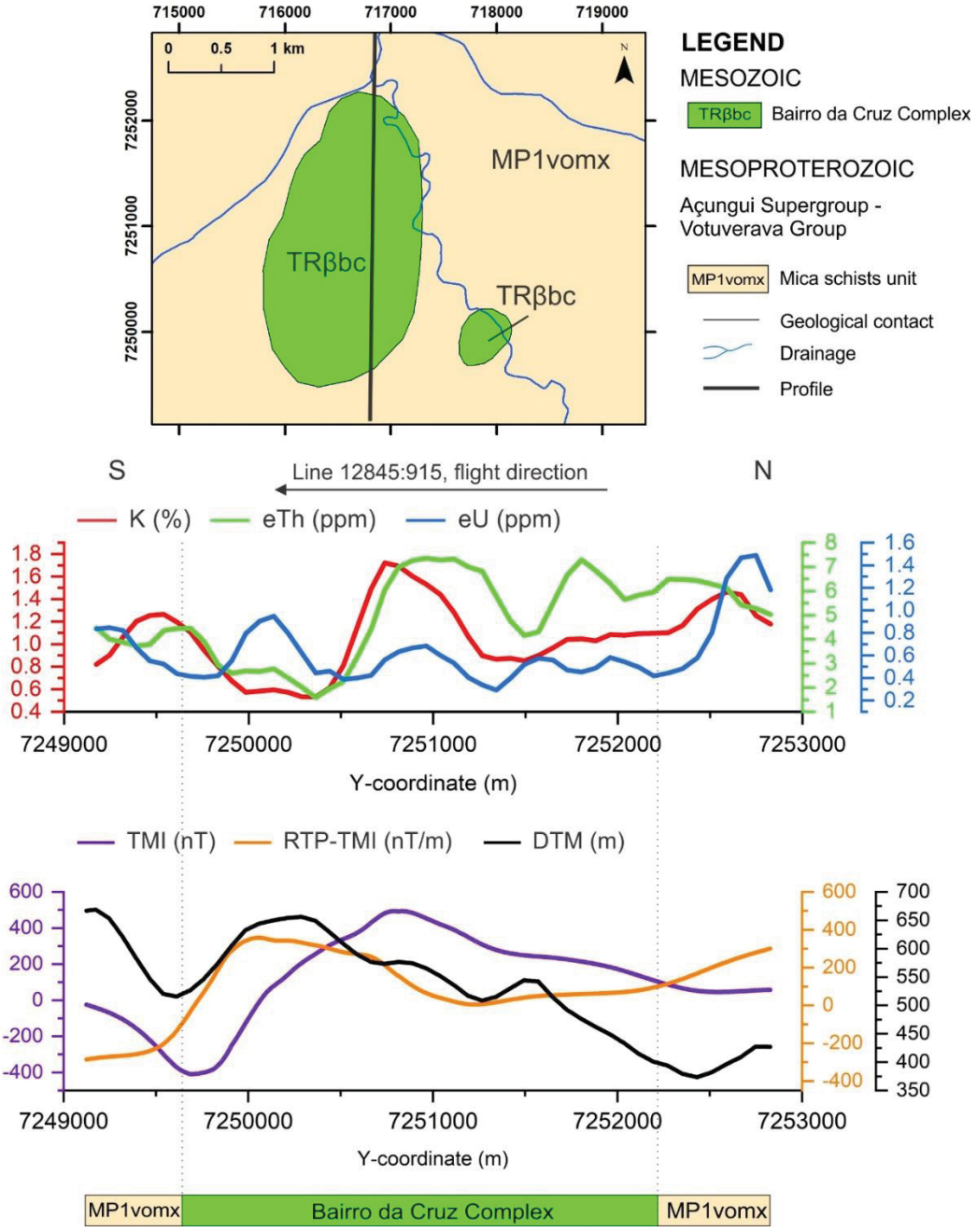

Figure 29. Flight line L12845:915 profile for radioelements (K, eTh, and eU) and magnetic data (TMI, RTP-TMI) alongside DTM values from Bairro da Cruz Complex.

Total magnetic intensity (TMI) revealed the lowest values on the south area of Bairro da Cruz (**Figure 29**), reaching -400 nT and maximum (over 500 nT) in the central part of the profile. TMI slightly diminish to 100 nT northward along the profile. RTP-TMI results showed some good correlation positioning the TMI anomaly over the central area, although it has located the anomaly more towards the southern part of Bairro da Cruz. It is important to highlight the fact this intrusion may have not been mapped in the literature using a fine-detail scale, and thus, our results suggest that BC geological contacts may be extended in the south direction where the RTP-TMI is positioned.

5.5.6.2 Banhadão Complex

The profile data for Banhadão Complex can be visualized in **Figure 30**. K distribution has displayed levels between 0.6 and 2.2%. The highest concentration of this radioelement is located between the Phlogopite melteigeite (KΛbam) and Pink nepheline syenite (KΛbansr) units in the central part of Banhadão. The Sodalite syenite (KΛbass) unit, which is suited for the exploration of ornamental rocks, showed the lowest values for K, eTh, and eU with 0.6%, 18 ppm, and 4 ppm, respectively. Equivalent uranium values in the Banhadão Complex increased gradually from its southern part reaching its peak between the Gray nepheline syenite (KΛbansc) and Pink nepheline syenite (KΛbansr) geological contact and then slowly decreasing until dropping in the Sodalite syenite (KΛbass) lithofacies. The figure for equivalent thorium is somewhat similar to the eU one, although it is more erratic with sharper increases and decreases in some points over the profile.

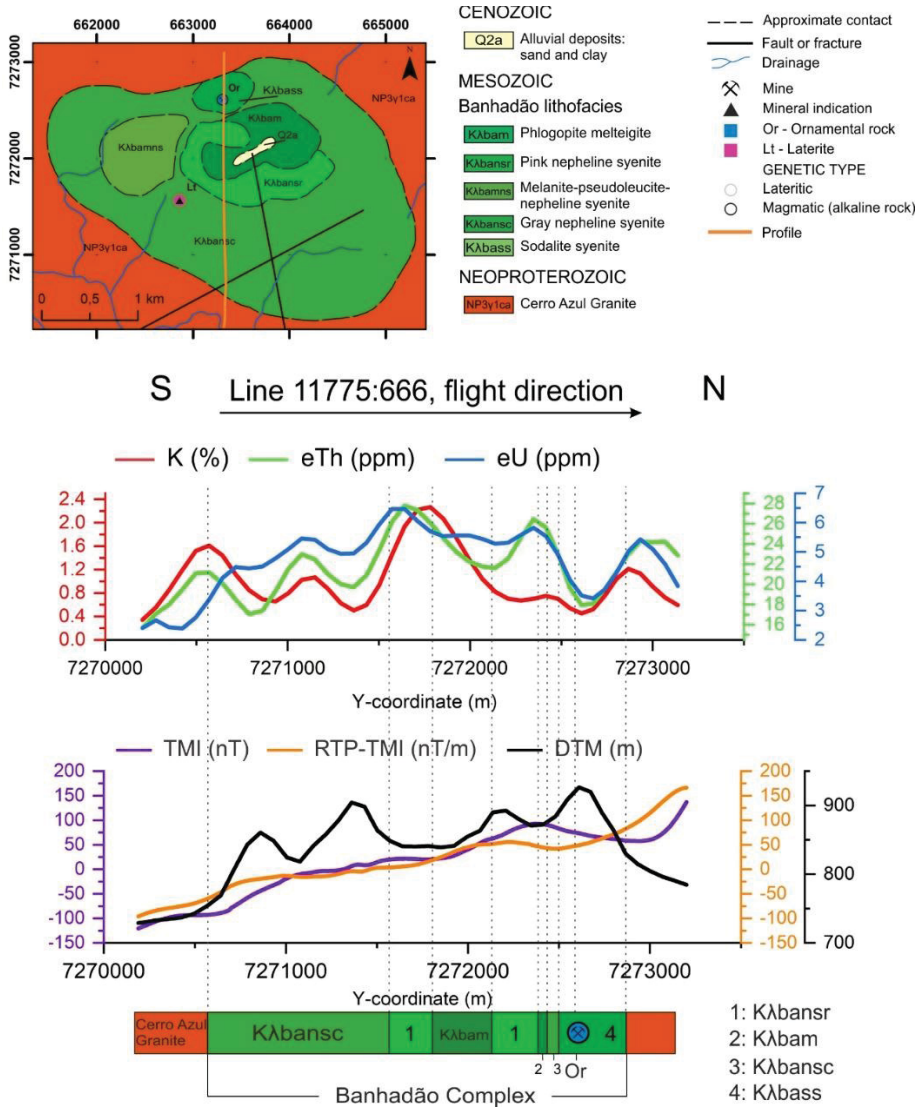

Figure 30. Flight line L11775:666 profile for radioelements (K, eTh, and eU) and magnetic data (TMI, RTP-TMI) alongside DTM values from Banhadão Complex.

TMI and RTP-TMI values slightly increased from south to north of the Banhadão Complex showing negative values in the Gray nepheline syenite (Kλbansc) unit and slowly went up to 100 nT in the northernmost part of the profile inside the Banhadão suite. The lack of any highs or lows between the lithofacies suggests that there is no significant contrast of magnetic susceptibility in this intrusion.

5.5.6.3 Itapirapuã Nepheline syenite

Figure 31 provides an overview of the radioelements concentrations and TMI data in the flight line 12035:677 which have flown in the Itapirapuã syenite. Ranging intervals for this intrusion are: 0 - 3.75% K, 20 - 37 ppm eTh and 2 - 14 ppm eU. What is interesting about the data in this profile is that all radioelements have peaked in virtually the same Y-coordinate (eTh peaked some meters near the south of this coordinate), located in the center of the Itapirapuã Nepheline syenite. In addition, a local low near the northern part of the peak described above is observed for K, eTh, and eU then followed northward by a local high.

Along the N-S profile (**Figure 31**), the magnetic data displayed negative levels. The figures for the Itapirapuã Nepheline syenite are around -100 nT (minimum) and -50 nT (maximum). The RTP-TMI and TMI profile remained practically stable over the Itapirapuã intrusion. The small difference between the maximum and minimum values indicates that there is a paucity of major contrast of magnetic susceptibility over this intrusion. In addition, the magnetic response appeared to be unaffected by the Fe mineralization near the profile.

5.5.6.4 Barra do Itapirapuã Carbonatite

This carbonatite body displayed higher concentrations of eU and eTh than its country rock (**Figure 32**), i.e. Cerro Azul Granite. The maximum values of these radioelements for the Barra do Itapirapuã intrusion are 45 ppm eU and 550 ppm eTh and they are located in the southernmost part of the Barra do Itapirapuã profile. These values then steadily drop towards the north of the profile. On the other hand, the opposite occurs for the K data. Its distribution starts decreasing when entering in the southern portion of the Barra do Itapirapuã, reach a small high around 1.0% and then plunge to near zero to start rising near the contact with Cerro Azul Granite. Then, this figure remains almost constant until rising above 3.0% at the end of the profile.

With respect to the magnetic profile, the TMI remained almost constant, situated between -50 and 0 nT. A local low is observed near the center of the carbonatite while the RTP-TMI displayed a local peak in the same position, even though it is an attenuated response in relation to the TMI data. This finding and the TMI grid data (**Figure 15**) are contrary to

previous studies (Drenth 2014; Thomas et al. 2016) which have suggested that carbonatite intrusions have circular, oval, strong magnetic signatures in their edges. However, the local TMI low in the profile (**Figure 32**) is somewhat consistent with those authors' claims that carbonatite cores coincide with magnetic lows.

No correlation was detected between the Fe and REE mineralizations and the gamma-ray spectrometric/magnetic responses in the Barra do Itapirapuã profile.

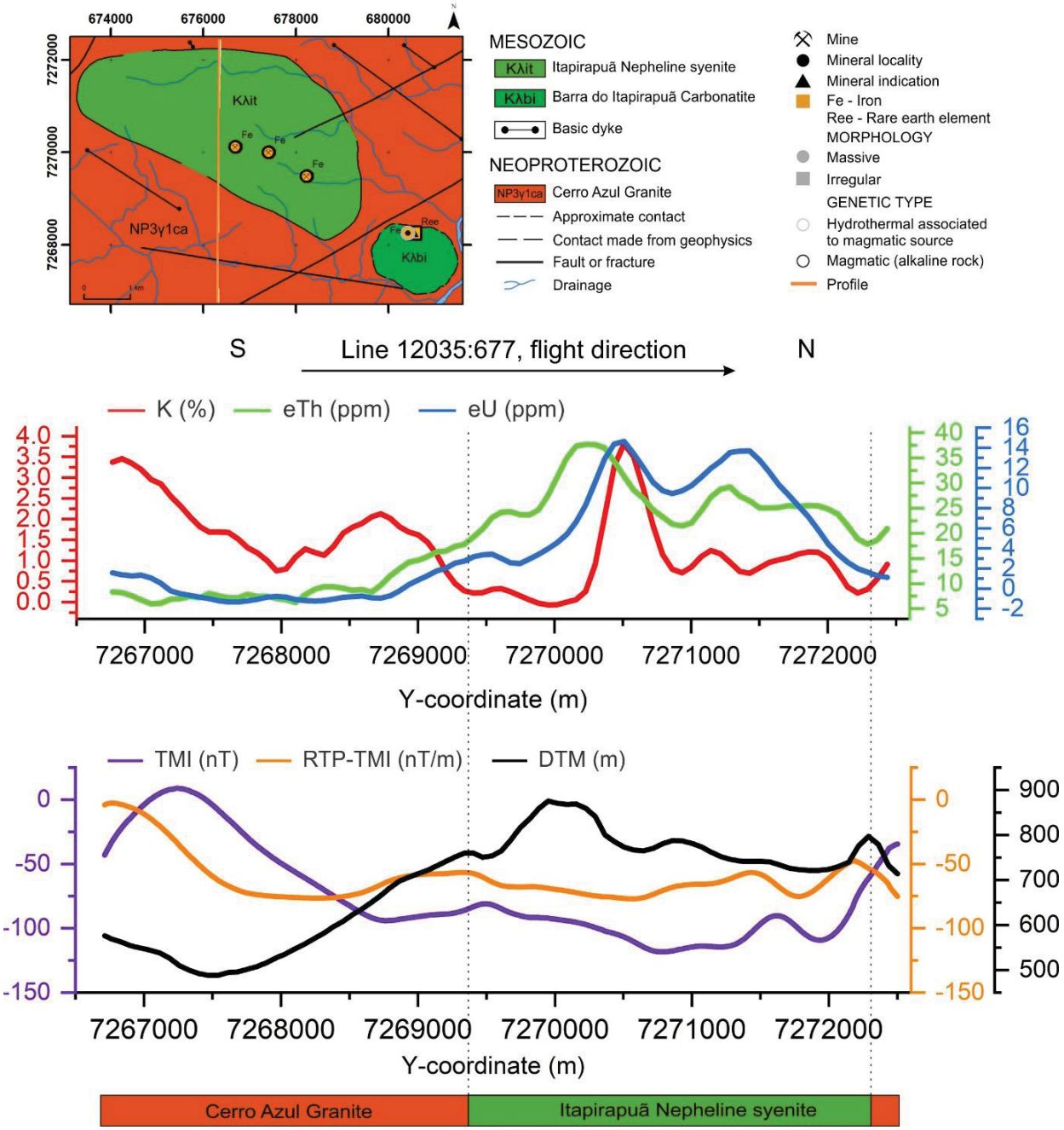

Figure 31. Flight line L12035:677 profile for radioelements (K, eTh, and eU) and magnetic data (TMI, RTP-TMI) alongside DTM values from Itapirapuã Nepheline syenite.

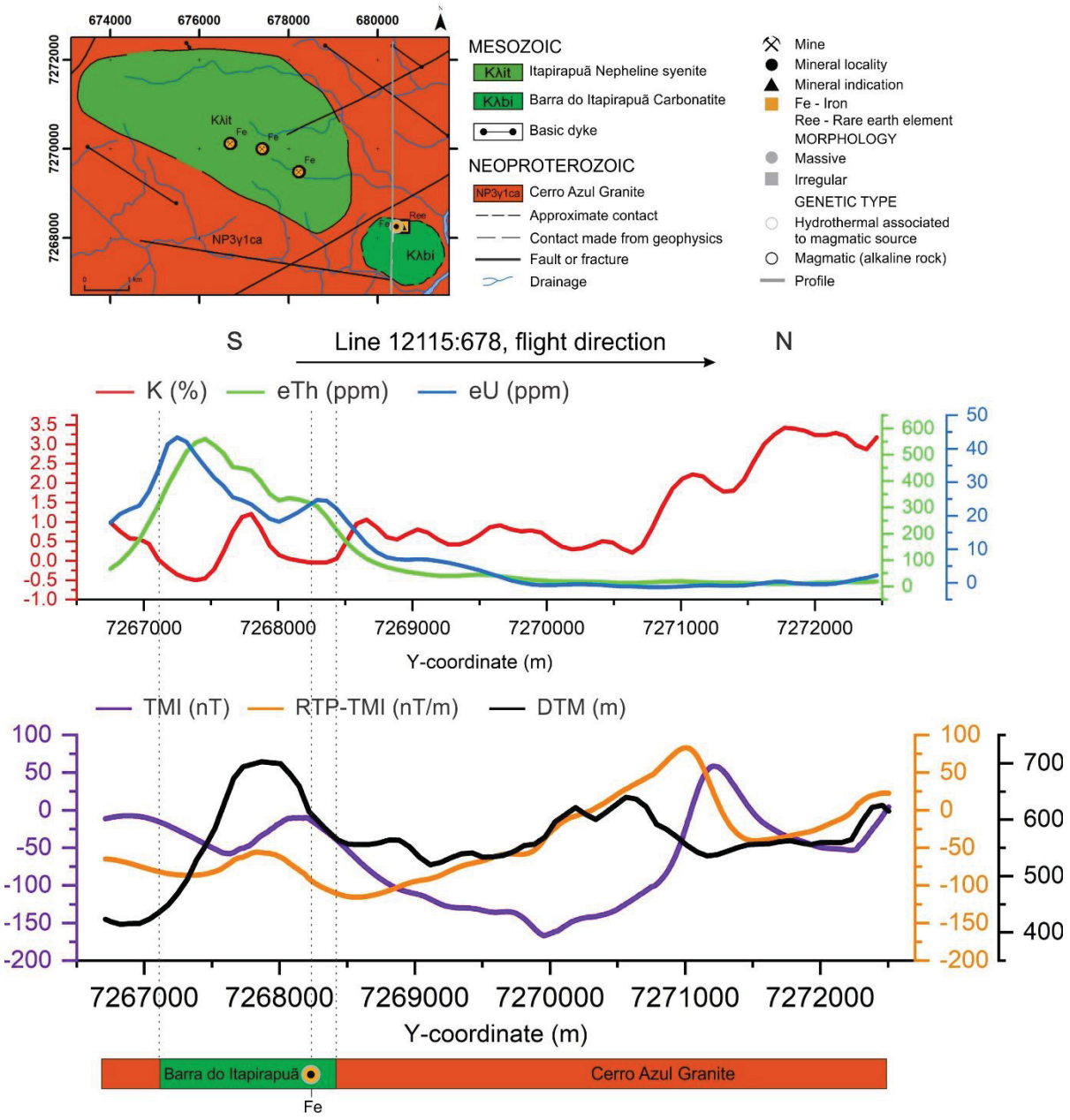

Figure 32. Flight line L12115:678 profile for radioelements (K, eTh, and eU) and magnetic data (TMI, RTP-TMI) alongside DTM values from Barra do Itapirapuã Carbonatite.

5.5.6.5 Barra do Teixeira Phonolite

This suite intruded in the Cerro Azul Granite displayed in its profile data (**Figure 33**) K distributions situated between 0.25 and 1.75% while eTh and eU figures range from 7 to 10 ppm and 1.5 to 2 ppm, respectively. The southern part of the phonolite is characterized by showing high values of eU while there is a decrease of K and eTh from the south to the central part of this body. There is a sharp rise of K along with eTh in the northern region of the Barra do Teixeira profile that continued into the Cerro Azul Granite. Overall, the highest radioactive element concentrations are situated in the north of the phonolite.

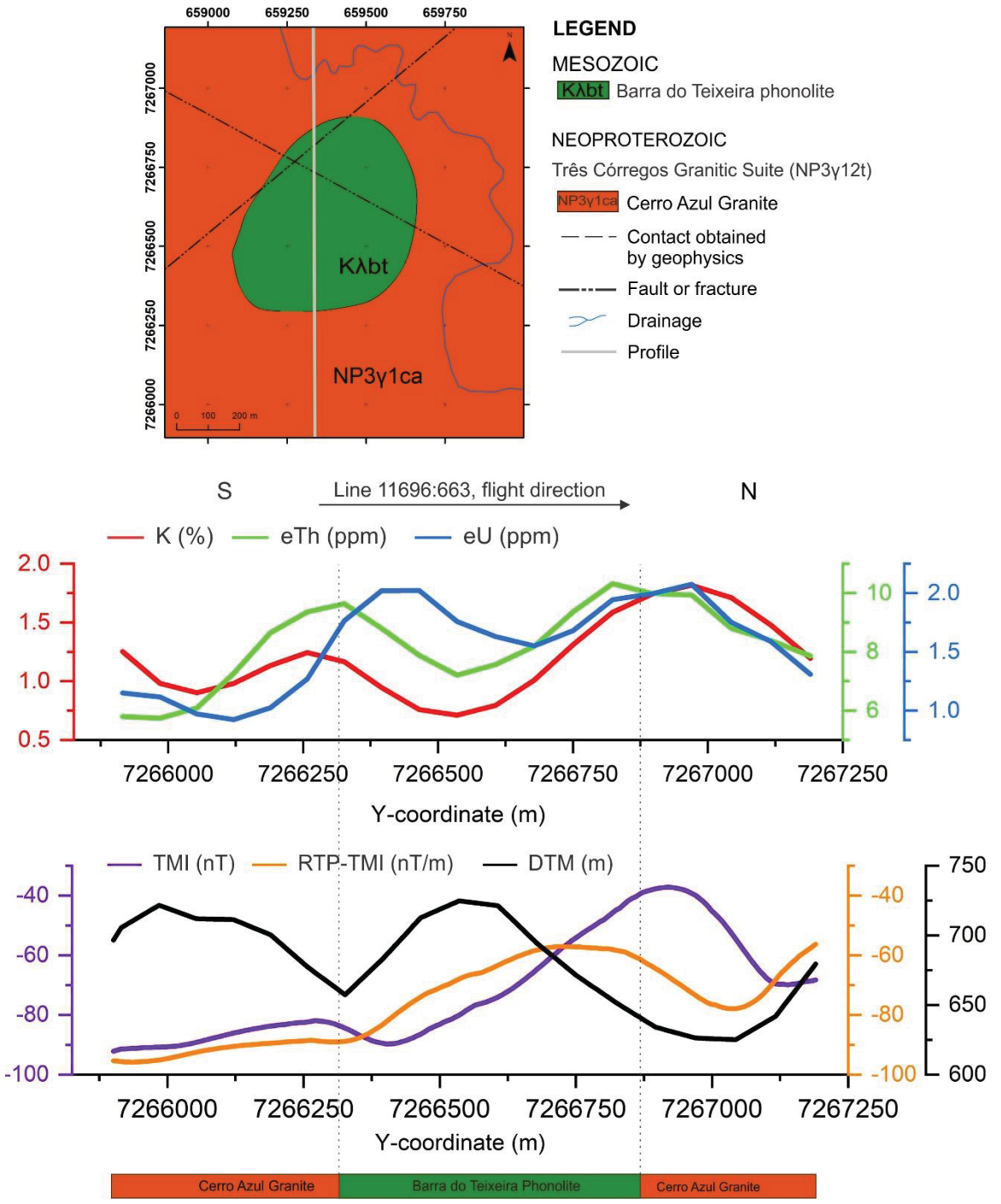

Figure 33. Flight line L11696:663 profile for radioelements (K, eTh, and eU) and magnetic data (TMI, RTP-TMI) alongside DTM values from Barra do Teixeira Phonolite.

The entire profile demonstrated negative values of TMI, ranging from -90 to -40 nT. The RTP-TMI data showed similar results. However, its profile seems attenuated in comparison with the TMI and has positioned the peak of this response over the center of the Barra do Teixeira phonolite.

5.5.6.6 José Fernandes Gabbro

Along the N-S José Fernandes Gabbro profile (**Figure 34**), maximum and minimum values inside this suite are: 0.75 - 2.0% K, 8 - 10 ppm eTh, 0.25 - 3.5 ppm eU. The lowest radioelement values of the profile are positioned over the JF suite, most to its central part. In this region, K and eTh levels decline from south to north while eU displays a local high, but three times lower than the peak of the Bairro da Serra Formation (MPbs), the highest for this radioelement along the profile.

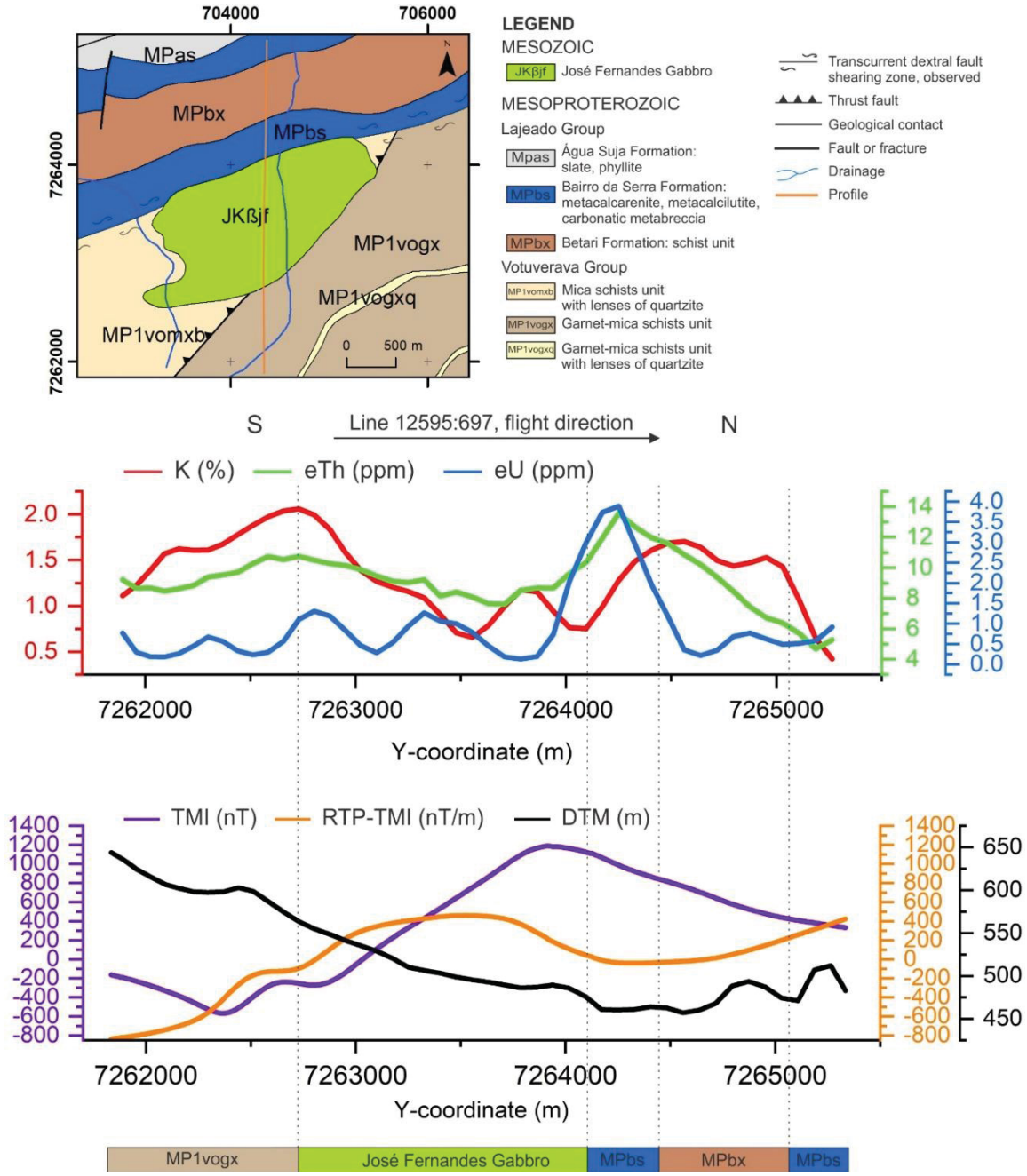

Figure 34. Flight line L12595:697 profile for radioelements (K, eTh, and eU) and magnetic data (TMI, RTP-TMI) alongside DTM values from José Fernandes Gabbro.

The range of TMI data for the JF gabbro boundaries is -200 to 1200 nT. This anomaly was characterized as having normal polarity for the Earth's southern hemisphere (**Figure 23a**) (negative value on the south lobe and positive on the north) while its RTP-TMI response has positioned a peak over the central part of the body, even though there is an attenuation of more than 600 nT in comparison with the TMI highest value. In other words, the amplitude of the TMI response is around 1800 nT whereas the RTP for the same data is 1200 nT.

5.5.6.7 Mato Preto Complex

Two profiles are illustrated for the Mato Preto Complex, one for its western area (**Figure 35**) and other for its eastern counterpart (**Figure 36**)

The profile located on the Mato Preto western portion (**Figure 35**) comprised K, eTh, and eU concentrations varying from 2.0 - 4.5%, 50 - 325 ppm, and 2.5 to 27.5 ppm, respectively. The most remarkable result is that there is a steady increase northward of eTh and eU reaching their maximum concentrations in the carbonatite lithofacies (Kλmpc) while the lowest potassium levels are located over this eTh and eU maxima. This is in good agreement with the profile of the Barra do Itapirapuã carbonatite (**Figure 32**), which showed a similar pattern for these radioelements distribution, i.e. high contents of eTh and eU with a low of potassium levels juxtaposed. The detection of different lithotypes in the BIT carbonatite may be only detected in the potassium profile, where there are some slight increases and decreases in its concentration.

Responses from TMI and RTP-TMI (**Figure 35**) displayed a smooth decrease of magnetic signal from south to north in the Mato Preto suite. Starting around 20 nT (southern area), the signal slowly dropped until it achieved over -60 nT in the northern portion. It is worth noting that the RTP of this signal has demonstrated virtually an identical response, both in shape and values, of TMI data.

Any correlation between the cooper and fluorine mineralization was not observed along the profile for both radiometric and magnetic data.

The eastern portion of Mato Preto is comprised only by the undifferentiated alkaline rocks unit (Kλmpi). Its profile (**Figure 36**) has the highest concentrations of eTh and eU in comparison with its country rock, schists from Água Clara Formation. Registering around 225 ppm eTh and 10 ppm eU, these peaks are situated in the central-south area of the Mato Preto suite. Like its eastern counterpart, there is a potassium depletion (around 0.25%) stacked in the same position of eTh and eU peaks. This response seems consonant with a carbonatite radiometric signature (i.e. eTh and eU highs and K lows with unusual values of eTh, above

100 ppm), hence indicating that the undifferentiated alkaline rocks unit (Kλmpi) could host carbonatite bodies.

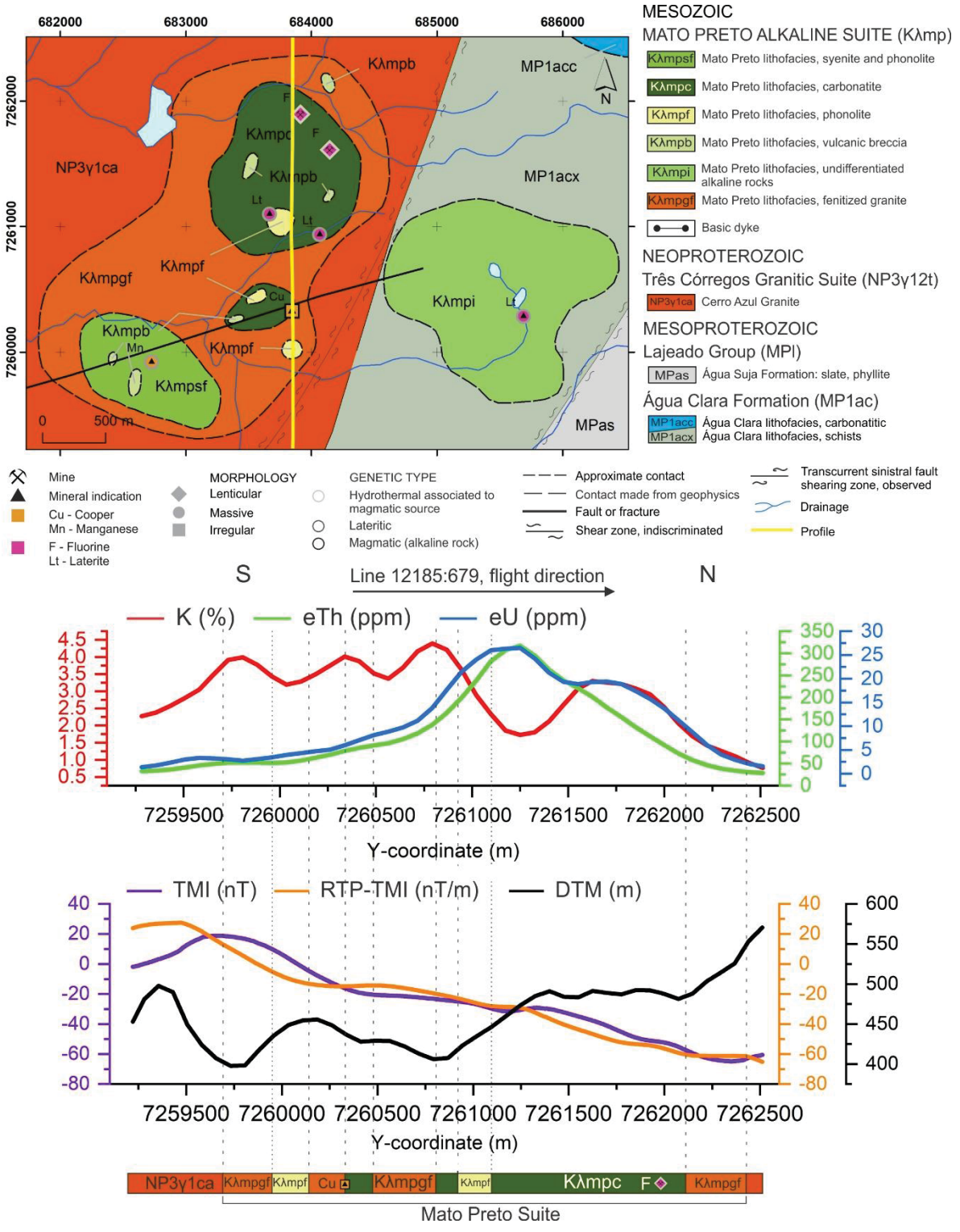

Figure 35. Flight line L12185:679 profile for radioelements (K, eTh, and eU) and magnetic data (TMI, RTP-TMI) alongside DTM values from Mato Preto Complex.

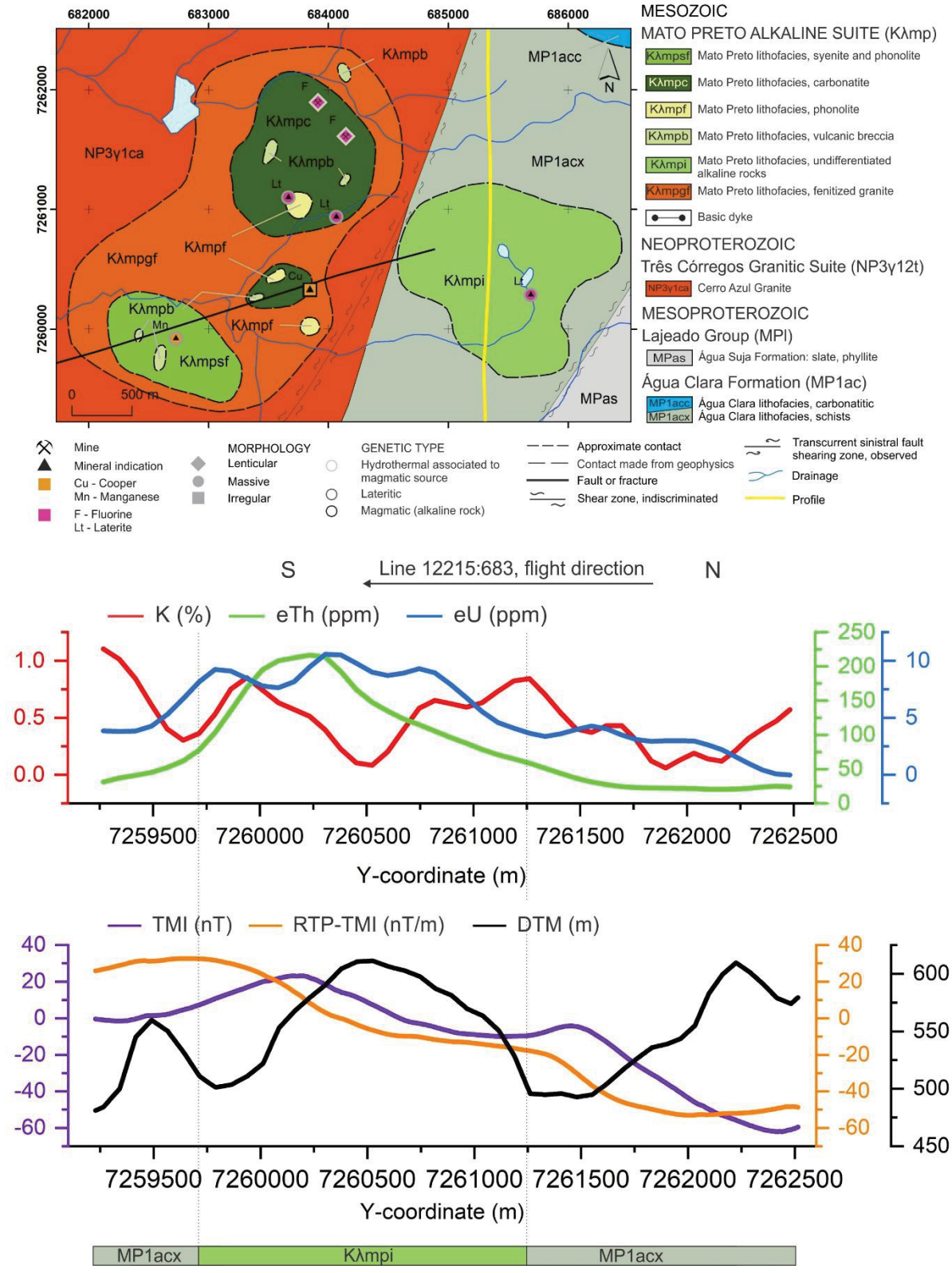

Figure 36. *Flight line L12215:683 profile for radioelements (K, eTh, and eU) and magnetic data (TMI, RTP-TMI) alongside DTM values from Mato Preto Complex*.

On the question of its magnetic profile, the undifferentiated alkaline rocks unit showed a small amplitude interval from the TMI response. The minimum found was -10 nT (in the

north) while its maximum was 20 nT approximately (in the south). Moreover, this positive peak is located in the same position as the eTh highest levels.

5.5.6.8 Tunas Complex

Profiles from flight lines 12325:684 and 12405:686 showing the radioelements levels and magnetic responses along the digital terrain model were displayed in **Figure 37** and **Figure 38**, respectively. Both profiles from Tunas could be characterized as the most erratic series between the complexes studied in this work. They displayed a large variety of ups and downs along the gamma-ray spectrometric and magnetic data. This result may be explained by the fact that those profiles comprise different rock types, including quaternary deposits, and also by the abrupt changes observed in the digital terrain model data. This variation in the DTM could influence the geomorphic processes and thus the rock/soil responses of gamma-rays (Wilford et al. 1997).

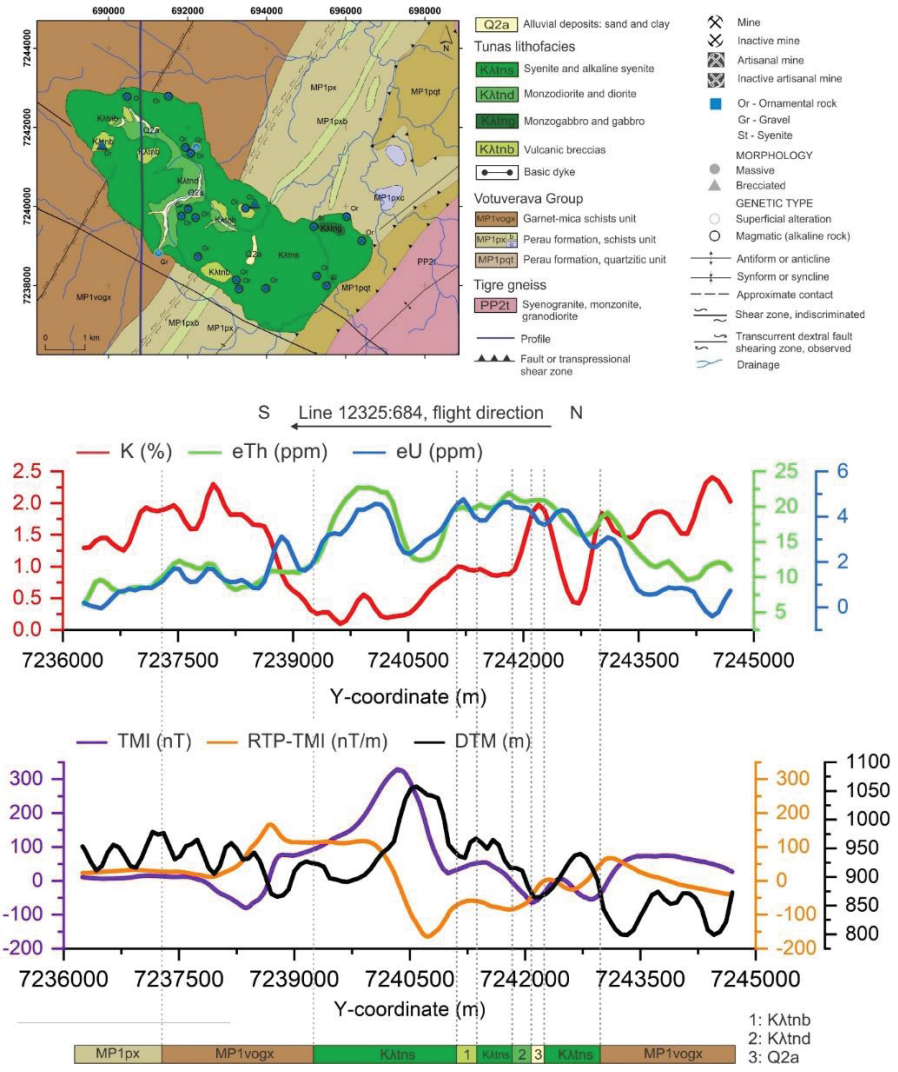

Figure 37. *Flight line L12325:684 profile for radioelements (K, eTh, and eU) and magnetic data (TMI, RTP-TMI) alongside DTM values from Tunas Complex.*

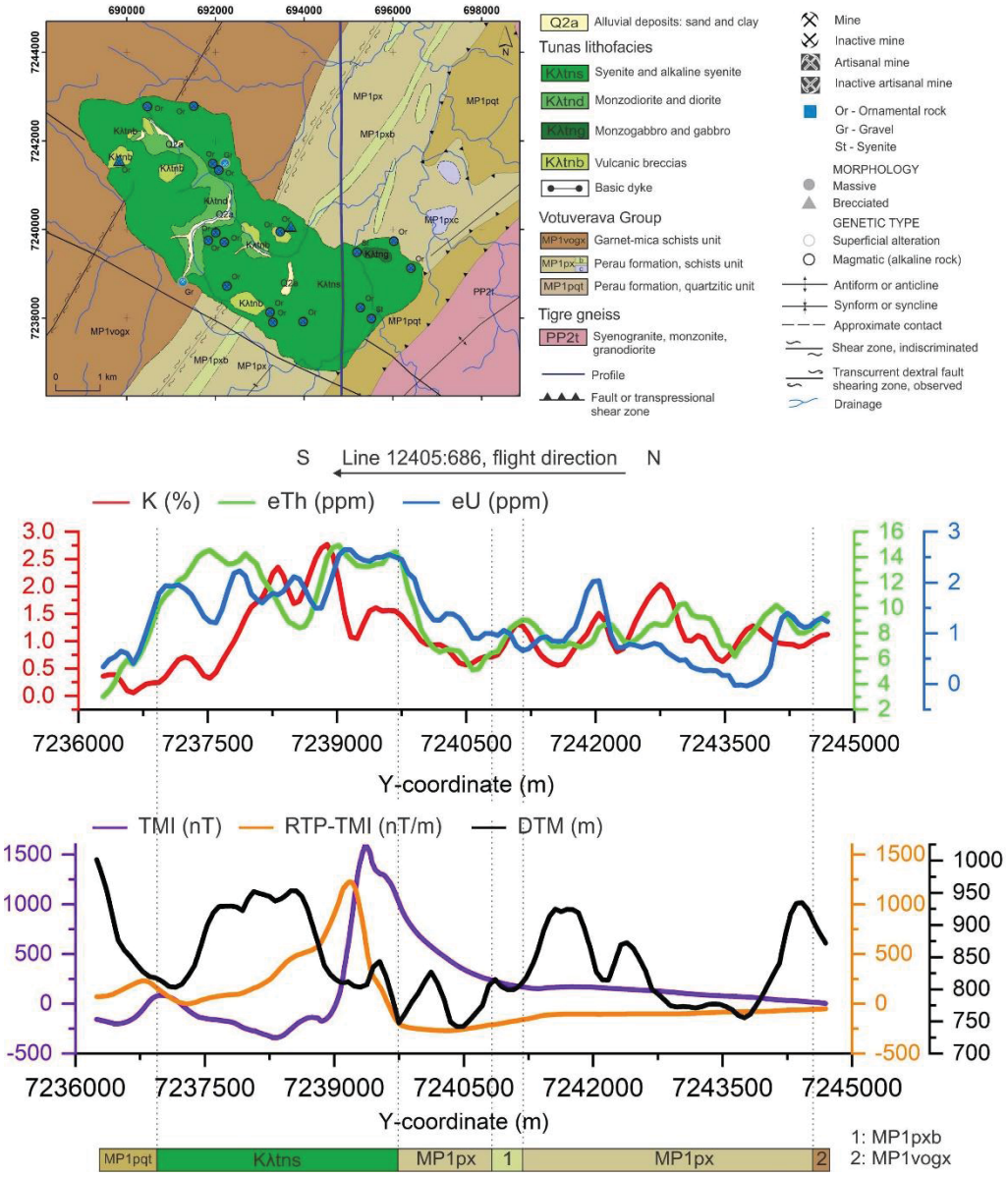

Figure 38. *Flight line L12405:686 profile for radioelements (K, eTh, and eU) and magnetic data (TMI, RTP-TMI) alongside DTM values from Tunas Complex*.

Line 12325:684 profile (**Figure 37**) demonstrated the highest levels of equivalent thorium and uranium inside the Tunas Complex. These concentrations are approximately 22.5 and 5 ppm, respectively, and are located on the syenite and alkaline syenite unit (KΛtns). This lithotype also carries the lowest quantities of K in the profile, i.e. almost 0.0 to 0.5%. This radioelement increased in the monzodiorite and diorite unit (KΛtnd), even though its concentration is less than in the country rocks of Tunas.

The magnetic data for this profile (**Figure 37**) has a significant amplitude. The TMI data has a maximum above 300 nT, which coincides with the highest levels of eTh and eU, and a minimum of -50 nT. The anomaly starts negative in the south and then steadily rises to positive values northward until changes its polarity in the northernmost part of Tunas Complex.

Although considerable attenuation has been observed for the RTP-TMI profile, it has peaked near the central axis of TMI anomaly (between 7238250 and 7239000 coordinates).

Figure 38 illustrates the results for line 12405:686, situated in the east of Tunas. Similar to its west profile, eTh and eU top levels are placed in the Tunas suite, i.e. syenite and alkaline syenite (Kλtns) lithofacies. Equivalent thorium results are 14 ppm with a local low of around 9 ppm in the center of this unit while eU erratic increase from south to north peaking almost 3 ppm inside of Kλtns lithofacies. Potassium quantities for Tunas eastern portion are somewhat higher, 1.0 to 1.5 ppm more than in the 12325:684 profile (western region). In addition, K concentrations in the syenite and alkaline syenite (Kλtns) lithofacies are higher than the Tunas country rocks in the eastern profile, i.e line 12405:686, while the opposite is seen in the western profile (**Figure 37**).

The eastern part of Tunas is magnetically stronger than its western region. The TMI profile showed peak to peak values around -300 nT and 1500 nT, an amplitude interval five times higher than the one demonstrated in the western profile (**Figure 37**). Additionally, the reduced to the pole signal in the eastern profile did not show any substantial attenuation in contrast to the western counterpart of Tunas.

5.6 CONCLUSIONS

High-resolution airborne geophysical data provides a powerful component for geologic interpretation where the rocks of interest do not have borehole data or access to their outcropped area is difficult. Prior works have documented geophysical evaluation of alkaline provinces in Brazil. However, these studies have been not focused on magnetic and radiometric data, especially the latter. In this work, we characterized geophysical the Ponta Grossa Arch Alkaline Province, whose extent has been targeted to mineral exploration for several decades.

We found that the igneous bodies of this province are composed mainly of shallow magnetic sources while dipolar anomalies with little to no interference of remnant magnetism were associated with some of these rocks. Modeling showed good agreement with magnetic susceptibilities values of alkaline rocks and gabbros reported in the literature, even though the shape and geometry of the PGAAP rocks could not be representative of the known geology. Further research should be carried out to establish the magnetization vector from the rocks modeled in this study as well as to confirm the intensity of remanent magnetism in those to better constrain inversions.

Our analyses displayed that these rocks are mainly enriched in eTh, which supports other works regarding alkaline complexes. In addition, we found the radiometric data useful to

distinguish complexes that host carbonatites from those that do not contain them. However, our approach to create a general classification based on radioelements for alkaline rocks was unsuccessful due to the lack of clear patterns. More information on radiometric data, such as conducting small-scale ground geophysical surveys, would help us to establish a greater degree of accuracy on this matter. Most notably, this is the first study to our knowledge to investigate in detail the magnetic and radiometric responses from alkaline bodies in the Ponta Grossa Arch, thus it has contributed to the understanding of geophysical signatures of alkaline provinces.

5.7 ACKNOWLEDGMENTS

We thank the Geological Survey of Brazil (CPRM) for providing the airborne geophysical data. F.J.F. Ferreira was supported in this research by the National Council for Scientific and Technological Development (CNPq, Brazil) (contract 303826/2018-5). The authors thank O.A. de Souza Filho and W.R. Borges for their reviews as part of the first author's M.Sc. thesis committee.

5.8 ARTICLE REFERENCES

Airo M. 2015. Geophysical signatures of mineral deposit types – synopsis. In: Airo M. (ed.) Geophysical signatures of mineral deposit types. Espoo: Geological Survey of Finland, Special Paper 58, p. 9-70. Available at: <http://tupa.gtk.fi/julkaisu/specialpaper/sp_058.pdf>. Accessed on: Oct. 18, 2018.

Airo M., Hyvönen E., Lerssi J., Leväniemi H., Routsalainen A. 2014. Tips and tools for the application of GTK´s airborne geophysical data. Geological Survey of Finland, Report of Investigation 215, 33 p. Available at: <https://pdfs.semanticscholar.org/cf86/fe5b9c1ab425575dd36bc1305487e6cf80d3.pdf>. Accessed on: Oct. 20, 2018.

Algarte J.P. 1972. A influência dos arqueamentos cratônicos no condicinamento das alcalinas dos Estados de São Paulo e Paraná. In: Congresso Brasileiro de Geologia, 26, Belém. Proceedings, v.1, p. 65-69.

Almeida F.F.M. 1983. Relações tectônicas das rochas alcalinas mesozóicas da região meridional da plataforma sul-americana. Revista Brasileira de Geociências, **13:**139-158. https://doi.org/10.25249/0375-7536.1983133139158

Almeida V.V. 2016. Petrologia do Gabro José Fernandes e sua relação temporal com o magmatismo mesozoico toleítico e alcalino no arco de Ponta Grossa. PhD thesis, Universidade de São Paulo, São Paulo, 274 p. http://doi.org/10.11606/T.44.2017.tde-30032017-083933

Almeida V.V., Janasi V.A., Azzone R.G., Faleiros F.M. 2019. Crustal contamination and genesis of transitional alkaline-tholeiitic intrusions: Insights from the José Fernandes Suite, Paraná Magmatic Province, Brazil. Lithos, **342-343:**59-75. https://doi.org/10.1016/j.lithos.2019.05.023

Alva-Valdivia L.M., López-Loera H. 2011. A review of iron oxide transformations, rock magnetism and interpretation of magnetic anomalies: El Morro Mine (Brazil), a case study. Geofísica Internacional, **50(3):**341-362.

Baranov V. 1957. A new method for interpretation of aeromagnetic maps: pseudo-gravimetric anomalies. Geophysics, **22:**359–383. https://doi.org/10.1190/1.1438369

Baranov V. and Naudy H. 1964. Numerical calculation of the formula of reduction to the magnetic pole. Geophysics, **29:**67–79. https://doi.org/10.1190/1.1439334

Blakely R.J., Connard G.G., Curto J.B. 2016. Tilt Derivative Made Easy. Technical note – Geosoft. Available at: <https://www.geosoft.com/media/uploads/resources/tilt_derivative_made_easy_07-2016.pdf>. Accessed on: Dec 30, 2019.

Briggs I.C. 1974. Machine contouring using minimum curvature. Geophysics, **39(1):**39-48. https://doi.org/10.1190/1.1440410

Brumatti M. and Almeida V.V. 2014. Rochas Alcalinas: Áreas de Registro, Iguape e Cerro Azul. Anexo III: Atualização da cartografia geológica da Folha Cerro Azul SG.22-X-B-IV. Estados de São Paulo e Paraná. São Paulo: CPRM, Escala 1:100.000.

Brumatti M. and Tomita S.A. 2014. Mapa geológico da folha Vila Branca – SG.22-X-B-IV-1. Escala 1:50000. São Paulo: CPRM.

Brumatti M., Almeida V.V., Lopes A.P., Campos F.F., Perrotta M.M., Mendes D., Pinto L.G.R., Palmeira L.C.M. 2015. Metalogenia das províncias minerais do Brasil: rochas alcalinas da porção meridional do cinturão Ribeira, estados de São Paulo e Paraná. CPRM, Informe de Recursos Minerais, Série Províncias Minerais do Brasil, 6:1-79.

Chmyz L., Ribeiro J.C., Zaramella D.R. 2011. Análise faciológica do Gabro José Fernandes (Adrianópolis, PR) e considerações preliminares do seu potencial econômico. In: VII Encontro Internacional de Produção Científica CESUMAR. Proceedings, v. 1, p. 1-5.

Clark D.A. 1997. Magnetic petrophysics and magnetic petrology: aids to geological interpretation of magnetic surveys. AGSO Journal of Australian Geology and Geophysics, **17(2):**83-103. http://pid.geoscience.gov.au/dataset/ga/81495

Clark D.A. 1999. Magnetic petrology of igneous intrusions: implications for exploration and magnetic interpretation. Exploration Geophysics, **30:**5-26. https://doi.org/10.1071/EG999005

Clark D.A. and Emerson D.W. 1991. Notes on rock magnetization characteristics in applied geophysical studies. Exploration Geophysics, **22(3):**547-555. https://doi.org/10.1071/EG991547

Comin-Chiaramonti P. and Gomes C.B. (eds.). 2005. *Mesozoic to Cenozoic alkaline magmatism in the Brazilian Platform*. São Paulo, EdUSP/Fapesp, 752 p.

Comin-Chiaramonti P., Gomes C.B., Ruberti E., Antonini P., Censi P. 2001. Mato Preto alkaline-carbonatite complex: geochemistry and isotope (O-C, Sr-Nd) constraints. Geochimica Brasiliensis, **15:**23-24. http://dx.doi.org/10.21715/gb.v15i1.181

Cordani U.G. and Hasui Y. 1968. Idades K-Ar de rochas alcalinas do primeiro planalto do Estado do Paraná. In: Congresso Brasileiro de Geologia, 22, Belo Horizonte. Proceedings, v. 1, p. 149-153.

Cowan D.R. and Cowan S. 1993. Separation Filtering Applied to Aeromagnetic Data. Exploration Geophysics, **24(3-4):**429–436. https://doi.org/10.1071/eg993429

CPRM - Geological Survey of Brazil. 1978. Projeto Aerogeofísico Serra do Mar Sul. CPRM/DNPM, Rio de Janeiro.

CPRM - Geological Survey of Brazil. 2011. Programa Geologia do Brasil (PGB) – Projeto aerogeofísico Paraná-Santa Catarina: relatório final do levantamento e processamento dos dados magnetométricos e gamaespectrométricos. Volume I. Lasa Prospecções, 326 p.

Curto J.B., Vidotti R.M., Fuck R.A., Blakely R.J., Alvarenga C.J.S., Dantas E.L. 2014. The tectonic evolution of the Transbrasiliano Lineament in northern Paraná Basin, Brazil, as inferred from aeromagnetic data. Journal of Geophysical Research: Solid Earth, **119(3):**1544–1562. https://doi.org/10.1002/2013jb010593

Drenth B.J. 2014. Geophysical expression of a buried niobium and rare earth element deposit: The Elk Creek carbonatite, Nebraska, USA. Interpretation, **2(4):**SJ23–SJ33. https://doi.org/10.1190/int-2014-0002.1

Efimov A.V. 1978. Multiplikativniyi pokazatel dlja vydelenija endogennych rud aerogamma-spectrometriceskim dannym. In: Metody rudnoj geofiziki. Naucno proizvodstvennoje objedinenie geofizica, Leningrado, 59-68.

Ferreira F.J.F. 1982. Integração de dados aeromagnéticos e geológicos: configuração e evolução tectônica do Arco de Ponta Grossa. MS thesis, Universidade de São Paulo, São Paulo, 186 p. https://doi.org/10.11606/d.44.1983.tde-14082013-161535

Ferreira F.J.F. and Algarte J.P. 1979. O comportamento aeromagnetométrico – cintilométrico das principais rochas alcalinas dos Estados de São Paulo e Paraná. In: Simpósio Regional de Geologia, 2, Rio Claro. Proceedings, v. 2, p. 195-208.

Ferreira F.J.F., Algarte J.P., Theodorovicz A., Martins F.A.G., Monma R., Silva R.B., Tassinari C.G.C., Rodrigues E.P., Coutinho J.V.M. 1987. O Complexo alcalino de Pariquera-Açu. In: Simpósio Regional de Geologia, 6, Sociedade Brasileira de Geologia. Proceedings, v. 1, p. 159-171.

Ferreira F.J.F., Fruchting A., Guimarães G.B., Alves L.S., Martin V.M.O., Ulbrich H.H.G.J. 2009. Levantamentos Gamaespectrométricos em Granitos Diferenciados. II: O Exemplo do Granito Joaquim Murtinho, Complexo Granítico Cunhaporanga, Paraná. Geologia USP. Série Científica, **9(1):**55–72. https://doi.org/10.5327/z1519-874x2009000100004

Ferreira F.J.F., Moraes R.A.V., Ferrari M.P., Vianna R.B. 1981. Contribuição ao estudo do Alinhamento Estrutural de Guapiara. In: Simpósio Regional de Geologia, 3, São Paulo, Sociedade Brasileira de Geologia. Proceedings, v. 1, p. 226-240.

Fitton J.G. and Upton B.G.J. (eds.). 1987. *Alkaline igneous rocks*. Geological Society, special publication, 30, 568 p.

Ford K.L., Dilabio R.N.W., Rencz A.N. 1988. Geological, geophysical and geochemical studies around the Allan Lake carbonatite, Algonquin Park, Ontario. Journal of Geochemical Exploration, **30(1-3):**99–121. https://doi.org/10.1016/0375-6742(88)90054-4

Forman J.M.A. and Angeiras A.G. 1981. Poços de Calderas and Itataia: Two case histories of uranium exploration in Brazil. In: International Atomic Energy Agency. Uranium Exploration Case Histories, p. 99–139.

Galbraith J. H. and Saunders D.F. 1983. Rock classification by characteristics of aerial gamma-ray measurements. Journal of Geochemical Exploration, **18(1):**49–73. https://doi.org/10.1016/0375-6742(83)90080-8

Gill R. 2010. *Igneous rocks and processes: a practical guide*. John Wiley & Sons. 472 p.

Gnojek I. and Prichystal A. 1985. A new zinc mineralization detected by airborne gamma-ray spectrometry in Northern Moravia (Czechoslovakia). Geoexploration, **23(4):**491-502. https://doi.org/10.1016/0016-7142(85)90076-6

Gomes C.B. 1970. Petrologia do maciço alcalino de Itapirapuã, São Paulo. Boletim do Instituto de Geociências e Astronomia da USP, **1:**77-188. https://doi.org/10.11606/issn.2316-9001.v1i0p77-197

Gomes C.B. and Comin-Chiaramonti P. (eds.). 2017. *Magmatismo alcalino continental da região meridional da plataforma brasileira*. EdUSP/Fapesp, 608 p.

Gomes C.B. and Comin-Chiaramonti P. 2005. An introduction to the alkaline and alkaline carbonatitic magmatism in and around the Paraná Basin. In: Gomes C.B. and Comin-Chiaramonti P. (eds.). Mesozoic to Cenozoic Alkaline Magmatism in the Brazilian Platform. EdUSP/Fapesp, p. 21-29.

Gomes C.B., Azzone R.G., Ruberti E., Vasconcelos P.M., Sato K., Rojas G.E.E. 2018. New age determinations for the Banhadão and Itapirapuã complexes in the Ribeira Valley, southern Brazil. Brazilian Journal of Geology, **48:**1-12. https://doi.org/10.1590/2317-4889201820170094

Gomes C.B., Barbieri M., Beccaluva L., Brotzu P., Conte A., Garbarino C., Macciotta G., Melluso L., Morbidelli L., Ruberti E., Scheibe L.F., Tamura R.M., Traversa G. 1987. Petrological and geochemical studies of alkaline rocks from continental Brazil: 2. The Tunas massif, State of Paraná. Geochimica Brasiliensis, **1(2):**201-234.

Gomes C.B., Ruberti E., Comin-Chiaramonti P., Azzone R.G. 2011. Alkaline magmatism in the Ponta Grossa Arch, SE Brazil: a review. Journal of South American Earth Sciences, **32(2):**152-168. http://dx.doi.org/10.1016/j.jsames.2011.05.003

Grant J.A. 1998. Ten things the textbooks don't tell you about processing and archiving airborne gamma-ray spectrometric data. In: Geological Survey of Canada. Current Research n. 1998-D, Eastern Canada and national and general programs, p. 83-87. https://doi.org/10.4095/209538

Hama M., Algarte J.P., Paiva I.P., Rodrigues J.C. 1977. Idades K/Ar do maciço alcalino do Banhadão e do complexo Bairro da Cruz. In: Simpósio Regional de Geologia, 1, São Paulo. Proceedings, v. 1, p. 170-178.

Isles D.J. and Rankin L.R. 2013. *Geological Interpretation of Aeromagnetic Data*. Society of Exploration Geophysicists and the Australian Society of Exploration Geophysicists. 365 p. http://dx.doi.org/10.1190/1.9781560803218.

Kaefer L.Q. and Algarte J.P. 1972. Maciço alcalino do Banhadão: estudos preliminares. In: Congresso Brasileiro de Geologia, 26, Belém-PA. Proceedings, v. 1, p. 55-64.

Killeen P.G. 1979. Gamma ray spectrometric methods in uranium exploration-application and interpretation. In: Hood P.J. (ed.). Geophysics and geochemistry in the search for metallic ores. Geological Survey of Canada, Economic Geology Report, **31:**163-230. http://dx.doi.org/10.4095/106049.

Leão-Santos M., Li Y., Moraes R. 2015. Application of 3D magnetic amplitude inversion to iron oxide-copper-gold deposits at low magnetic latitudes: A case study from Carajás Mineral Province, Brazil. Geophysics, **80(2):**B13–B22. https://doi.org/10.1190/geo2014-0082.1

Li Y. 2017. From Susceptibility to Magnetization: Advances in the 3D Inversion of Magnetic Data in the Presence of Significant Remanent Magnetization. In: Tschirhart V. and Thomas M.D. (eds.) Proceedings of Exploration 17: Sixth Decennial International Conference on Mineral Exploration, p. 239–260.

Li Y. and Oldenburg D.W. 1996. 3-D Inversion of Magnetic Data. Geophysics, **61:**394-408. http://dx.doi.org/10.1190/1.1443968

Li Y., Shearer S.E., Haney M.M., Dannemiller N. 2010. Comprehensive approaches to 3D inversion of magnetic data affected by remanent magnetization. Geophysics, **75(1):**L1–L11. https://doi.org/10.1190/1.3294766

Loureiro F.E.L. and Tavares J.R. 1983. Duas novas ocorrências de carbonatitos: Mato Preto e Barra do Rio Itapirapuã. Revista Brasileira de Geociências, **13:**7-11. https://doi.org/10.25249/0375-7536.19831310711

Louro V.H.A, Mantovani M.S.M., Ribeiro V.B. 2017. Integrated geologic and geophysical interpretation of the Buraco da Velha copper deposit (Rondônia, Brazil): A basis for exploring in related environments. Geophysics, **82(3):**B121-B133. https://doi.org/10.1190/geo2016-0345.1

Louro V.H.A., Negrão A.P., Castro L.G., Ferreira F.J.F. 2019. Canoas geophysical anomaly: A possible alkaline body or unusual anomaly caused by mafic dykes in the Ponta Grossa Arch, Brazil? Journal of Applied Geophysics, 170, 103857, preprint. https://doi.org/10.1016/j.jappgeo.2019.103857

Mantovani M.S.M., Louro V.H.A., Ribeiro V.B., Requejo H.S., Santos R.P.Z. 2016. Geophysical analysis of Catalão I alkaline–carbonatite complex in Goiás, Brazil. Geophysical Prospecting, **64(1):**216-227. https://doi.org/10.1111/1365-2478.12283

Marangoni Y.R. and Mantovani M.S.M. 2013. Geophysical signatures of the alkaline intrusions bordering the Paraná Basin. Journal of South American Earth Sciences, **41:**83-89. https://doi.org/10.1016/j.jsames.2012.08.004

Miller H.G. and Singh V. 1994. Potential field tilt — a new concept for location of potential field sources. Journal of Applied Geophysics, **32:**213–217. https://doi.org/10.1016/0926-9851(94)90022-1

Morais S.M., Faleiros F.M., Costa V.S., Gomes S.D., Chieregati L.A., Rodrigues S.W.O. et al. 2012. Mapa geológico da Folha Apiaí. Escala 1:100000. Geological Survey of Brazil (CPRM).

Paine J., Haederle M., Flis M. 2001. Using transformed TMI data to invert for remanently magnetised bodies. Exploration Geophysics, **32(3/4):** 238–242. https://doi.org/10.1071/eg01238

Pereira W.R., Mantovani M.S.M., Santos R.P.Z. 2010. Análise geofísica do complexo Alcalino do Barreiro, Araxá-MG. Simpósio Brasileiro de Geofísica, 4, Proceedings, p. 1-5. https://doi.org/10.22564/4simbgf2010.038

Piccirillo E.M. and Melfi A.J. (eds.) 1988. *The Mesozoic flood volcanism from the Paraná Basin (Brazil). Petrogenetic and geophysical aspects*. São Paulo: IAG-USP, 600p.

Piccirillo E.M., Bellieni G., Cavazzini G., Comin-Chiaramonti P., Petrini R., Melfi A.J., Pinese J.P.P., Zantedeschi P., De Min A. 1990. Lower Cretaceous dyke swarms from the Ponta Grossa Arch: Petrology, Sr-Nd isotopes and genetic relationships with the Paraná flood volcanics. Chemical Geology, **89:**19-48. https://doi.org/10.1016/0009-2541(90)90058-F

Pilkington M. and Beiki M. 2013. Mitigating remanent magnetization effects in magnetic data using the normalized source strength. Geophysics, **78:**J25-J32. https://doi.org/10.1190/geo2012-0225.1

Raposo M.I.B. and Ernesto M. 1995. An Early Cretaceous paleomagnetic pole from Ponta Grossa dikes (Brazil): implications for the South American Mesozoic apparent polar wander path. J. Geophys. Res. Solid Earth, **100(B10):**20095–20109. https://doi.org/10.1029/95JB01681

Reid A.B., Allsop J.M., Granser H., Millett A.J., Somerton I.W. 1990. Magnetic interpretation in three dimensions using Euler deconvolution. Geophysics, **55(1):**80-91. https://doi.org/10.1190/1.1442774

Riccomini C., Velázquez V.F., Gomes C.B. 2005. Tectonic controls of the Mesozoic and Cenozoic Alkaline Magmatism in Central-Southeastern Brazilian Platform. In: Gomes C.B. and Comin-Chiaramonti P. (eds). Mesozoic to Cenozoic Alkaline Magmatism in the Brazilian Platform, p. 32-55.

Ruberti E., Castorina F., Censi P., Gomes C.B., Speziale S., Comin-Chiaramonti P. 1997. REE-C-O-Sr-Nd systematic in carbonatites from Barra do Itapirapuã and Mato Preto in Southern Brazil. In: South American Symposium on Isotope Geology, 1, Campos do Jordão, Proceedings, p. 271-275.

Ruberti E., Gomes C.B., Comin-Chiaramonti P. 2005. The alkaline magmatism from the Ponta Grossa Arch. In: Comin-Chiaramonti P. and Gomes C.B. (eds.) Mesozoic to Cenozoic alkaline magmatism in the Brazilian Platform. São Paulo, Edusp/Fapesp, p. 473-522.

Rugenski A. 2006. Investigação geofísica dos complexos alcalinos do sul e sudeste do Brasil. PhD thesis, Universidade de São Paulo, 352 p. https://doi.org/10.11606/t.14.2019.tde-26032013-093128

Santos R.V., Dardenne M.A., Matsui E. 1990. Geoquímica de isótopos de carbono e oxigênio dos carbonatitos do Complexo Alcalino de Mato Preto, Paraná, Brasil. Revista Brasileira de Geociências, **20(1-4):**153-158. https://doi.org/10.25249/0375-7536.1990153158

Saunders D.F., Branch J.F., Thompson C.K. 1994. Tests of Australian aerial radiometric data for use in petroleum reconnaissance, Geophysics, **59:**411-419. https://doi.org/10.1190/1.1443603

Saunders D.F., Terry S.A., Burson K.R., Branch J.F., Thompson C.K. 1993. Relation of thorium-normalizaed surface and aerial radiometric data to subsurface petroleum accumulations. Geophysics, **58:**1417-1427. https://doi.org/10.1190/1.1443357

Saunders D.F., Terry S.A., Thompson C.K. 1987. Test of National Uranium Resource Evaluation gamma-ray spectral data in petroleum reconnnaissance, Geophysics, **52:**1547-1556. https://doi.org/10.1190/1.1442271

Siga Jr. O., Gomes C.B., Sato K. Passarelli C.R. 2007. O Maciço Alcalino de Tunas, PR: Novos Dados Geocronológicos. Geologia USP Série Científica, **7(2):**71-80. https://doi.org/10.5327/Z1519-874x2007000200005

Sonoki I.K. and Garda G.M. 1988. Idades K/Ar de rochas alcalinas do Brasil meridional e Paraguai oriental: compilação e adaptação às novas constantes de decaimento. Boletim do Instituto de Geociências da USP, Série Científica, **19:**63-85. https://doi.org/10.11606/issn.2316-8986.v19i0p63-85

Spector A. and Grant F.S. 1970. Statistical models for interpreting aeromagnetic data. Geophysics, **35(2):**293-302. https://doi.org/10.1190/1.1440092

Swain C.J. 1976. A FORTRAN IV program for interpolating irregularly spaced data using the difference equations for minimum curvature. Computers & Geosciences, **1:**231-240. https://doi.org/10.1016/0098-3004(76)90071-6

Thomas M.D., Ford K.L., Keating P. 2016. Review paper: Exploration geophysics for intrusion-hosted rare metals. Geophysical Prospecting, **64(5):**1275–1304. https://doi.org/10.1111/1365-2478.12352

Ulbrich H. and Gomes C.B. 1981. Alkaline rocks from continental Brazil. Earth-Science Reviews, **17(1-2):**135-154. https://doi.org/10.1016/0012-8252(81)90009-x

Ussami N., Kolisnyk A., Raposo M.I.B., Ferreira F.J.F., Molina E.C., Ernesto M. 1994. Detectabilidade magnética de diques do Arco de Ponta Grossa: um estudo integrado de magnetometria terrestre/aérea e magnetismo de rocha. Revista Brasileira de Geociências, **21:**317-327. https://doi.org/10.25249/0375-7536.1991317327

Vasconcellos E.M.G. 1995. Petrologia e geoquímica de diques e "plugs" alcalinos da região do Vale do Ribeira, divisa dos Estados do Paraná e São Paulo. PhD thesis, Universidade de São Paulo, 202 p. https://doi.org/10.11606/t.44.1995.tde-28102015-105327

Vasconcellos E.M.G. and Gomes C.B. 1998. Diques e "plugs" alcalinos da região do Vale do Ribeira, Divisa dos Estados do Paraná e São Paulo: características petrográficas e geoquímicas. Geochimica Brasiliensis, **12:**123-143. https://doi.org/10.11606/issn.2316-8986.v29i0p97-124

Verplanck P.L. and Gosen, B.S.V. 2011. Carbonatite and alkaline intrusion-related rare earth element deposits - A deposit model: U.S. Geological Survey Open-File Report 2011-1256, 6 p. http://dx.doi.org/10.3133/ofr20111256

Vieira A.J. 1973. Geologia do centro e nordeste do Paraná e centro-sul de São Paulo. In: Congresso Brasileiro de Geologia, 27, Aracaju, Proceedings, v.3, p. 259-277.

Wilford J.R., Bierwirth P.N., Craig M.A. 1997. Application of airborne gamma-ray spectrometry in soil/regolith mapping and applied geomorphology. AGSO Journal of Australian Geology and Geophysics, **17(2):**201-216. http://pid.geoscience.gov.au/dataset/ga/81503

6 COMPLEMENTARY RESULTS

6.1 FLIGHT HEIGHT OF LINES

The plot below (**Figure 39**) demonstrates the average survey height for each line of the totality of the CPRM (2011) Paraná-Santa Catarina project. Its representation was divided into two categories: radiometrics and magnetics. The total average flight height for each type of data is almost equal, with the radiometric survey presenting 163 m while the magnetic one is slightly above, comprising 165 m. These values exceeded the nominal flight height (i.e. 100 m) expressed in the report from CPRM (2011). It is also noted that a significant amount of lines are situated above 300 m, maybe because of aircraft security reasons according to the CPRM (2011) report. Some lines showed even higher values (**Figure 39**). For example, lines 131168 (822 m) and 12937 (775 m) are above the 700 m threshold. These lines were not located in the study area, however.

Thus, the results suggest that the flight height of airborne surveys should be verified by the interpreter even when the report of the contractor displays the nominal survey height, which can be a piece of misleading information. Aerogeophysical signal, which is strongly dependent on the sensor height, could be attenuated where outliers in the survey height are present.

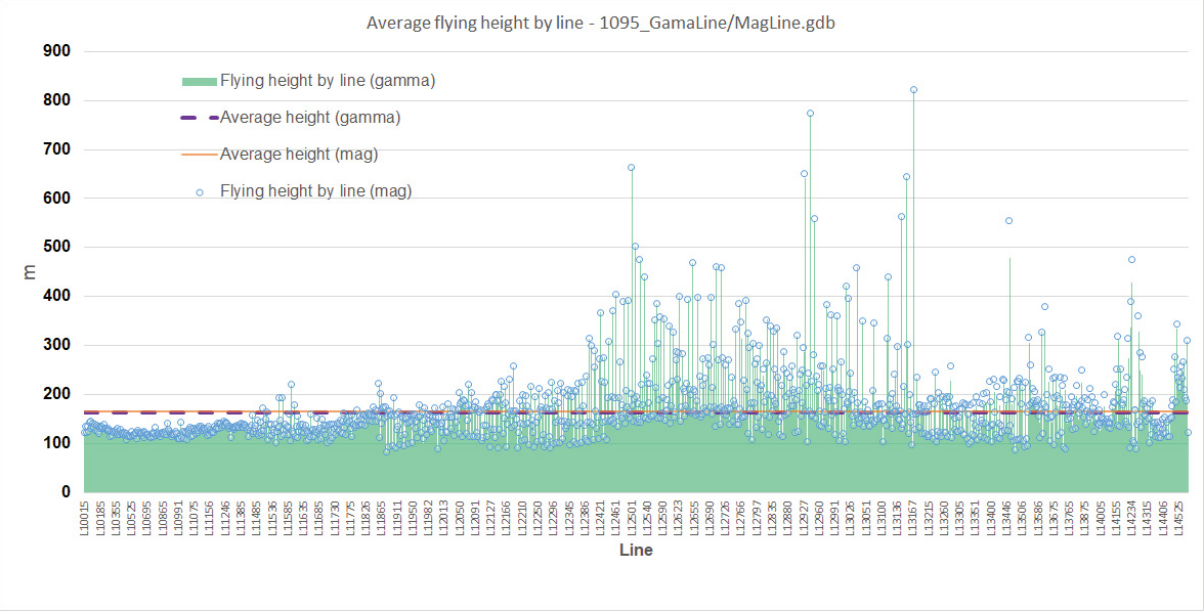

Figure 39. Average survey height by each line of the CPRM Paraná-Santa Catarina airborne survey project. Note that not all the lines were labeled on the x-axis due to the lack of proper space in the chart.

7 FINAL REMARKS

7.1 FINDINGS

This section outlines the major results and findings and emphasizes the contributions to the understanding of airborne magnetic and radiometric signatures in alkaline, alkalic-carbonatitic, and gabbros complexes. The igneous rocks analyzed in this thesis were: Bairro da Cruz, Banhadão, Itapirapuã, Barra do Itapirapuã, Barra do Teixeira, José Fernandes, Mato Preto, and Tunas.

Depth estimates from the radially averaged power spectrum, Euler 3D deconvolution, and tilt angle revealed mainly magnetic sources with an average of 500 m, indicating shallow sources. Total magnetic field anomaly and filtering techniques applied in the study area displayed that Bairro da Cruz, José Fernandes, and Tunas complexes are the bodies with significant magnetic responses. Dipolar anomalies with little to no interference of remanent magnetism were associated with these complexes. Magnetic susceptibility models from different filtering techniques were generated for the three igneous rocks. The results showed good agreement with magnetic susceptibilities values of alkaline rocks and gabbros, even though the shape and geometry of the rocks modeled could not be representative of the known geology. A possible explanation for this might be the lack of constraints used in the inversions since there is no information about the alkaline complexes' magnetic properties and/or borehole data that defined their emplacement depths.

With respect to radiometrics, results from gridded and profile data demonstrated that no general classification based on radioelements for alkaline rocks could be implemented due to the lack of clear patterns. The igneous rocks studied in this thesis are mainly enriched in eTh over eU and K, which supports other works regarding alkaline complexes. In addition, complexes that host carbonatites, i.e. Barra do Itapirapuã and Mato Preto, showed the highest contents of eTh and eU in comparison to other complexes that do not contain carbonatites.

7.2 FUTURE WORK

Further research is hence needed to confirm the state of magnetization of the igneous rocks in the study area as well as to confirm the intensity of remanent magnetism in those modeled bodies to constrain future modeling.

More information on radiometric data, such as conducting small-scale ground geophysical surveys, would help in establishing a greater degree of accuracy on the radioactive element concentrations and also to corroborate the existence of higher eTh/other radioelements levels relation verified in this work.

REFERENCES

Airo M. 2015. Geophysical signatures of mineral deposit types – synopsis. In: Airo M. (ed.) Geophysical signatures of mineral deposit types. Espoo: Geological Survey of Finland, Special Paper 58, p. 9-70. Available at: <http://tupa.gtk.fi/julkaisu/specialpaper/sp_058.pdf>. Accessed on: Oct. 18, 2018.

Airo M., Hyvönen E., Lerssi J., Leväniemi H., Routsalainen A. 2014. Tips and tools for the application of GTK´s airborne geophysical data. Geological Survey of Finland, Report of Investigation 215, 33 p. Available at: <tupa.gtk.fi/julkaisu/tutkimusraportti/tr_215.pdf>. Accessed on: Oct. 20, 2018.

Algarte J.P. 1972. A influência dos arqueamentos cratônicos no condicionamento das alcalinas dos Estados de São Paulo e Paraná. In: Congresso Brasileiro de Geologia, 26, Belém. Proceedings, v.1, p. 65-69.

Alkmim F.F. 2015. Geological Background: A Tectonic Panorama of Brazil. In: Vieira B.C. et al. (eds.). Landscapes and Landforms of Brazil, World Geomorphological Landscapes. Springer: Dordrecht, 9-17. https://doi.org/10.1007/978-94-017-8023-0_2

Almeida F.F.M. 1966. Origem e evolução da plataforma brasileira. 2ª Semana de Estudos Geológicos. Universidade Federal do Rio Grande do Sul, Porto Alegre, Anais, 45-128.

Almeida F.F.M. 1967. Origem e evolução da Plataforma Brasileira. DNPM-DGM Boletim, **241:**5-36.

Almeida F.F.M. 1971. Condicionamento tectônico do magmatismo alcalino mesozóico do Sul do Brasil e do Paraguai Oriental. Anais da Academia Brasileira de Ciências, **43:**835-836.

Almeida F.F.M. 1972. Tectono-magmatic activation of the South American Platform and associated mineralization. 24th International Geological Congress, Montreal, Proceedings, Section 3, 339-346.

Almeida F.F.M. 1983. Relações tectônicas das rochas alcalinas mesozóicas da região meridional da plataforma sul-americana. Revista Brasileira de Geociências, **13:**139-158. https://doi.org/10.25249/0375-7536.1983133139158

Almeida F.F.M., Brito-Neves B.B., Carneiro C.D.R. 2000. Origin and evolution of the South American platform. Earth Science Reviews, **50:**77–111. https://doi.org/10.1016/S0012-8252(99)00072-0

Almeida F.F.M., Hasui Y., Brito-Neves B.B., Fuck R.A. 1981. Brazilian structural provinces: an introduction. Earth Science Reviews, **17:**1–21. https://doi.org/10.1016/0012-8252(81)90003-9

Almeida R.I.R. 1982. O Arco de Ponta Grossa: uma proposta de configuração a partir da interpretação de dados de sensoriamento remoto. MSc thesis, Instituto Nacional de Pesquisas Espaciais (INPE), São Paulo, 108 p.

Almeida V.V. 2016. Petrologia do Gabro José Fernandes e sua relação temporal com o magmatismo mesozoico toleítico e alcalino no arco de Ponta Grossa. PhD thesis, Universidade de São Paulo, São Paulo, 274 p. http://doi.org/10.11606/T.44.2017.tde-30032017-083933

Almeida V.V., Janasi V.A., Azzone R.G., Faleiros F.M. 2019. Crustal contamination and genesis of transitional alkaline-tholeiitic intrusions: Insights from the José Fernandes Suite, Paraná Magmatic Province, Brazil. Lithos, **342-343:**59-75. doi:10.1016/j.lithos.2019.05.023

Almeida V.V., Janasi V.A., Heaman L.M., Shaulis B.J., Hollanda M.H.B.M., Renne P.R. 2017. Contemporaneous alkaline and tholeiitic magmatism in the Ponta Grossa Arch, Paraná-Etendeka Magmatic Province: constraints from U-Pb zircon/baddeleyite and 40Ar/39Ar phlogopite dating of the José Fernandes Gabbro and mafic dykes. Journal of Volcanology and Geothermal Research, **355:**55-65. doi: 10.1016/j.jvolgeores.2017.01.018

Alva-Valdivia L.M., López-Loera H. 2011. A review of iron oxide transformations, rock magnetism and interpretation of magnetic anomalies: El Morro Mine (Brazil), a case study. Geofísica Internacional, **50(3):**341-362.

Andrade F.R., Möller P., Lüders V., Dulski P., Gilg, H. 1999. Hydrothermal rare earth elements mineralization in the Barra do Itapirapuã carbonatite, southern Brazil: behaviour of selected trace elements and stable isotopes (C, O). Chemical Geology, **155(1-2)**:91–113. doi:10.1016/s0009-2541(98)00143-0

Arioli E.E., Salazar Jr. 2015. Geologia e Recursos Minerais do estado do Paraná. MINEROPAR - Minerais do Paraná. Report. 128 p. Retrieved from: https://www.documentador.pr.gov.br/documentador/pub.do?action=d&uuid=@gtf-escriba-minerop@1ea55ed3-62f5-4050-b1b9-9efe73ef7630 Accessed 10/jul/2019.

Baranov V. 1957. A new method for interpretation of aeromagnetic maps: pseudo-gravimetric anomalies. Geophysics, **22:**359–383. https://doi.org/10.1190/1.1438369

Baranov V. and Naudy H. 1964. Numerical calculation of the formula of reduction to the magnetic pole. Geophysics, **29:**67–79. https://doi.org/10.1190/1.1439334

Barbosa O. 1941. Geologia e petrologia da região de Apiaí, estado de São Paulo. Universidade de São Paulo. Admission thesis for professor.

Billings S. and Richards D. 2000. Quality control of gridded aeromagnetic data. Exploration Geophysics, **31:**611-616. https://doi.org/10.1071/EG00611

Blakely R.J. 1995. Potential theory in gravity and magnetic applications. Cambridge, Cambridge University Press, 441 p. https://doi.org/10.1017/CBO9780511549816

Blakely R.J., Connard G.G., Curto J.B. 2016. Tilt Derivative Made Easy. Technical note – Geosoft. Retrieved from <https://www.geosoft.com/media/uploads/resources/tilt_derivative_made_easy_07-2016.pdf> Accessed 30/dec/2019.

Briggs I.C. 1974. Machine contouring using minimum curvature. Geophysics, **39(1):**39-48. https://doi.org/10.1190/1.1440410

Brumatti M. and Almeida V.V. 2014. Rochas Alcalinas: Áreas de Registro, Iguape e Cerro Azul. Anexo III: Atualização da cartografia geológica da Folha Cerro Azul SG.22-X-B-IV. Estados de São Paulo e Paraná. São Paulo: CPRM, Escala 1:100.000.

Brumatti M. and Almeida V.V. 2015. Rochas Alcalinas: Áreas de Registro, Iguape e Cerro Azul. Anexo IV: Mapas geológicos e geoquímicos dos corpos alcalinos na Folha Cerro Azul, SG.22-X-B-IV. Estados de São Paulo e Paraná. São Paulo: CPRM, Escala 1:100.000.

Brumatti M. and Tomita S.A. 2014a. Geologia e recursos minerais das folhas Vila Branca – SG.22-X-B-IV-1 e Ribeira – SG.22-X-B-IV-2, estados de São Paulo e Paraná, escala 1:50.000. São Paulo: CPRM.

Brumatti M. and Tomita S.A. 2014b. Mapa geológico da folha Vila Branca – SG.22-X-B-IV-1. Escala 1:50000. São Paulo: CPRM.

Brumatti M., Almeida V.V., Lopes A.P., Campos F.F., Perrotta M.M., Mendes D., Pinto L.G.R., Palmeira L.C.M. 2015. Metalogenia das províncias minerais do Brasil: rochas alcalinas da porção meridional do cinturão Ribeira, estados de São Paulo e Paraná. CPRM, Informe de Recursos Minerais, Série Províncias Minerais do Brasil, 6:1-79.

Carvalho P.F. and Pinto E.A. 1937. Reconhecimento geológico da região sul da Série Assunguy. Boletim do Serviço Geológico e Mineralógico, 71, 29p.

Castro F.R., Oliveira S.P., Souza, J., Ferreira F.J.F. 2018. Combining tilt derivative filters: new approaches to enhance magnetic anomalies. Brazilian Journal of Geophysics, **36(3):**335-343. http://dx.doi.org/10.22564/rbgf.v36i3.1956

Chmyz L., Ribeiro J.C., Zaramella D.R. 2011. Análise faciológica do Gabro José Fernandes (Adrianópolis, PR) e considerações preliminares do seu potencial econômico. In: Proceedings of VII Encontro Internacional de Produção Científica CESUMAR, v. 1, p. 1-5.

Choppin G.R. 1988. Humics and Radionuclide Migration. Radiochimica Acta, **44-45(1):**23-28. doi:10.1524/ract.1988.4445.1.23

Clark D.A. 1997. Magnetic petrophysics and magnetic petrology: aids to geological interpretation of magnetic surveys. AGSO Journal of Australian Geology and Geophysics, 17(2):83-103. http://pid.geoscience.gov.au/dataset/ga/81495

Clark D.A. 1999. Magnetic petrology of igneous intrusions: implications for exploration and magnetic interpretation. Exploration Geophysics, **30:**5-26. https://doi.org/10.1071/EG999005

Clark D.A. and Emerson D.W. 1991. Notes on rock magnetization characteristics in applied geophysical studies. Exploration Geophysics, **22(3):**547-555. https://doi.org/10.1071/EG991547

Comin-Chiaramonti P. and Gomes C.B. (eds.). 2005. *Mesozoic to Cenozoic alkaline magmatism in the Brazilian Platform*. São Paulo, EdUSP/Fapesp, 752 p.

Comin-Chiaramonti P., Castorina F., Cundari A., Petrini R., Gomes C.B. 1995. Dykes and sills from eastern Paraguay: Sr and Nd systematics. In: Baer G. and Heiman A. (eds.) Physics and chemistry of dykes. Rotterdam: Balkema, 267-278.

Comin-Chiaramonti P., Cundari A., DeGraff J.M., Gomes C.B., Piccirillo E.M. 1999. Early Cretaceous-Tertiary magmatism in eastern Paraguay (western Paraná Basin): geological, geophysical and geochemical relationships. Journal of Geodynamics, **28:**375-391. https://doi.org/10.1016/S0264-3707(99)00016-2

Comin-Chiaramonti P., Gomes C.B., Ruberti E., Antonini P., Censi P. 2001. Mato Preto alkaline-carbonatite complex: geochemistry and isotope (O-C, Sr-Nd) constraints. Geochimica Brasiliensis, **15:**23-24. http://dx.doi.org/10.21715/gb.v15i1.181

Comin-Chiaramonti, P., Cundari A., Piccirillo E.M., Gomes C.B., Castorina F., Censi P., De Min A., Marzoli A., Speziale S., Velázquez V.F. 1997. Potassic and sodic igneous rocks from eastern Paraguay: their origin from the lithospheric mantle and genetic relationships with the associated Paraná flood tholeiites. Journal of Petrology, **38:**495-528. https://doi.org/10.1093/petroj/38.4.495

Cooper G.R.J. and Cowan D.R. 2006. Enhancing potential field data using filters based on the local phase. Computers & Geosciences, **32:**1585-1591. https://doi.org/10.1016/j.cageo.2006.02.016

Cordani U.G. and Hasui Y. 1968. Idades K-Ar de rochas alcalinas do primeiro planalto do Estado do Paraná. In: Anais do 22º Congresso Brasileiro de Geologia, Belo Horizonte, SBG, **1:**149-153.

Cordell L. and Grauch J.S. 1985. Mapping basement magnetization zones from aeromagnetic data in the San Juan Basin, New Mexico. In: 52nd Annual International Meeting, SEG, Expanded Abstracts, 246–247. https://doi.org/10.1190/1.1826915

Cowan D.R. and Cowan S. 1993. Separation Filtering Applied to Aeromagnetic Data. Exploration Geophysics, **24(3-4):**429–436. doi:10.1071/eg993429

CPRM - Geological Survey of Brazil and DNPM - National Department of Mineral Production. 1977. Projeto Leste do Paraná. Folha Curitiba SG.22-X-D-I. 234p.

CPRM - Geological Survey of Brazil. 1978a. Projeto Aerogeofísico Serra do Mar Sul. CPRM/DNPM, Rio de Janeiro.

CPRM - Geological Survey of Brazil. 1978b. Projeto Aerogeofísico São Paulo-Rio de Janeiro. CPRM/DNPM, Rio de Janeiro.

CPRM - Geological Survey of Brazil. 2011. Programa Geologia do Brasil (PGB) – Projeto aerogeofísico Paraná-Santa Catarina: relatório final do levantamento e processamento dos dados magnetométricos e gamaespectrométricos. Volume I. Lasa Prospecções, 326 p.

Curto J.B., Vidotti R.M., Fuck R.A., Blakely R.J., Alvarenga C.J.S., Dantas E.L. 2014. The tectonic evolution of the Transbrasiliano Lineament in northern Paraná Basin, Brazil, as inferred from aeromagnetic data. Journal of Geophysical Research: Solid Earth, **119(3):**1544–1562. https://doi.org/10.1002/2013jb010593

Darnley A.G. 1972. Airborne gamma-ray survey techniques. In: Uranium prospecting handbook: Institution of Mining&Metallurgy, 174–211.

Dentith M. and Mudge S.T. 2014. Geophysics for the Mineral Exploration Geoscientist. Cambridge University Press, 454p. https://doi.org/10.1017/cbo9781139024358

Dickson B.L. and Scott K.M. 1997. Interpretation of aerial gamma-ray surveys – adding the geochemical factors. AGSO Journal of Australian Geology & Geophysics, **17(2):**187-200. http://pid.geoscience.gov.au/dataset/ga/81502

Drenth B.J. 2014. Geophysical expression of a buried niobium and rare earth element deposit: The Elk Creek carbonatite, Nebraska, USA. Interpretation, **2(4):**SJ23–SJ33. https://doi.org/10.1190/int-2014-0002.1

Efimov A.V. 1978. Multiplikativniyi pokazatel dlja vydelenija endogennych rud aerogamma-spectrometriceskim dannym. In: Metody rudnoj geofiziki. Naucno proizvodstvennoje objedinenie geofizica, Leningrado, 59-68.

Evjen H.M. 1936. The place of vertical gradient in gravitational interpretations. Geophysics, **1(1):**127-136. https://doi.org/10.1190/1.1437067

Faleiros F.M., Morais S.M., Costa V.S. 2012. Geologia e recursos minerais da folha Apiaí SG.22-X-B-V: escala 1:100.000: estados de São Paulo e Paraná. São Paulo: CPRM. Programa Geologia do Brasil, Programa Levantamentos Geológicos Básicos do Brasil.

Ferreira F.J.F. 1982. Integração de dados aeromagnéticos e geológicos: configuração e evolução tectônica do Arco de Ponta Grossa. MS thesis, Universidade de São Paulo, São Paulo, 186 p. https://doi.org/10.11606/d.44.1983.tde-14082013-161535

Ferreira F.J.F. and Algarte J.P. 1979. O comportamento aeromagnetométrico – cintilométrico das principais rochas alcalinas dos Estados de São Paulo e Paraná. In: Simpósio Regional de Geologia, 2, Rio Claro. Atas, **2:**195-208.

Ferreira F.J.F., Algarte J.P., Theodorovicz A., Martins F.A.G., Monma R., Silva R.B., Tassinari C.G.C., Rodrigues E.P., Coutinho J.V.M. 1987. O Complexo alcalino de Pariquera-Açu. In: Proceedings of VI Simpósio Regional de Geologia. Sociedade Brasileira de Geologia, **1:**159-171.

Ferreira F.J.F., Daitx E.C., Moraes M.C. 1984. Nova contribuição do magmatismo Mesozóico associada ao Arco de Ponta Grossa: o Complexo Gabróide Barra do Estrela. Anais do XXXIII do Congresso Brasileiro de Geologia, Rio de Janeiro, 1693-1706.

Ferreira F.J.F., Fruchting A., Guimarães G.B., Alves L.S., Martin V.M.O., Ulbrich H.H.G.J. 2009. Levantamentos Gamaespectrométricos em Granitos Diferenciados. II: O Exemplo do Granito Joaquim Murtinho, Complexo Granítico Cunhaporanga, Paraná. Geologia USP, Série Científica, **9(1):**55–72. doi:10.5327/z1519-874x2009000100004

Ferreira F.J.F., Moraes R.A.V., Ferrari M.P., Vianna R.B. 1981. Contribuição ao estudo do Alinhamento Estrutural de Guapiara. In: Atas do III Simpósio Regional de Geologia, São Paulo SP: Sociedade Brasileira de Geologia, **1:**226-240.

Ferreira F.J.F., Souza J., Bongiolo A.B.S., Castro L.G. 2013. Enhancement of the total horizontal gradient of magnetic anomalies using the tilt angle. Geophysics, **78:**33-41. https://doi.org/10.1190/geo2011-0441.1

Fitton J.G. and Upton B.G.J. (eds.). 1987. Alkaline igneous rocks. Geological Society, special publication, 30, 568 p.

Ford K.L., Dilabio R.N.W., Rencz A.N. 1988. Geological, geophysical and geochemical studies around the Allan Lake carbonatite, Algonquin Park, Ontario. Journal of Geochemical Exploration, **30(1-3):**99–121. doi:10.1016/0375-6742(88)90054-4

Forman J.M.A. and Angeiras A.G. 1981. Poços de Calderas and Itataia: Two case histories of uranium exploration in Brazil. In: International Atomic Energy Agency. Uranium Exploration Case Histories, p. 99-139.

Fuck R.A. 1972. Geologia do maciço alcalino de Tunas, Paraná, Brasil. PhD thesis, Universidade de São Paulo, 82p. https://doi.org/10.11606/t.44.2016.tde-10062016-095215

Galbraith J. H. and Saunders D.F. 1983. Rock classification by characteristics of aerial gamma-ray measurements. Journal of Geochemical Exploration, **18(1):**49–73. doi:10.1016/0375-6742(83)90080-8

García-Abdeslem J. and Ness G.E. 1994. Inversion of the power spectrum from magnetic anomalies. Geophysics, **59(3):**391-404. https://doi.org/10.1190/1.1443601

Geosoft. 2010. montaj MAGMAP Filtering - 2-D Frequency Domain Processing of Potential Field Data: Extension for Oasis montaj v7.1. Tutorial and User Guide, 73 p.

Gibson S.A., Thompson R.N., Leonardos O.H., Dickin A.P., Mitchell J.G. 1995. The Late Cretaceous impact of the Trindade mantle plume: evidence from large-volume, mafic, potassic magmatism in SE Brazil. Journal of Petrology, **36:**189-229. https://doi.org/10.1093/petrology/36.1.189

Gibson S.A., Thompson R.N., Weska R.K., Dickin A.P., Leonardos O.H. 1997. Late Cretaceous rift-related upwelling and melting of the Trindade starting mantle plume head beneath western Brazil. Contributions to Mineralogy and Petrology, **126:**303-314. https://doi.org/10.1007

Gill R. 2010. Igneous rocks and processes: a practical guide. John Wiley & Sons. 472 p.

Gimenez Filho A., Janasi V.A., Campanha G.A.C., Teixeira W., Trevizoli Júnior L.E. 2000. U-Pb dating and Rb-Sr isotope geochemistry of the eastern portion of the Três Córregos batholith, Ribeira fold belt, São Paulo. Revista Brasileira de Geociências, **30:**45-50. https://doi.org/10.25249/0375-7536.2000301045050

Gnojek I. and Prichystal A. 1985. A new zinc mineralization detected by airborne gamma-ray spectrometry in Northern Moravia (Czechoslovakia). Geoexploration, **23(4):**491-502. https://doi.org/10.1016/0016-7142(85)90076-6

Gomes C.B. 1970. Petrologia do maciço alcalino de Itapirapuã, São Paulo. Boletim do Instituto de Geociências e Astronomia da USP, **1:**77-188. https://doi.org/10.11606/issn.2316-9001.v1i0p77-197

Gomes C.B. and Comin-Chiaramonti P. (eds.) 2017. Magmatismo alcalino continental da região meridional da plataforma brasileira. EdUSP/Fapesp, 608 p.

Gomes C.B. and Comin-Chiaramonti P. 2005. An introduction to the alkaline and alkaline carbonatitic magmatism in and around the Paraná Basin. In: Gomes C.B. and Comin-Chiaramonti P. (eds). Mesozoic to Cenozoic Alkaline Magmatism in the Brazilian Platform. 21-29.

Gomes C.B., Azzone R.G., Ruberti E., Vasconcelos P.M., Sato K., Rojas G.E.E. 2018. New age determinations for the Banhadão and Itapirapuã complexes in the Ribeira Valley, southern Brazil. Brazilian Journal of Geology, **48:**1-12. https://doi.org/10.1590/2317-4889201820170094

Gomes C.B., Barbieri M., Beccaluva L., Brotzu P., Conte A., Garbarino C., Macciotta G., Melluso L., Morbidelli L., Ruberti E., Scheibe L.F., Tamura R.M., Traversa G. 1987. Petrological and geochemical studies of alkaline rocks from continental Brazil: 2. The Tunas massif, State of Paraná. Geochimica Brasiliensis, **1(2):**201-234.

Gomes C.B., Ruberti E., Comin-Chiaramonti P., Azzone R.G. 2011. Alkaline magmatism in the Ponta Grossa Arch, SE Brazil: a review. Journal of South American Earth Sciences, **32(2):**152-168. http://dx.doi.org/10.1016/j.jsames.2011.05.003

Grant F.S. and Dodds J. 1972. MAGMAP FFT Processing System Development Notes. Paterson Grant and Watson Ltd, Canada.

Grant J.A. 1998. Ten things the textbooks don't tell you about processing and archiving airborne gamma-ray spectrometric data. In: Geological Survey of Canada. Current Research n. 1998-D, Eastern Canada and national and general programs, 83-87. https://doi.org/10.4095/209538

Grauch V.J.S. and L. Cordell. 1987. Limitations of determining density or magnetic boundaries from the horizontal gradient of gravity or pseudogravity data: Geophysics, **52:**118–121. http://dx.doi.org/10.1190/1.1442236

Hama M., Algarte J.P., Paiva I.P., Rodrigues J.C. 1977. Idades K/Ar do maciço alcalino do Banhadão e do complexo Bairro da Cruz. In: Atas do I Simpósio Regional de Geologia, São Paulo. São Paulo: Sociedade Brasileira de Geologia. **1:**170-178.

Haney M., C. Johnston, Y. Li, M. Nabighian. 2003. Envelopes of 2D and 3D magnetic data and their relationship to the analytic signal: Preliminary results: 73rd Annual International Meeting, SEG Expanded Abstracts, 596–599. https://doi.org/10.1190/1.1817997

Hart S.R. 1988. Heterogeneous mantle domains: signatures, genesis and mixing chronologies. Earth and Planetary Science Letters, **90:**273-296. https://doi.org/10.1016/0012-821X(88)90131-8

Hidalgo-Gato M.C. and Barbosa V.C.F. 2015. Edge detection of potential-field sources using scale-space monogenic signal: Fundamental principles. Geophysics, **80:**J27-J36. https://doi.org/10.1190/geo2015-0025.1

Hinze W.J., Von Frese R.R.B., Saad A.H. 2013. Gravity and magnetic exploration: Principles, practices, and applications. Cambridge University Press. 525p.

Holden E.J., Wong J.C., Kovesi P., Wedge D., Dentith M., Bagas L. 2012. Identifying structural complexity in aeromagnetic data: An image analysis approach to greenfields gold exploration. Ore Geology Reviews, **46:**47–59. doi:10.1016/j.oregeorev.2011.11.002

Holden E.J., Wong J.C., Wedge D., Martis M., Lindsay M., Gessner K. 2016. Improving assessment of geological structure interpretation of magnetic data: An advanced data analytics approach. Computers & Geosciences, **87:**101–111. doi:10.1016/j.cageo.2015.11.010

Horsfall K.R. 1997. Airborne magnetic and gamma ray data acquisition. AGSO Journal of Australian Geology & Geophysics, **17(2):**159-174. http://pid.geoscience.gov.au/dataset/ga/81489

IAEA - International Atomic Energy Agency. 1991. Airborne gamma ray spectrometer surveying. Technical Reports Series, 323, 97 p.

IAEA - International Atomic Energy Agency. 2003. Guidelines for radioelement mapping using gamma ray spectrometry data. IAEA TECDOC, 1363, 184 p.

IBGE - Brazilian Institute of Geography and Statistics. 2019. Acesso e uso de dados geoespaciais. Manuais Técnicos em Geociências, n.14, Rio de Janeiro.

Isles D.J. and Rankin L.R. 2013. Geological Interpretation of Aeromagnetic Data. Society of Exploration Geophysicists and the Australian Society of Exploration Geophysicists. 365p. http://dx.doi.org/10.1190/1.9781560803218

Jenkins II R.E. 1987. Geology of the Clugger fluorite deposit, Mato Preto, Paraná, Brazil. Revista Brasileira de Geociências, **17:**288–294. https://doi.org/10.25249/0375-7536.1987288294

Kaefer L.Q. and Algarte J.P. 1972. Maciço alcalino do Banhadão: estudos preliminares. XXVI Congresso Brasileiro de Geologia. Anais, Belém-PA, 1-55-64.

Killeen P.G. 1979. Gamma ray spectrometric methods in uranium exploration-application and interpretation. In: Hood P.J. Geophysics and geochemistry in the search for metallic ores. Geological Survey of Canada, Economic Geology Report **31:**163-230. http://dx.doi.org/10.4095/106049

Langmuir D. and Herman J.S. 1980. The mobility of thorium in natural waters at low temperatures. Geochimica et Cosmochimica Acta, **44(11):**1753–1766. doi:10.1016/0016-7037(80)90226-4

Leão-Santos M., Li Y., Moraes R. 2015. Application of 3D magnetic amplitude inversion to iron oxide-copper-gold deposits at low magnetic latitudes: A case study from Carajás Mineral Province, Brazil. Geophysics, **80(2):**B13–B22. https://doi.org/10.1190/geo2014-0082.1

Li X. 2006a. Understanding 3D analytic signal amplitude. Geophysics, **71(2):**L13-L16. https://doi.org/10.1190/1.2184367

Li X. 2006b. On “Theta map: Edge detection in magnetic data” (C. Wijns, C. Perez, P. Kowalczyk. 2005. Geophysics, 71:L39–L43). Geophysics, **71(3):**X11-X12. http://dx.doi.org/10.1190/1.2194525

Li Y. 2017. From Susceptibility to Magnetization: Advances in the 3D Inversion of Magnetic Data in the Presence of Significant Remanent Magnetization. In: Tschirhart V. and Thomas M.D. (eds.) Proceedings of Exploration 17: Sixth Decennial International Conference on Mineral Exploration, 239–260.

Li Y. and Oldenburg D.W. 1996. 3-D Inversion of Magnetic Data. Geophysics, **61:**394-408. http://dx.doi.org/10.1190/1.1443968

Li Y., Shearer S.E., Haney M.M., Dannemiller N. 2010. Comprehensive approaches to 3D inversion of magnetic data affected by remanent magnetization. Geophysics, **75(1):**L1–L11. https://doi.org/10.1190/1.3294766

Loureiro F.E.L. and Tavares J.R. 1983. Duas novas ocorrências de carbonatitos: Mato Preto e Barra do Rio Itapirapuã. Revista Brasileira de Geociências, **13:**7-11. https://doi.org/10.25249/0375-7536.19831310711

Louro V.H.A, Mantovani M.S.M., Ribeiro V.B. 2017. Integrated geologic and geophysical interpretation of the Buraco da Velha copper deposit (Rondônia, Brazil): A basis for exploring in related environments. Geophysics, **82(3):**B121-B133. https://doi.org/10.1190/geo2016-0345.1

Louro V.H.A., Negrão A.P., Castro L.G., Ferreira F.J.F. 2019. Canoas geophysical anomaly: A possible alkaline body or unusual anomaly caused by mafic dykes in the Ponta Grossa Arch, Brazil? Journal of Applied Geophysics, 170, 103857, preprint. https://doi.org/10.1016/j.jappgeo.2019.103857

Luyendyk A.P.J. 1997. Processing of airborne magnetic data. AGSO Journal of Australian Geology and Geophysics, **17(2):**31-38. Geoscience Australia, Canberra. http://pid.geoscience.gov.au/dataset/ga/81490

Mantovani M.S.M., Louro V.H.A., Ribeiro V.B., Requejo H.S., Santos R.P.Z. 2016. Geophysical analysis of Catalão I alkaline–carbonatite complex in Goiás, Brazil. Geophysical Prospecting, **64(1):**216-227. https://doi.org/10.1111/1365-2478.12283

Mantovani M.S.M., Rugenski A., Diogo L.A., Shukowsky W. 2005. Integrated geophysical investigation of a possible new alkaline occurrence in SE Brazil. Journal of South American Earth Sciences, **20(3):**259–266. https://doi.org/10.1016/j.jsames.2005.05.011

Marangoni Y.R. and Mantovani M.S.M. 2013. Geophysical signatures of the alkaline intrusions bordering the Paraná Basin. Journal of South American Earth Sciences, **41:**83-89. 10.1016/j.jsames.2012.08.004

Melcher G.C., Cordani U.G., Damasceno E.C., Girardi V.A.V., Gomes C.B., Melfi A.J. 1971. Geologia das rochas Pré-Cambrianas do Vale do Rio Ribeira de Iguape. In: XXV Congresso Brasileiro de Geologia, Boletim Especial, 1:193-194.

Melcher G.C., Gomes, C.B., Cordani, U.G., Bettencourt, J.S., Damasceno, E.C., Girardi, V.A.V., Melfi, A.J. 1973. Geologia e petrologia das rochas metamórficas e graníticas associadas do Vale do Rio Ribeira de Iguape, SP e PR. Revista Brasileira de Geociências, **3:**97-123. https://doi.org/10.25249/0375-7536.197397123

Miller H.G. and Singh V. 1994. Potential field tilt — a new concept for location of potential field sources. Journal of Applied Geophysics, **32:**213–217. https://doi.org/10.1016/0926-9851(94)90022-1

Milner S.C., Le Roex A.P., O'Connor J.M. 1995. Age of Mesozoic rocks in northwestern Namibia, and their relationship to continental breakup. Journal of the Geological Society, **152:**97-104. https://doi.org/10.1144/gsjgs.152.1.0097

Minty B.R.S. 1997. Fundamentals of airborne gamma-ray spectrometry. AGSO Journal of Australian Geology and Geophysics, **17(2):**39-50. http://pid.geoscience.gov.au/dataset/ga/81491

Minty B.R.S. 2011. Short note: on the use of radioelement ratios to enhance gamma-ray spectrometric data. Exploration Geophysics, **42:**116-120. https://doi.org/10.1071/EG10011

Mitchinson D., Fournier D., Heagy L., Kang S. 2017. Geophysical Toolkit for Geologists. Retrieved from http://toolkit.geosci.xyz/index.html Accessed 20-dec-2020.

Moraes Rego L.F., Almeida F.F.M. 1946. Seção geológica de Capela da Ribeira a Curitiba. Universidade de São Paulo, Separata de Geologia e Metalurgia, **3:**5-30.

Morais S.M., Faleiros F.M., Costa V.S., Gomes S.D., Chieregati L.A., Rodrigues S.W.O. et al. 2012. Mapa geológico da Folha Apiaí. Escala 1:100000. Geological Survey of Brazil (CPRM).

Moro P.S., Vidotti R.M., Dantas E.L. 2018. Structural framework from gravity and magnetic data in the paleo/mesoproterozoic Araí rift-sag Basin, Central Brazil. Geophysics, **83:**B195-B207. https://doi.org/10.1190/geo2017-0627.1

Nabighian M.N. 1972. The analytic signal of two-dimensional magnetic bodies with polygonal cross section: its properties and use for automated anomaly interpretation. Geophysics, **37:**507-17. https://doi.org/10.1190/1.1440276

Nabighian M.N. 1974. Additional comments on the analytic signal of two-dimensional magnetic bodies with polygonal cross section, Geophysics, **39:**85-92. https://doi.org/10.1190/1.1440416

Nabighian M.N. 1984. Toward a three-dimensional automatic interpretation of potential field data via generalized Hilbert transforms: Fundamental relations. Geophysics, **49:**780-786. https://doi.org/10.1190/1.1441706

Nabighian M.N., Grauch V.J.S., Hansen R.O., LaFehr T.R., Li Y., Peirce J.W., Phillips J.D., Ruder M.E. 2005. The historical development of the magnetic method in exploration. Geophysics, **70(6):**33ND-61ND. https://doi.org/10.1190/1.2133784

Paine J., Haederle M., Flis M. 2001. Using transformed TMI data to invert for remanently magnetised bodies. Exploration Geophysics, **32(3/4):**238–242. https://doi.org/10.1071/eg01238

Pereira B.M. and Ferreira F.J.F. 2018. Recognition of gold mineralization favorability zones through airborne gamma-ray spectrometry and magnetometry in Brusque and Botuverá region, southern Brazil. Brazilian Journal of Geophysics, **36(3):**361-374. doi:10.22564/rbgf.v36i3.1953

Pereira W.R., Mantovani M.S.M., Santos R.P.Z. 2010. Análise geofísica do complexo Alcalino do Barreiro, Araxá-MG. Extended Abstract, 4º Simpósio Brasileiro de Geofísica, 1-5. https://doi.org/10.22564/4simbgf2010.038

Pesce A., Gimenez M.E., Gianni G.M., Folguera A., Martinez P. 2019. Magnetic characterization of a retroarc extensional basin: The Loncopué Trough. Journal of South American Earth Sciences, **89:**55-62. https://doi.org/10.1016/j.jsames.2018.11.001

Piccirillo E.M. and Melfi A.J. (eds.) 1988. The Mesozoic flood volcanism from the Paraná Basin (Brazil). Petrogenetic and geophysical aspects. São Paulo: IAG-USP, 600 p.

Piccirillo E.M., Bellieni G., Cavazzini G., Comin-Chiaramonti P., Petrini R., Melfi A.J., Pinese J.P.P., Zantedeschi P., De Min A. 1990. Lower Cretaceous dyke swarms from the Ponta Grossa Arch: Petrology, Sr-Nd isotopes and genetic relationships with the Paraná flood volcanics. Chemical Geology, **89:**19-48. https://doi.org/10.1016/0009-2541(90)90058-F

Pieruceti J.A. 1973. A intrusão básica de José Fernandes, PR. MSc thesis. Instituto de Geociências. Universidade de São Paulo. https://doi.org/10.11606/d.44.1973.tde-18092015-180434

Pieruceti J.A. and Gomes C.B. 1975. Aspectos mineralógico-petrográficos da intrusão de José Fernandes, PR. Anais da Academia Brasileira de Ciências, **47:**439-450.

Pilkington M. and Beiki M. 2013. Mitigating remanent magnetization effects in magnetic data using the normalized source strength. Geophysics, **78:**J25-J32. https://doi.org/10.1190/geo2012-0225.1

Pilkington M. and Tschirhart V. 2017. Practical considerations in the use of edge detectors for geologic mapping using magnetic data. Geophysics, **82(3):**J1-J8. doi: 10.1190/geo2016-0364.1

Pires A.C.B. 1995. Identificação geofísica de áreas de alteração hidrotermal, Crixás-Guarinos, Goiás. Revista Brasileira de Geociências, **25(1):**61-68. https://doi.org/10.25249/0375-7536.19956168

Ramos L.N.R.A., Pires A.C.B., Toledo C.L.B. 2014. Airborne gamma-ray spectrometric and magnetic signatures of Fazenda Nova Region, East portion of Arenópolis magmatic arc, Goiás. Brazilian Journal of Geophysics, **32(1):**123-140. http://dx.doi.org/10.22564/rbgf.v32i1.401

Raposo M.I.B. and Ernesto M. 1995. An Early Cretaceous paleomagnetic pole from Ponta Grossa dikes (Brazil): implications for the South American Mesozoic apparent polar wander path. Journal of Geophysical Research Solid Earth, **100(B10):**20095–20109. https://doi.org/10.1029/95JB01681

Reeves C. 2005. Aeromagnetic surveys: principles, practice and interpretation. Geosoft. 155p. Available at: https://www.geosoft.com/media/uploads/resources/technical-papers/Aeromagnetic_Survey_Reeves.pdf

Reid A.B., Allsop J.M., Granser H., Millett A.J., Somerton I.W. 1990. Magnetic interpretation in three dimensions using Euler deconvolution. Geophysics, **55(1):**80-91. https://doi.org/10.1190/1.1442774

Renne P.R., Glen J.M., Milner S.C., Duncan A.R. 1996. Age of Etendeka flood volcanism and associated intrusions in southwestern Africa. Geology, **24:**659-662. https://doi.org/10.1130/0091-7613(1996)024<0659:AOEFVA>2.3.CO;2

Riccomini C., Velázquez V.F., Gomes C.B. 2005. Tectonic controls of the Mesozoic and Cenozoic Alkaline Magmatism in Central-Southeastern Brazilian Platform. In: Gomes C.B. and Comin-Chiaramonti P. (eds). Mesozoic to Cenozoic Alkaline Magmatism in the Brazilian Platform, 32-55.

Roest W.R., Verhoef J., Pilkington M. 1992. Magnetic interpretation using the 3-D analytic signal. Geophysics, **57:**116-25. https://doi.org/10.1190/1.1443174

Ruberti E. 1984. Petrologia do maciço alcalino do Banhadão, PR. PhD Thesis. Universidade de São Paulo, 248 p. https://doi.org/10.11606/t.44.1984.tde-25102012-164727

Ruberti E. 1998. Petrologia e geoquímica das suítes carbonatíticas de Mato Preto (PR) e da Barra de Itapirapuã (PR-SP), Brasil. Associate professor thesis, Universidade de São Paulo, São Paulo, 211 p. https://doi.org/10.11606/t.44.2013.tde-29042013-151400

Ruberti E. and Gomes C.B. 1984. O Maciço alcalino do Banhadão, PR: geologia e petrografia. In: XXXIII Congresso Brasileiro de Geologia, Rio de Janeiro, Anais, **9:**4400-4412.

Ruberti E., Castorina F., Censi P., Gomes C.B., Speziale S., Comin-Chiaramonti P. 1997. REE-C-O-Sr-Nd systematic in carbonatites from Barra do Itapirapuã and Mato Preto in Southern Brazil. In: 1st South American Symposium on Isotope Geology, Campos do Jordão, Extended Abstracts, 271-275.

Ruberti E., Enrich G.E.R., Azzone R.G., Comin-Chiaramonti P., De Min A., Gomes C.B. 2012. The Banhadão Alkaline Complex, southeastern Brazil: source and evolution of potassic SiO2-undersaturated high-Ca magmatic series. Mineralogy and Petrology, **104:**63-80. https://doi.org/10.1007/s00710-011-0171-9

Ruberti E., Gomes C.B., Comin-Chiaramonti P. 2005. The alkaline magmatism from the Ponta Grossa Arch. In: Comin-Chiaramonti P. and Gomes C.B. (eds.) Mesozoic to Cenozoic alkaline magmatism in the Brazilian Platform. São Paulo, Edusp/Fapesp, 473-522.

Rugenski A. 2006. Investigação geofísica dos complexos alcalinos do sul e sudeste do Brasil. PhD thesis, Universidade de São Paulo, 352 p. https://doi.org/10.11606/t.14.2019.tde-26032013-093128

Santos R.V. and Dardenne M.A. 1988. Fluorita de Mato Preto: um caso particular de mineralização de fluorita associada a complexo alcalino carbonático. In: Proceedings of 35th Congresso Brasileiro de Geologia, **3:**1251-1261.

Santos R.V., Dardenne M.A., Matsui E. 1990. Geoquímica de isótopos de carbono e oxigênio dos carbonatitos do Complexo Alcalino de Mato Preto, Paraná, Brasil. Revista Brasileira de Geociências, **20(1-4):**153-158. https://doi.org/10.25249/0375-7536.1990153158

Saunders D.F., Branch J.F., Thompson C.K. 1994. Tests of Australian aerial radiometric data for use in petroleum reconnaissance, Geophysics, **59:**411-419. https://doi.org/10.1190/1.1443603

Saunders D.F., Terry S.A., Burson K.R., Branch J.F., Thompson C.K. 1993. Relation of thorium-normalizaed surface and aerial radiometric data to subsurface petroleum accumulations. Geophysics, **58:**1417-1427. https://doi.org/10.1190/1.1443357

Saunders D.F., Terry S.A., Thompson C.K. 1987. Test of National Uranium Resource Evaluation gamma-ray spectral data in petroleum reconnaissance, Geophysics, **52:**1547-1556. https://doi.org/10.1190/1.1442271

Sheriff R.E. 2002. Encyclopedic Dictionary of Applied Geophysics. Geophysical References Series 13. 4ed. Society of Exploration Geophysicists, Tulsa, Oklahoma, USA, 429p.

Siga Jr. O., Gomes C.B., Sato K. Passarelli C.R. 2007. O Maciço Alcalino de Tunas, PR: Novos Dados Geocronológicos. Geologia USP Série Científica, **7(2):**71-80. https://doi.org/10.5327/Z1519-874x2007000200005

Sigismondi M.E. 2019. Radial Averaged Power Spectrum Step by Step. Retrieved from https://www.researchgate.net/publication/332428035_RADIAL_AVERAGED_POWER_SPECTRUM_STEP_BY_STEP. Accessed 18 April 2019.

Silva D.C. 1984. Projeto Barra do Itapirapuã: Relatório de Pesquisa. Curitiba, MINEROPAR.

Silva D.C. 1994. Espectrometria de raios gama aplicada na classificação de granitóides. MSc thesis. IAG-USP, Universidade de São Paulo, 83p.

Silva D.C., Felipe R.S., Pontes J.B. 1981. Notas sobre as ocorrências de fluorita do Vale do Ribeira, PR. In: Proceedings of III Simpósio Sul-Brasileiro de Geologia. SBG, Curitiba, **1:**21-34.

Sonoki I.K. and Garda G.M. 1988. Idades K/Ar de rochas alcalinas do Brasil meridional e Paraguai oriental: compilação e adaptação às novas constantes de decaimento. Boletim do Instituto de Geociências da USP, Série Científica, **19:**63-85. https://doi.org/10.11606/issn.2316-8986.v19i0p63-85

Spector A. and Grant F.S. 1970. Statistical models for interpreting aeromagnetic data. Geophysics, **35(2):**293-302. https://doi.org/10.1190/1.1440092

Swain C.J. 1976. A FORTRAN IV program for interpolating irregularly spaced data using the difference equations for minimum curvature. Computers & Geosciences, **1:**231-240. doi:10.1016/0098-3004(76)90071-6

Tankard A.J., Uliana M.A., Welsink H.J., Ramos V.A., Turic M., França A.B., Milani E.J., Brito-Neves, B.B., Eyles N., Skarmeta J., Santa Ana H., Wiens F., Cirbián M., Paulsen O.L., Germs G.J.B., De Wit M.J., Machacha T., Miller, R. McG. 1995. Tectonic controls of basin evolution in southwestern Gondwana. In: Tankard A.J., Suarez R., Welsink H.J. (eds.) Petroleum basins of South America. AAPG Memoir **62:**5-52.

Telford W.M., Geldart L.P., Sheriff R.E. 1990. Applied Geophysics. 2ed. Cambridge University Press. 770 p. https://doi.org/10.1017/cbo9781139167932

Thomas M.D., Ford K.L., Keating P. 2016. Review paper: Exploration geophysics for intrusion-hosted rare metals. Geophysical Prospecting, 64(5):1275–1304. https://doi.org/10.1111/1365-2478.12352

Thompson D.T. 1982. EULDPH: A new technique for making computer assisted depth estimates from magnetic data. Geophysics, **47:**31–37. https://doi.org/10.1190/1.1441278

Thompson R.N., Gibson S.A., Mitchell J.G., Dickin A.P., Leonardos O.H., Brod J.A., Greenwood J.C. 1998. Migrating Cretaceous-Eocene magmatism in the Serra do Mar alkaline province, SE Brazil: melts from the deflected Trindade mantle plume. Journal of Petrology, **39:**1493-1526. https://doi.org/10.1093/petroj/39.8.1493

Trein E., Marini O.J., Fuck R.A. 1967. Rochas alcalinas do primeiro planalto do estado do Paraná. Boletim Paranaense de Geociências, 23-25:325-347.

Ulbrich H. and Gomes C.B. 1981. Alkaline rocks from continental Brazil. Earth-Science Reviews, **17(1-2):**135-154. https://doi.org/10.1016/0012-8252(81)90009-x

Ulbrich H.H.G.J., Demaiffe D., Vlach S.R.F., Ulbrich M.N.C. 2003. Geochemical and Sr, Nd and Pb isotope signatures of phonolites and nepheline syenites from Poços de Caldas alkaline massif, southeastern Brazil. 4th South American Symposium on Isotope Geology, Salvador, Short Papers, 698-701.

Ussami N., Kolisnyk A., Raposo M.I.B., Ferreira F.J.F., Molina E.C., Ernesto M. 1994. Detectabilidade magnética de diques do Arco de Ponta Grossa: um estudo integrado de magnetometria terrestre/aérea e magnetismo de rocha. Revista Brasileira de Geociências, **21:**317-327. https://doi.org/10.25249/0375-7536.1991317327

Vacquier V., Steenland N.C., Henderson R.G., Zietz I. 1951. Interpretation of Aeromagnetic Maps. Geological Society of America Memoirs. 150p. https://doi.org/10.1130/mem47-p1

Vasconcellos E.M.G. 1991. Investigações Geológicas e Petrológicas das Brechas Vulcânicas do Maciço de Tunas, PR. MSc thesis, Universidade de São Paulo, 128p. https://doi.org/10.11606/d.44.1991.tde-18092015-174124

Vasconcellos E.M.G. 1995. Petrologia e geoquímica de diques e "plugs" alcalinos da região do Vale do Ribeira, divisa dos Estados do Paraná e São Paulo. PhD thesis, Universidade de São Paulo, 202p. https://doi.org/10.11606/t.44.1995.tde-28102015-105327

Vasconcellos E.M.G. and Gomes C.B. 1992. Caracterização petrográfica de brechas vulcânicas no Complexo Alcalino de Tunas, PR. Revista Brasileira de Geociências, v.22, 3:269-274. https://doi.org/10.25249/0375-7536.1992269274

Vasconcellos E.M.G. and Gomes C.B. 1998. Diques e "plugs" alcalinos da região do Vale do Ribeira, Divisa dos Estados do Paraná e São Paulo: características petrográficas e geoquímicas. Geochimica Brasiliensis, **12:**123-143. https://doi.org/10.11606/issn.2316-8986.v29i0p97-124

Verplanck P.L. and Gosen, B.S.V. 2011. Carbonatite and alkaline intrusion-related rare earth element deposits - A deposit model: U.S. Geological Survey Open-File Report 2011-1256, 6p. http://dx.doi.org/10.3133/ofr20111256

Vieira A.J. 1973. Geologia do centro e nordeste do Paraná e centro-sul de São Paulo. In: Congresso Brasileiro de Geologia, 27, Aracaju, Anais, **3:**259-277.

Weihermann J. D., Ferreira F.J.F., Cury L.F., Silveira C.T. 2016. Gamma-ray spectrometry of granitic suites of the Paranaguá Terrane, Southern Brazil. Journal of Applied Geophysics, **132:**38–52. doi:10.1016/j.jappgeo.2016.06.017

Wijns C., Perez C., Kowalczyk P. 2005. Theta map: edge detection in magnetic data. Geophysics, 70:39-43. https://doi.org/10.1190/1.1988184

Wilford J.R., Bierwirth P.N., Craig M.A. 1997. Application of airborne gamma-ray spectrometry in soil/regolith mapping and applied geomorphology. AGSO Journal of Australian Geology and Geophysics, **17(2):**201-216. http://pid.geoscience.gov.au/dataset/ga/81503

APPENDIX 1 - ROUTINE TO CALCULATE THE AVERAGE FLIGHT HEIGHT BY LINE

1095_GamaLine.gdb/1095_MagLine.gdb from the PR-SC project should be exported as .csv files with the headers Line and ALTURA on the first row in the Oasis Montaj suite. The dataset should be on this form in the .csv file:

Line,ALTURA

L10015,95.95

L10015,98.2

L10015,99.17

L10015,98.17

L10015,95.76

...

Install the Python and R programming languages distribution called Anaconda, available at https://www.anaconda.com. In the Anaconda navigator, open the Spyder application and run the code:

```
import pandas as pd # import pandas package
import matplotlib.pyplot as plt # import matplot package


pd.set_option('display.max_rows', 1300) # define the maximum number of rows shown in the console
df = pd.read_csv (r'C:\Users\...\filename.csv')
#df = pd.read_csv (r'Path where the CSV file is stored\filename.csv')
mean1 = df['ALTURA'].mean()
print ('Total arithmetic mean: ' + str(mean1))


groupby_mean1 = df.groupby(['Line']).mean()
print('Mean of values, grouped by Line: ' + str(groupby_mean1))
```

This will generate the average survey height by each line and the total mean for the dataset. Then, this data should be exported to a graphing software to generate the plots. It should be noted that for large datasets sometimes not all the values are copied. If this is the case, try to increase the buffer for the console in Spyder options.

APPENDIX 2 - PARAMETERS USED FOR 3D INVERSIONS

All inverse modelings have the common parameters:

Sensor Elevation Channel	GPSALT
Data Sampling Optimization	Yes
Samples Per Cell	1
IGRF	Date: 2010-11-14
Cell sizes (m)	X = Y = 220, Z = 50
Constraints: Susceptibility	Starting Model Default Value: Default for system Parameter Reference Model Default Value: 0 Gradient Reference Model Default Value: 0 Upper Bounds Model Default Value: 1e+20 Lower Bounds Model Default Value: -1e+20 Parameter Weighting Model Default Value: 0.0001 EW Gradient Weighting Model Default Value: 1 NS Gradient Weighting Model Default Value: 1 Vertical Gradient Weighting Model Default Value: 1 Reweighting model None Active Model Default Value: 1 IRI Focus None Reweighting Model Default Value: 1
Global Settings	Acceleration Radius of Influence (m): 1000000 Computational Error Tolerance: 0.002 Regularization - Auto-Fit Data fit: 1 Attempts: 20

Bairro da Cruz parameters

Common parameters for Bairro da Cruz inversions:

IGRF	Field Strength (nT): 22823
Active Volume	Dimension (cells): X = 23 Y = 18 Z = 28 Mínima (m): X = 714746.5 Y = 7249123.3 Z = -1738.1 Maxima (m): X = 719403.2 Y = 7252827.4 Z = 778.3
Base and Padding	Dimension (cells): Base = 18 Horizontal Padding = 5

	Vertical Padding = 5 Cell expansion ratios: Base = 1.08 Horizontal Padding = 1.5 Vertical Padding = 1.5
Top of Model	Value: 778.25
Lin-Log Transition	Value: 279.58

ASVI-TMI inversion for Bairro da Cruz

Sensor channel of database	ASVI_TMI
Fit Error - Absolute	Value: 6.124
Background Trend - Linear	X Origin: 717088.1 Y Origin: 7250978.4 Intercept: 204.54 X Slope: -0.067616 Y Slope: 0.017413
IGRF	Inclination (degrees): 90 Declination (degrees): 0

RTP-TMI inversion for Bairro da Cruz

Sensor channel of database	RTP_TMI
Fit Error - Absolute	Value: 7.925
Background Trend - Linear	X Origin: 717088.1 Y Origin: 7250978.4 Intercept: 72.072 X Slope: -0.014055 Y Slope: 0.033434
IGRF	Inclination (degrees): -35 Declination (degrees): -19

TMI inversion for Bairro da Cruz

Sensor channel of database	TMI
Fit Error - Absolute	Value: 8.754
Background Trend - Linear	X Origin: 693590.4 Y Origin: 7240456.9 Intercept: 64.356 X Slope: 0.001767 Y Slope: 0.011024
IGRF	Inclination (degrees): -35 Declination (degrees): -19

VIAS-TMI inversion for Bairro da Cruz

Sensor channel of database	VIAS_TMI
Fit Error - Absolute	Value: 11.66
Background Trend - Linear	X Origin: 717088.1 Y Origin: 7250978.4 Intercept: 39.076 X Slope: -0.051989 Y Slope: -0.04967
IGRF	Inclination (degrees): 90 Declination (degrees): 0

José Fernandes parameters

Common parameters for José Fernandes inversions:

IGRF	Field Strength (nT): 22818
Active Volume	Dimension (cells): X = 18 Y = 17 Z = 26 Mínima (m): X = 702791.0 Y = 7261846.4 Z = -1458.9 Maxima (m): X = 706423.0 Y = 7265329.6 Z = 749.5
Base and Padding	Dimension (cells): Base = 17 Horizontal Padding = 5 Vertical Padding = 5 Cell expansion ratios: Base = 1.08 Horizontal Padding = 1.5 Vertical Padding = 1.5
Top of Model	Value: 749.5
Lin-Log Transition	Value: 320.32

ASVI-TMI inversion for José Fernandes

Sensor channel of database	ASVI_TMI
Fit Error - Absolute	Value: 12.04
Background Trend - Linear	X Origin: 704562.2 Y Origin: 7263608.9 Intercept: 383.68 X Slope: -0.053629 Y Slope: 0.034857
IGRF	Inclination (degrees): 90 Declination (degrees): 0

RTP-TMI inversion for José Fernandes

Sensor channel of database	RTP_TMI
Fit Error - Absolute	Value: 16.84
Background Trend - Linear	X Origin: 704562.2 Y Origin: 7263608.9 Intercept: 163.59 X Slope: 0.007905 Y Slope: -0.007015
IGRF	Inclination (degrees): -34.7 Declination (degrees): -19

TMI inversion for José Fernandes

Sensor channel of database	TMI
Fit Error - Absolute	Value: 15.03
Background Trend - Linear	X Origin: 704562.2 Y Origin: 7263608.9 Intercept: 162.19 X Slope: -0.05891 Y Slope: 0.21127
IGRF	Inclination (degrees): -34.7 Declination (degrees): -19

VIAS-TMI inversion for José Fernandes

Sensor channel of database	VIAS_TMI
Fit Error - Absolute	Value: 20.84
Background Trend - Linear	X Origin: 704562.2 Y Origin: 7263608.9 Intercept: 236.88 X Slope: -0.054994 Y Slope: -0.024392
IGRF	Inclination (degrees): 90 Declination (degrees): 0

Tunas parameters

Common parameters for Tunas inversions:

IGRF	Field Strength (nT): 22810
Active Volume	Dimension (cells): X = 49 Y = 39 Z = 31 Mínima (m): X = 688184.7 Y = 7236245.0 Z = -2377.0 Maxima (m): X = 698860.6 Y = 7244698.4 Z = 1065.5
Base and Padding	Dimension (cells): Base = 23 Horizontal Padding = 5 Vertical Padding = 5 Mínima (m): Cell expansion ratios: Base = 1.08 Horizontal Padding = 1.5 Vertical Padding = 1.5
Top of Model	Value: 1065.5
Lin-Log Transition	Value: 675.23

ASVI-TMI inversion for Tunas

Sensor channel of database	ASVI_TMI
Fit Error - Absolute	Value: 8.224
Background Trend - Linear	X Origin: 693590.4 Y Origin: 7240456.9 Intercept: 192.84 X Slope: 0.001085 Y Slope: -0.014093
IGRF	Inclination (degrees): 90 Declination (degrees): 0

RTP-TMI inversion for Tunas

Sensor channel of database	RTP_TMI
Fit Error - Absolute	Value: 9.381
Background Trend - Linear	X Origin: 693590.4 Y Origin: 7240456.9 Intercept: 39.966 X Slope: 0.011634 Y Slope: -0.026461

IGRF	Inclination (degrees): -34.9 Declination (degrees): -18.9

TMI inversion for Tunas

Sensor channel of database	TMI
Fit Error - Absolute	Value: 8.754
Background Trend - Linear	X Origin: 693590.4 Y Origin: 7240456.9 Intercept: 64.356 X Slope: 0.001767 Y Slope: 0.011024
IGRF	Inclination (degrees): -34.9 Declination (degrees): -18.9

VIAS-TMI inversion for Tunas

Sensor channel of database	VIAS_TMI
Fit Error - Absolute	Value: 21.03
Background Trend - Linear	X Origin: 693590.4 Y Origin: 7240456.9 Intercept: 127.15 X Slope: 0.019917 Y Slope: -0.080778
IGRF	Inclination (degrees): 90 Declination (degrees): 0

APPENDIX 3 - RADIOMETRIC IMAGES AND DIGITAL TERRAIN MODEL OF STUDY AREA

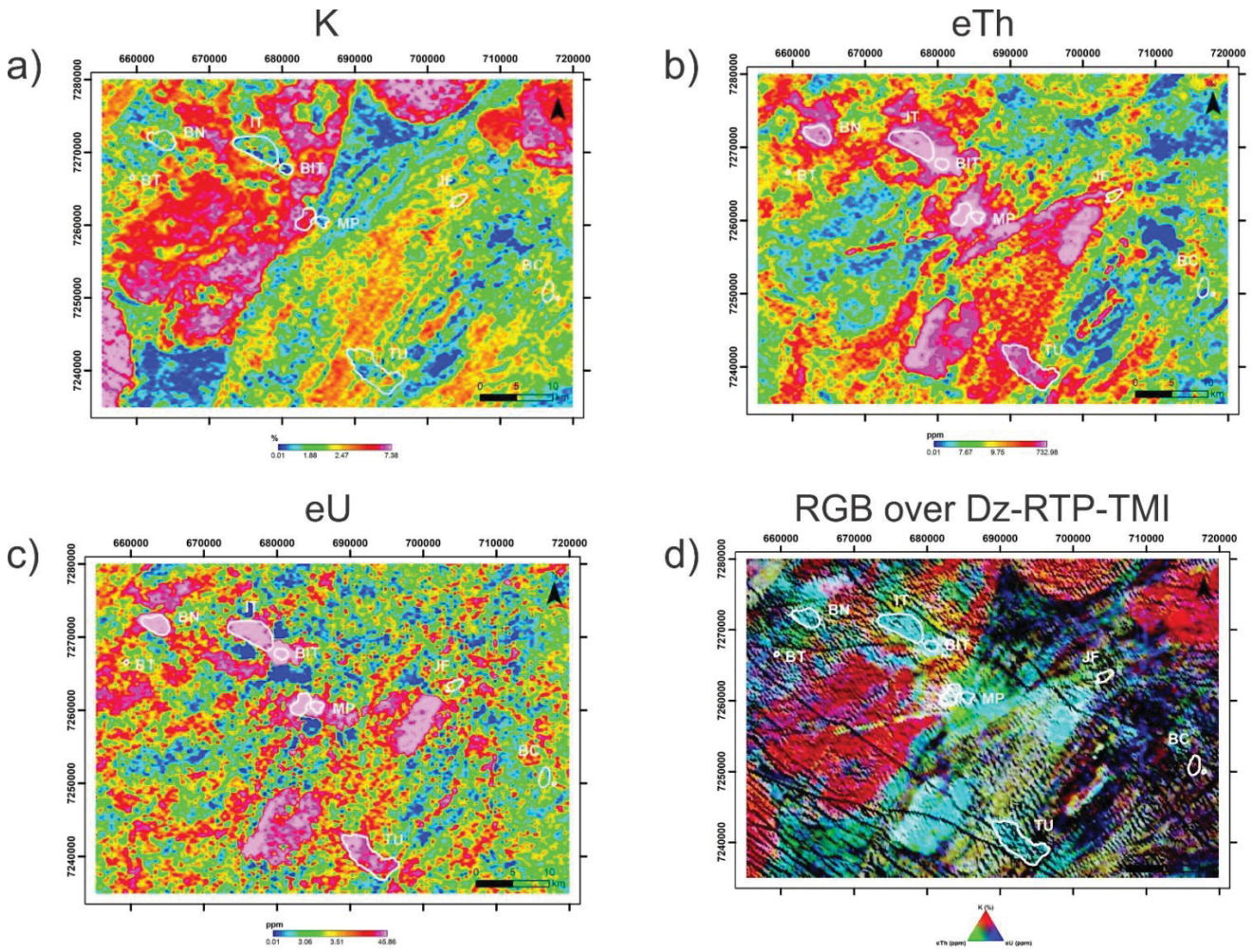

Figure 40. Gridded images of K, eTh, eU, and R-K/G-eTh/B-eU over the first vertical derivative. Intrusions: Bairro da Cruz (BC), Barra do Itapirapuã (BIT), Banhadão (BN), Barra do Teixeira (BT), Itapirapuã (IT), José Fernandes (JF), Mato Preto (MP), and Tunas (TU).

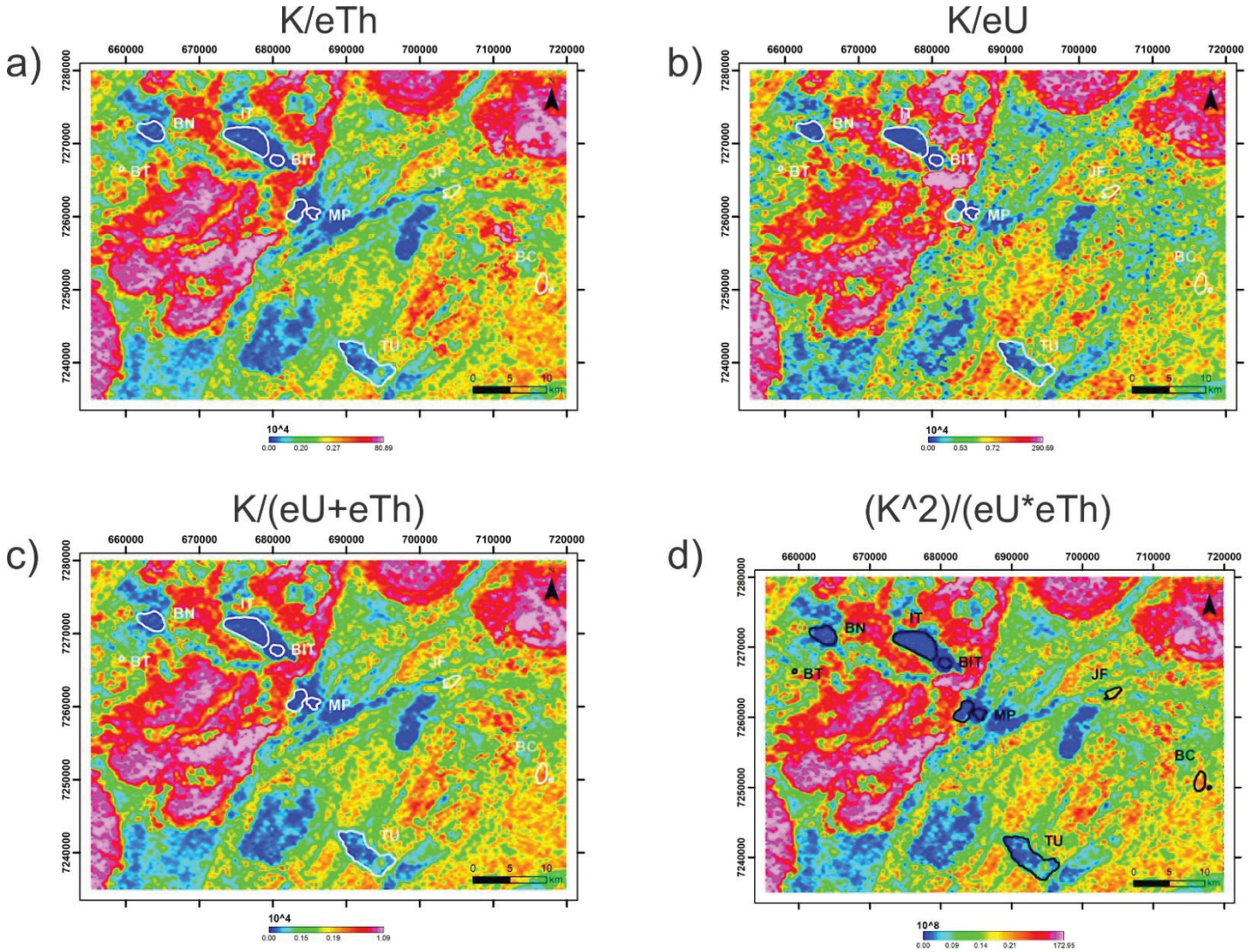

Figure 41. Gridded images of ratios K/eTh, K/eU, K/(eU+eTh), and (K^2)/(eU*eTh). Intrusions: Bairro da Cruz (BC), Barra do Itapirapuã (BIT), Banhadão (BN), Barra do Teixeira (BT), Itapirapuã (IT), José Fernandes (JF), Mato Preto (MP), and Tunas (TU).

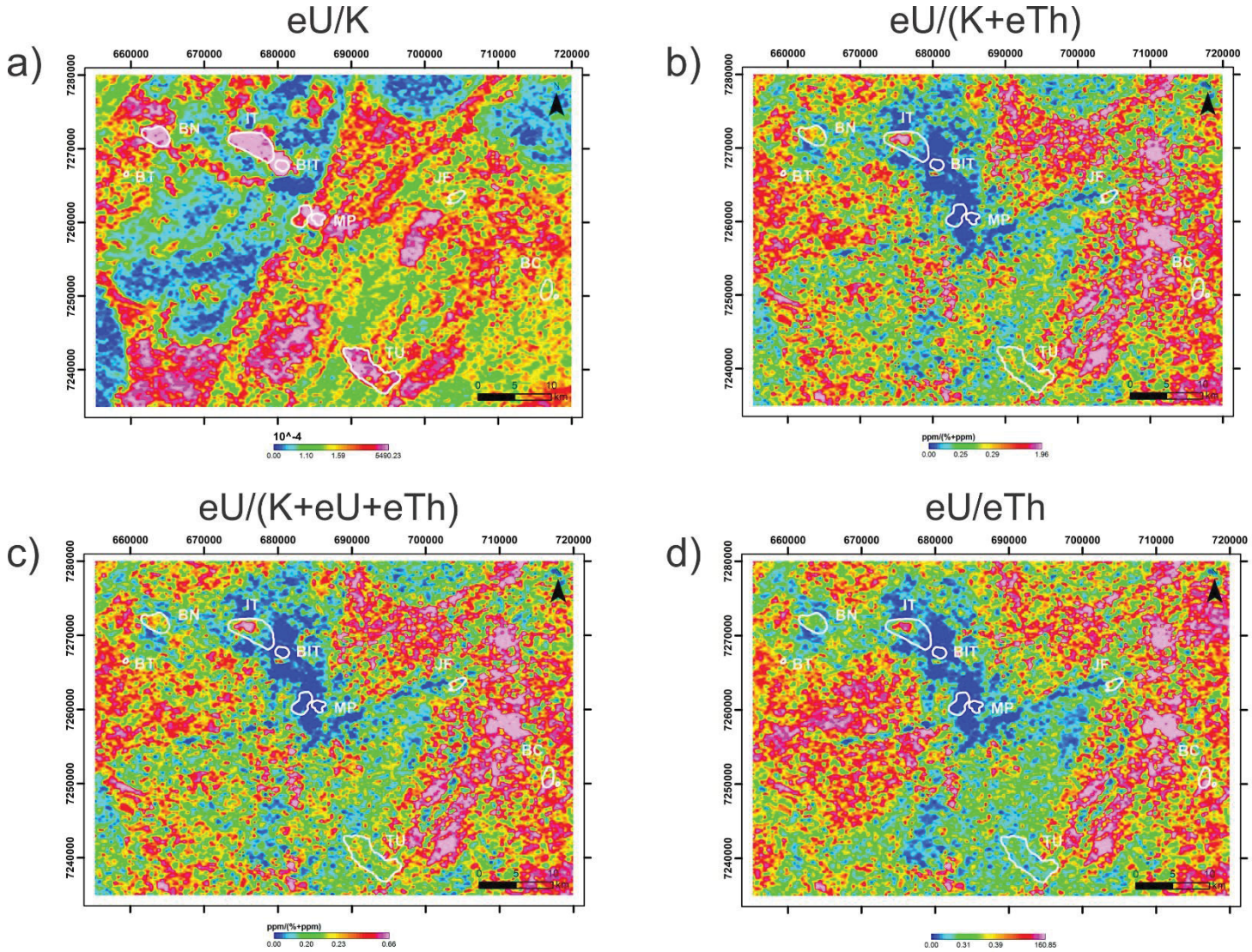

Figure 42. Gridded images of eU/K, eU/(K+eTh), eU/(K+eU+eTh), and eU/eTh. Intrusions: Bairro da Cruz (BC), Barra do Itapirapuã (BIT), Banhadão (BN), Barra do Teixeira (BT), Itapirapuã (IT), José Fernandes (JF), Mato Preto (MP), and Tunas (TU).

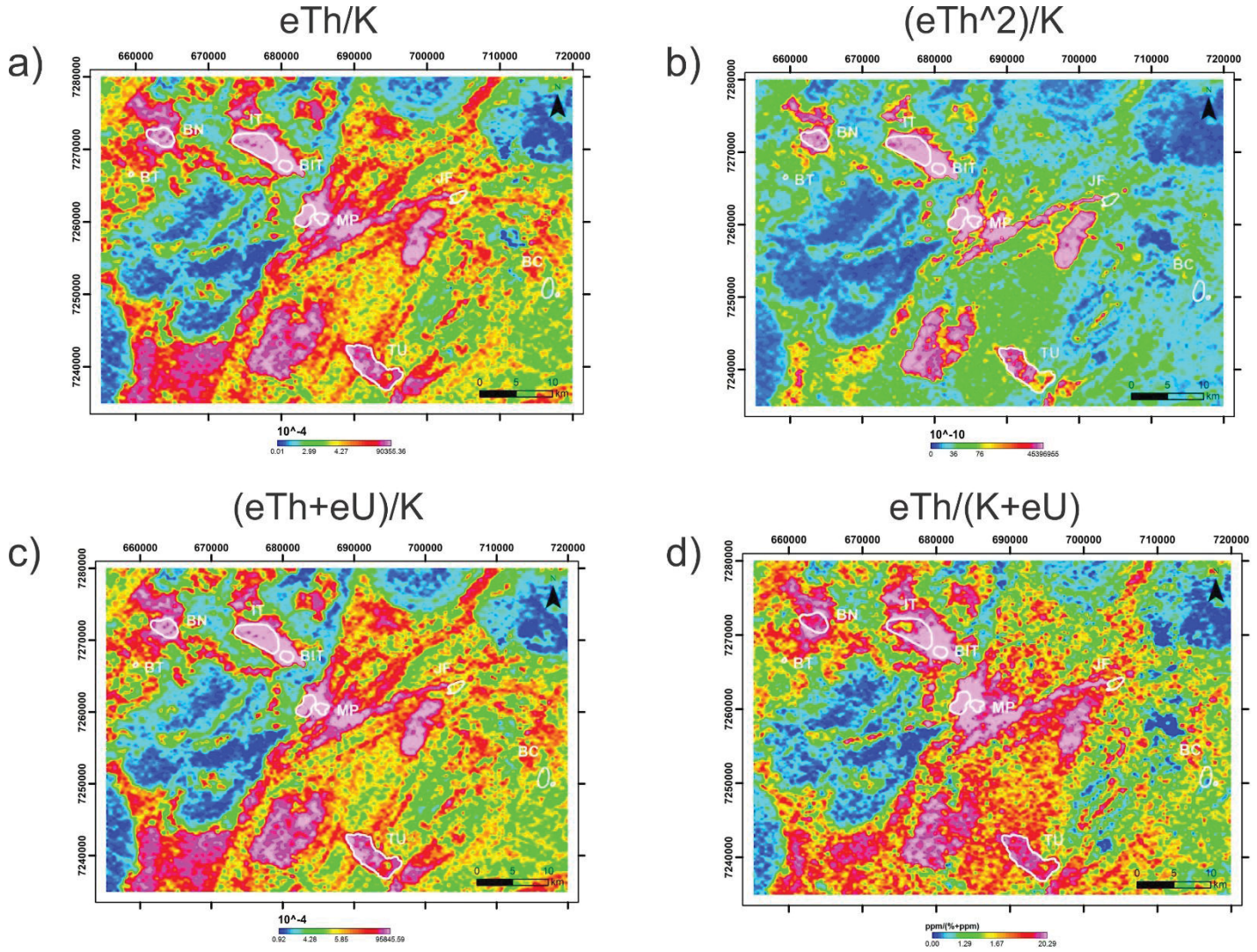

Figure 43. Gridded images of eTh/K, (eTh^2)/K, (eTh+eU)/K, and eTh/(K+eU). Intrusions: Bairro da Cruz (BC), Barra do Itapirapuã (BIT), Banhadão (BN), Barra do Teixeira (BT), Itapirapuã (IT), José Fernandes (JF), Mato Preto (MP), and Tunas (TU).

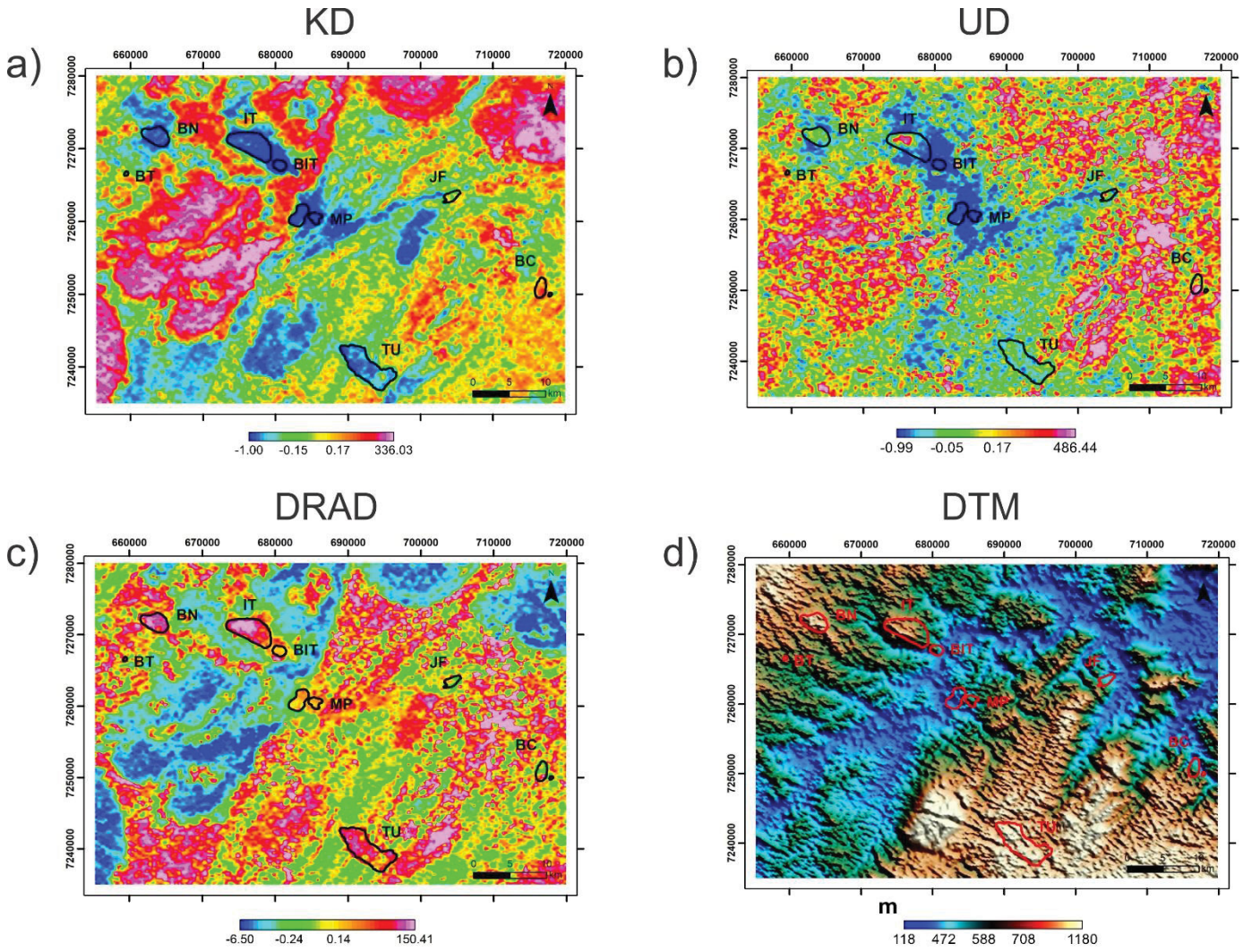

Figure 44. Gridded images of parameters KD, UD, DRAD, and Digital Terrain Model (DTM). Intrusions: Bairro da Cruz (BC), Barra do Itapirapuã (BIT), Banhadão (BN), Barra do Teixeira (BT), Itapirapuã (IT), José Fernandes (JF), Mato Preto (MP), and Tunas (TU).

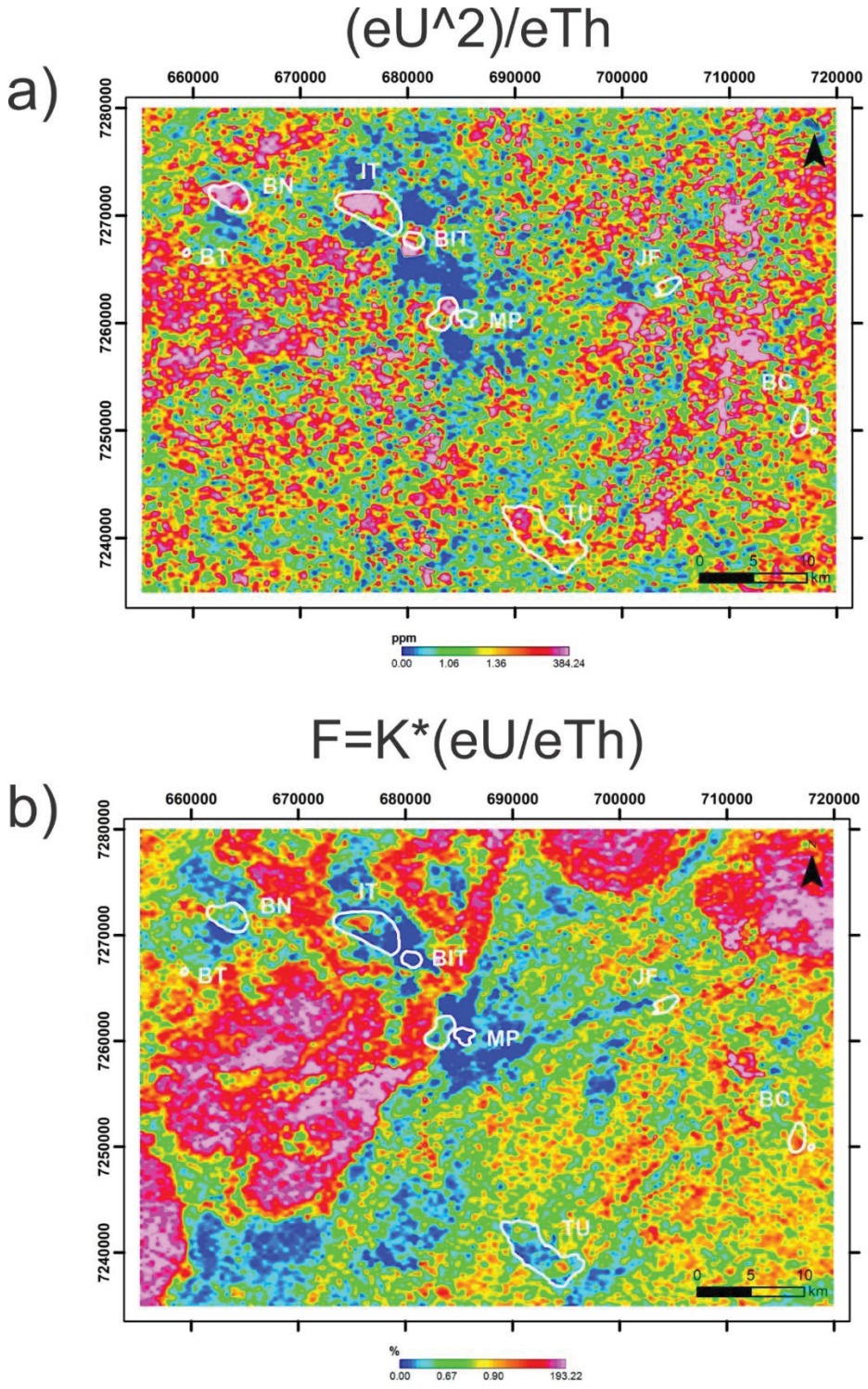

Figure 45. Gridded images of ratios (eU^2)/eTh and F=K*(eU/eTh). Intrusions: Bairro da Cruz (BC), Barra do Itapirapuã (BIT), Banhadão (BN), Barra do Teixeira (BT), Itapirapuã (IT), José Fernandes (JF), Mato Preto (MP), and Tunas (TU).